NOVEL DATA-BASED AND MODEL-BASED ALGORITHMS FOR PROCESS MONITORING AND EQUIPMENT DEGRADATION TRACKING

A Dissertation

by

MOHAMMED ZIYAN SHERIFF

Submitted to the Office of Graduate and Professional Studies of
Texas A&M University
in partial fulfillment of the requirements for the degree of

DOCTOR OF PHILOSOPHY

Chair of Committee,	Mohamed N. Nounou
Co-Chair of Committee,	Costas Kravaris
Committee Members,	Mahmoud El-Halwagi
	Hazem N. Nounou
	Mohammad Azizur Rahman
Head of Department,	Arul Jayaraman

December 2020

Major Subject: Chemical Engineering

ABSTRACT

Process monitoring is a critical component of many industries, required in order to maintain product quality and enhance process safety, thereby increasing economic benefits. Process monitoring methods provide a means of determining if a process is operating as expected, or if it is experiencing faulty or abhorrent conditions, e.g., process drifts or disturbances that disrupt the operation, which can result in plant shutdowns and economic losses due to down time and maintenance. Process monitoring methods can be broadly categorized into qualitative based models, quantitative based models, and data-based models. A primary objective of this work is to enhance the performance of monitoring algorithms by integrating the advantages of various data-driven and model-based methods. Data-based fault detection methods such as principal component analysis (PCA) and its extensions, will be integrated with composite hypothesis tests, such as the generalized likelihood ratio (GLR) charts in order to obtain superior fault detection performance when compared to conventional methods. The applicability of the developed fault detection algorithms will be examined using different illustrative examples, such as the Tennessee Eastman (TE) process. Monitoring process drifts and equipment degradation is another area of concern in process industries. Therefore, a second objective of this work is to develop an algorithm capable of detecting drifts in processes and equipment degradation, even when operating under control, by utilizing state estimation methods that are able to determine when a process is operating under sub-par conditions. The developed algorithm will be applied on an illustrative example of a heat exchanger,

using both simulated synthetic and experimental data, to demonstrate its simplicity and practical applicability. This should enable the process engineer to make better executive decisions regarding the running of the plant. Pipeline flow and leak detection, specifically in subsea pipelines is another important issue that needs to be addressed, and therefore a third objective of this work is to design and develop an experimental setup to collect different sensor measurements, and utilize different fault detection and classification algorithms in order to study pipeline flow behavior.

DEDICATION

This dissertation is dedicated to my parents, Omar Khayyam Sheriff and Firzana Zubair for their unconditional love, continued support, and instilling the importance of education in me from a very young age. Thank you.

ACKNOWLEDGEMENTS

As this work has been the result of many years of challenging and exciting research work, conducted on both campuses of Texas A&M University, i.e., College Station and Qatar, much of this would not have been possible without the support and encouragement of a number of people. I would like to take this opportunity to acknowledge those responsible for being my inspiration, motivation, and support system over the last few years.

First and foremost, I would like to thank those who played a direct role in shaping my personality and work ethic as an academic. Primarily my committee chair, Dr. Mohamed Nounou, for his excellent vision and guidance throughout the course of my time as a graduate student at Texas A&M University. As a first-generation college student, I was beyond blessed to land an advisor who was the perfect mentor, providing me with encouragement and support when required, and letting me take over the reigns as I gained experience. My co-chairs, Dr. Nazmul Karim and Dr. Costas Kravaris, also provided unwavering support and invaluable guidance over the last few years, encouraging me to think long-term and attempt to solve real problems that were applicable to the broader engineering industry. Other members of my committee, Dr. Mahmoud El-Halwagi and Dr. Hazem Nounou, also deserve gratitude for their valuable insight, input and advice.

Second, I would like to thank the members of the different research groups I have been fortunate enough to be a part of. From Dr. Nounou's group: Nour, Shameel, Byanne, Mohamed, Noor. From Dr. Karim's research group: Chiru, Jon, Melanie, Tejasvi,

Xinghua. From Dr. Kravaris's group: Zhaoyang, Sunjeev, Joshiba, Mengxi. I am thankful for their time and the chance to brainstorm and engage in intellectual discussions, and for also providing me with important feedback during the course of conducting research and finalizing my dissertation.

Special thanks also go out to all faculty, staff, and students on both campuses of Texas A&M University, in College Station and in Qatar, for making my undergraduate and graduate experiences truly memorable, and for providing a great learning environment, both inside and outside the classroom. Ashley deserves a special mention for being patient and taking the time to personally address all queries I have had related to all of the administrative paperwork I have had to handle.

As a third culture adult who has had the opportunity to live, study, and work in multiple countries, I have met a number of individuals from different backgrounds, who have become life-long friends. Therefore, in addition to members of the various research groups, I would also like to thank Joe, Raid, Shaik, Dhabia, Maria Christina, Sufiyan, Mary, Tamanna, and Nour.

Last, but most certainly not least, I would like to thank my family for their unconditional love, and continued support and encouragement over the last three decades. Mom, dad, and my brother Zaahid, through your hard work and selflessness you have motivated me to accomplish goals and ambitions I would not have been able to pursue otherwise. As always, I hope to continue to develop personally and professionally, in both academia and the industry, and I do hope I make you all proud.

CONTRIBUTORS AND FUNDING SOURCES

Contributors

This work was supervised by a dissertation committee consisting of Professor Mohamed Nounou, Professor Costas Kravaris, and Professor Mahmoud El-Halwagi of the Department Chemical Engineering, Professor Hazem Nounou of the Department of Electrical Engineering, and Professor Azizur Rahman of the Department of Petroleum Engineering.

Funding Sources

Graduate study was primarily supported by NPRP grant NPRP7-1172-2-439 from the Qatar National Research Fund (a member of Qatar Foundation). Additional financial support for research was received from Texas A&M University's Response Research Seed Grant RRSG 2019-482192.

Additional support was also received through the Paul and Ellen Deisler Fellowship from the Department of Chemical Engineering at Texas A&M University, and the Graduate Teaching Fellowship from the College of Engineering at Texas A&M University.

TABLE OF CONTENTS

Page

LIST OF FIGURES

Page

LIST OF TABLES

Page

1. INTRODUCTION

Statistical process monitoring is an integral component of many process industries. Continuous monitoring of these processes is essential in order to maintain product quality and enhance process safety, thereby ensuring that the process remains economically profitable by minimizing down-time and maximizing profits. Walter Shewhart brought attention to the importance of statistical quality control for industrial applications while working as an engineer for Bell Systems [1], [2]. Shewhart explained that monitoring different stages of a process and carrying out early detection and correction of abnormalities is economically beneficial, as opposed to identification and disposal of a faulty final product [3].

Process monitoring methods can be classified using many different methods. The authors in [4]–[6] broadly categorize process monitoring methods into quantitative based models, qualitative based models, and data based (or process history based) models. Different processes and process units can be defined using fundamental principles, such as mass and energy balances. Quantitative model-based techniques utilize these definitions to construct process models that can be utilized to determine if process data deviates from expected values, i.e., to detect faults. Examples of such models are state estimations methods, i.e., Kalman filter methods, and other observer based methods [7], [8]. On the other hand, in the absence of well-defined quantitative models, qualitative relationships between different variables may be used in order to classify different types of data and determine the cause of a fault. Fault trees are examples of qualitative model

based techniques [9]. In the event that process data is available, and there is a lack of a well-defined process model or if the process model is complex, data-based monitoring techniques are often employed [10]. A broad range of data-based process techniques exist, and they are often applied to monitor different processes [11], [12].

A primary objective of this work is to improve existing data-based process monitoring methods, with an emphasis on improving the fault detection and classification performance of the widely used principal component analysis (PCA) method, and its various extensions. Recently, hypothesis testing methods have grown in popularity within the statistical process monitoring industry as they bring in solid theoretical contribution to the field [11], [13]. One method that has demonstrated superior fault detection performance is the generalized likelihood ratio (GLR) technique, and this work will demonstrate how fault detection algorithms can be developed in order to capture its advantages and enhance the overall fault detection and classification performance. Different fault detection and classification algorithms that were developed through the course of this thesis work will be presented, along with applications. The performance of the different fault detection algorithms will be evaluated using three fault detection metrics: the missed detection rate, the false alarm rate, and the out-of-control average run length (ARL_1). The missed detection rate quantifies the percentage of observations that go undetected in the faulty region, while the false alarm rate quantifies the percentage of observations that are incorrectly flagged as faults in the non-faulty region. ARL_1 measures the number of observations it takes for a particular technique to flag a fault in the faulty region, i.e., it measures the speed of detection.

Many plants operate continuously and have process controllers in place in order to ensure that the desired set point is being achieved, e.g., quality of product, or output characteristic (physical parameter), by adjusting the manipulated variable. However, in reality, different process can experience a degradation in the process model itself, i.e., process drift whose existence and impact might be tough to ascertain when operating a system under control. E.g., a heat exchanger can experience different degrees of fouling over time for a variety of reasons leading to a change in the process model, but if the process is operating under control the manipulated variable (in this case, the amount of heating or cooling utility), can be varied in order to ensure that the desired set point is being achieved. In such cases a more accurate representation of the current equipment (or plant) degradation is required in order to determine the cost associated with operating under sub-par conditions. Therefore, a second objective of this work focuses on using available quantitative models, namely state and parameter estimation methods such as the different available Kalman filters, to demonstrate how they can be utilized in order to obtain a more accurate representation of the current operating region of the process and equipment degradation [14]. Urgency of required maintenance can then be determined, which would in turn increase economic benefits by reducing operational costs as a result of carrying out required maintenance. It is important to note that for certain applications monitoring equipment degradation can help avert catastrophic incidents with regards to safety as well.

Chronic leak detection, i.e., small pipeline leaks, can lead to significant releases of greenhouse gases resulting in substantial environmental pollution. If leaks go undetected

and are not addressed in a timely manner, the fracture in the pipeline can propagate, leading to larger releases to the environment, which can lead to fires or explosions [15]. This highlights the importance of implementing efficient leak detection and localization techniques, especially for harsh conditions such as subsea and arctic conditions, as these conditions present additional barriers. Therefore, a third objective of this work is to critically examine existing leak detection and localization literature, in order to guide the design and development of an experimental setup that can be used to study fluid behavior in the event of a leak. Since industrial processes provide an abundance of sensor measurements, an additional objective is the study of fluid behavior in pipelines to examine if redundant pressure sensor measurements can be utilized to predict flow rates from different operating conditions, in the absence or malfunctioning of a flow meter.

The following section will provide a more detailed introduction to data-based models, before introducing Principal Component Analysis (PCA), and its various extensions, that were developed in order to increase the robustness of the PCA model.

1.1. Principal Component Analysis (PCA) and its extensions

Data-based models can be further classified into univariate monitoring methods, i.e., where only trends within a single variable are monitored, and multivariate monitoring methods, i.e., where trends within a variable and correlation between variables are monitored. Once a data-based process model has been developed, the current observation can be compared to its expected value, resulting in the production of process residuals [16]. The Shewhart chart was one of the first univariate charts developed, and functions

by observing process residuals and determining if they exceed acceptable limits [17]. The Shewhart chart is only concerned with the process residual at the current time instant, and is therefore mainly efficient at detecting only fairly large deviations in the process residuals [16], [18]. Therefore, incorporating process memory to fault detection charts may allow trends in the data to be observed, like in the case of process drifts or sustained faults. This led to the development of the exponentially (or geometric) weighted moving average (EWMA) and cumulative sum (CUSUM) charts so that that a broader range of faults, i.e., deviations, could be detected [19]–[22].

Multivariate extensions of the above univariate charts have also been developed [23]–[25]. However, these multivariate extensions ignore possible cross correlation that might be present between the different variables. Since industrial processes may contain process variables that are correlated, it is important to utilize techniques that model or capture the cross-correlation present. All multivariate techniques require collection of vast amounts of data from multiple sensors monitoring the different process variables. Computational efficiency is required when dealing with vast amounts of data collection. Dimensionality reductions techniques have been developed in order to reduce the computational load experienced when analyzing data from complex processes that require the monitoring of multiple variables [26]. They can be of two types: input-output based models, or input-based models. Partial Least Squares (PLS) is an example of an input-output based model, and these techniques are often used if there are many explanatory variables, that are possibly correlated, and relationships can be drawn between the input and output variables [27]. On the other hand, input based models utilize the input variables

in order to observe correlations between different variables [28]. One example of an input-based model is Principal Component Analysis (PCA). Many process industries utilize PCA due to its computational simplicity and efficiency for most processes [29], [30]. The following section introduces the conventional PCA model.

1.1.1. Principal Component Analysis (PCA)

PCA is a linear dimensionality reduction technique that performs well for many linear and approximately linear processes [11], [31]. PCA is still a popular choice for use by many engineering and process industries due to its computational simplicity. A given data matrix **X**, of *m* process variables, and *n* observations can be represented utilizing a linear sum of the given variables [29]:

$$\mathbf{X} = \mathbf{T}\mathbf{P}^{\mathrm{T}} \tag{1}$$

where, **T** and **P**, represent the principal component (PCs), and loading vectors, respectively. The loading vectors are orthogonal and can be obtained from the covariance matrix $(\mathbf{\Sigma})$ of **X** as shown [29]:

$$\mathbf{\Sigma} = \frac{1}{n-1}\mathbf{X}^{\mathrm{T}}\mathbf{X} = \mathbf{P}\mathbf{\Lambda}\mathbf{P}^{\mathrm{T}} \text{ with } \mathbf{P}\mathbf{P}^{\mathrm{T}} = \mathbf{I}_m \tag{2}$$

where, $\mathbf{\Lambda} = diag(\lambda_1, \lambda_2, \ldots, \lambda_m)$ is the diagonal matrix made up of the eigenvectors provided by the *m* PCs, and $\mathbf{I}_m$ is the identity matrix. Dimensionality reduction is carried out in order to improve the computational efficiency of PCA. This is accomplished by capitalizing on the correlation between the different process variables, and using a lower number of PCs to represent the original data set. A number of methods can be utilized in

order to decide on the appropriate number of PCs to retain, e.g., cumulative percent variance (CPV), scree plot, cross validation [32], [33]. CPV is utilized by many authors as it is computationally simple [28]:

$$CPV\left(l\right)=\frac{\sum_{i=1}^{l}\lambda_i}{trace\left(\mathbf{\Sigma}\right)}\times 100\,. \tag{3}$$

The choice of the number of PCs to retain depends on the number it takes to achieve a certain CPV value, e.g., 95%. The original data matrix can now be expressed using retained (l) PCs, and the ignored (m-l) PCs as follows [29]:

$$\mathbf{X}=\mathbf{T}\mathbf{P}^{\mathrm{T}}=\left[\hat{\mathbf{T}}\tilde{\mathbf{T}}\right]\left[\hat{\mathbf{P}}\tilde{\mathbf{P}}\right]^{\mathrm{T}}, \tag{4}$$

where $\hat{\mathbf{T}}\in\mathbb{R}^{n\times l}$, $\tilde{\mathbf{T}}\in\mathbb{R}^{n\times(m-l)}$, $\hat{\mathbf{P}}\in\mathbb{R}^{m\times l}$, and $\tilde{\mathbf{P}}\in\mathbb{R}^{m\times(m-l)}$. Expanding this expression [29]:

$$\mathbf{X}=\hat{\mathbf{T}}\hat{\mathbf{P}}^{\mathrm{T}}+\tilde{\mathbf{P}}\tilde{\mathbf{T}}^{\mathrm{T}}=\overbrace{\mathbf{X}\hat{\mathbf{P}}\hat{\mathbf{P}}^{\mathrm{T}}}^{\hat{\mathbf{X}}}+\overbrace{\mathbf{X}\left(\mathbf{I}_m-\hat{\mathbf{P}}\hat{\mathbf{P}}^{\mathrm{T}}\right)}^{\mathbf{E}}, \tag{5}$$

where, $\hat{\mathbf{X}}$ and **E** represents the data modeled using just the retained $\left(l\right)$ PCs, and model residuals, respectively.

Once the PCA model has been constructed using the fault-free (training) data, which are collected under normal operating conditions, fault detection charts can then be applied in order to determine if a process is experiencing faults. Two indices are often utilized in order to detect faults: the Hotelling's T^2 statistic, which focuses on faults in the PC space, and Q statistic, which focuses on faults in the residual space [34], [35]. Authors have shown that the Q chart is better able to detect smaller faults than the T^2 chart [36].

The T^2 statistic can be computed as follows [37]:

$$T^2 = x^{\mathrm{T}}\hat{\mathbf{P}}\hat{\mathbf{\Lambda}}^{-1}\hat{\mathbf{P}}^{\mathrm{T}}x\,. \tag{6}$$

The fault detection (or control) limits can be computed using a 95-99% confidence interval applied on the distribution of the T^2 statistic computed using training data. Alternatively, the fault detection limits can also be computed theoretically using formulae widely available in literature [34].

The Q statistic is also known as the squared prediction error (SPE), which measures the projection of the observation on the residual space, and is computed as follows [11]:

$$Q = e^{\mathrm{T}}e\,. \tag{7}$$

Like the T^2 chart, the fault detection limits for the Q statistic can be computed either empirically or theoretically [36].

The PCA model is widely used as it is computationally simple, and function well for linear and approximately linear process. However, industrial process might not always be approximately linear. Therefore, a more robust technique is required in order to handle the nonlinearity of certain processes. One such technique based on extending the application of PCA to nonlinear process will be described in the next section.

1.1.2. Kernel Principal Component Analysis (KPCA)

A popular extension of PCA to nonlinear applications is the KPCA algorithm. The KPCA algorithm functions by transforming the nonlinear data to a high-dimensional feature space, where linear PCA becomes applicable [38]. It is difficult to know the exact

nonlinear transformation that forces the nonlinear data matrix to be linear in the feature space. According to Mercer's theorem, an orthogonal semi-definite function can be used in order to map the data in the feature space, rather than knowing the explicit function. This nonlinear function is referred to as the kernel function and is the dot product of the mapped data in the feature space denoted as follows [39]:

$$K\left(\mathbf{X}_i, \mathbf{X}_j\right) = \Phi\left(\mathbf{X}_i\right)\Phi\left(\mathbf{X}_j\right). \tag{8}$$

A number of different kernels have been utilized in order to facilitate the nonlinear mapping [39]:

- Radial basis function (RBF): $K\left(\mathbf{X}, \mathbf{Y}\right) = \exp\left(\frac{-\left\|\mathbf{X}-\mathbf{Y}\right\|^2}{c}\right)$,
- Polynomial function: $K\left(\mathbf{X}, \mathbf{Y}\right) = \left\langle \mathbf{X}, \mathbf{Y} \right\rangle^d$,
- Sigmoid function: $K\left(\mathbf{X}, \mathbf{Y}\right) = \tanh\left(\beta_0 \left\langle \mathbf{X}, \mathbf{Y} \right\rangle + \beta_1\right)$,

where, c, d, β_0, and β_1 are parameters that need to be tuned for the different nonlinear kernel transformations in order to ensure that the transformed data matrix is approximately linear. PCA seeks to find the PCs by minimizing the information loss in the input space, while KPCA does this is the hyper-dimensional feature (F) space. The covariance in the feature space is computed as follows [39]:

$$\mathbf{C}^F = \frac{1}{n}\sum_{j=1}^{n} \Phi\left(\mathbf{X}_j\right)\Phi\left(\mathbf{X}_j\right)^T \tag{9}.$$

Like PCA, the PCs can be found by diagonalizing the covariance matrix. This is accomplished by solving the following eigenvalue problem in the feature space [39]:

$$\lambda \mathbf{v} = \mathbf{C}^F \mathbf{v}, \tag{10}$$

where, $\lambda \geq 0$ and represent the eigenvalues. This is solved by the deriving the following equation [39]:

$$n\lambda\alpha = K\alpha, \tag{11}$$

where, K and α are the $n \times n$ kernel matrix and eigenvectors, respectively. For testing data vector $\mathbf{X}$, the PCs (t) are extracted by projecting $\Phi(\mathbf{X})$ onto the eigenvectors $\mathbf{v}_k$ in the feature space where $k = 1,\ldots l$ [39]:

$$\mathbf{t}_k = \left\langle \mathbf{v}_k, \Phi(\mathbf{X}) \right\rangle = \sum_{i=1}^{N} \alpha_i^k \left\langle \Phi(\mathbf{X}_i) \Phi(\mathbf{X}) \right\rangle. \tag{12}$$

Before the KPCA model is constructed, the data in the high dimensional space needs to be mean centered as follows [39]:

$$\mathbf{K} = \mathbf{K} - 1_n \mathbf{K} - \mathbf{K} 1_n + 1_n \mathbf{K} 1_n \text{ where, } 1_n = \frac{1}{n} \begin{vmatrix} 1 & \cdots & 1 \\ \vdots & \ddots & \vdots \\ 1 & \cdots & 1 \end{vmatrix} \in R^{n \times n}. \tag{13}$$

The fault detection charts for the KPCA model can be computed similar to their conventional counterparts. The variation in the KPCA model is captured by the T^2 statistic as follows [39]:

$$T^2 = \left[\mathbf{t}_1, \ldots, \mathbf{t}_l\right] \Lambda^{-1} \left[\mathbf{t}_1, \ldots, \mathbf{t}_l\right]^T. \tag{14}$$

Like its linear counterpart the fault detection limits of the T^2 chart can be computed empirically or computationally [39].

For the Q statistic to be computed, the feature vector $\Phi(\mathbf{X})$ needs to be reconstructed. This is accomplished by projecting $\mathbf{t}_k$ into the feature space utilizing $\mathbf{v}_k$ [39]:

$$\hat{\Phi}_n(\mathbf{X}) = \sum_{k=1}^{n} \mathbf{t}_k \mathbf{v}_k \,. \tag{15}$$

The Q statistic can now be computed [39]:

$$Q = \left\| \Phi(\mathbf{X}) - \hat{\Phi}_l(\mathbf{X}) \right\|^2 . \tag{16}$$

Once again the fault detection limits for the Q statistic can be computed either empirically or computationally [39].

Measurement residuals collected from process industries may contain high levels of noise, deviate from normality, and can be autocorrelated, and these might adversely affect the performance of the conventional methods [16], [35]. Bakshi developed a multiscale principal component analysis (MSPCA) model in order to address these issues [35], [40], [41]. Due to the multiscale nature of the wavelet coefficients, MSPCA has shown to be an appropriate mechanism to model behavior changes over time and frequency, and the following section will briefly describe multiscale wavelet based representation of data and the MSPCA model [36].

1.1.3. Multiscale Principal Component Analysis (MSPCA)

1.1.3.1. Wavelet-based multiscale representation of data

Wavelet-based representation of data is a powerful signal processing tool, that is capable of providing efficient separation of stochastic and deterministic features in available data [16], [35], [41]–[43]. Utilizing the time-domain data, i.e., measurements collected from sensors, a courser approximation of the given data can be obtained by convoluting the original data using a low pass filter (*h*), derived from a scaling basis function that has the following form [36]:

$$\phi_{ij}(t) = \sqrt{2^{-j}}\,\phi\left(2^{-j}t - k\right), \tag{17}$$

where, *j* and *k* are the discretized dilation and translation parameters, respectively. The difference between the original and approximated data, also known as the detail signal, is obtained by convoluting the original data using a high pass filter (*g*), derived from a wavelet basis function of the following form [36]:

$$\psi_{ij}(t) = \sqrt{2^{-j}}\,\psi\left(2^{-j}t - k\right). \tag{18}$$

This approximation can be repeated multiple times on the subsequent scaled data, and the original data can be reconstructed using the sum of the last scaled signal, and all details signals [36]:

$$x(t) = \sum_{k=1}^{n2^{-J}} a_{Jk}\phi_{Jk} + \sum_{j=1}^{J}\sum_{k=1}^{n2^{-J}} d_{jk}\psi_{jk}(t), \tag{19}$$

where, n, and J, are the number of observations and the maximum possible decomposition depth, respectively. A schematic illustration of the wavelet-based multiscale representation procedure is provided in Figure 1.

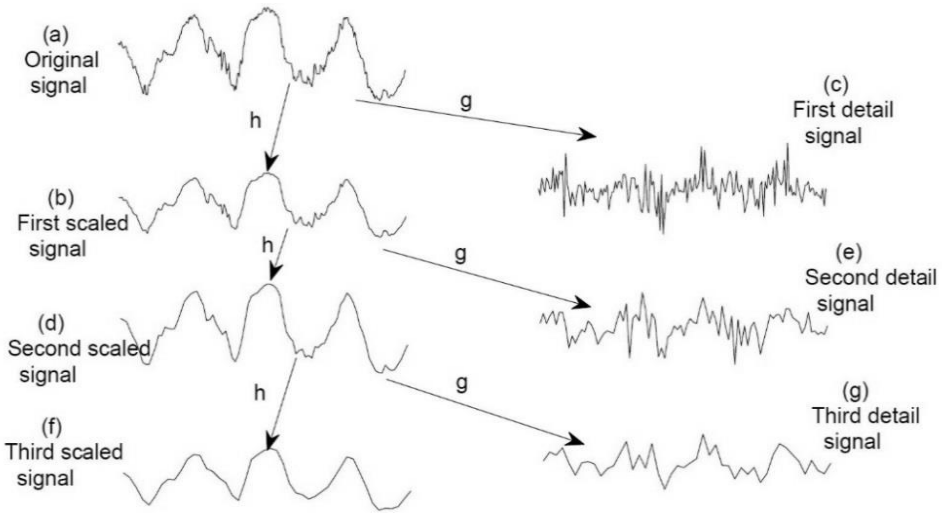

Figure 1. Schematic illustration of wavelet-based multiscale representation of data.

1.1.3.2. MSPCA model description

The MSPCA model was developed by Bakshi in order to combine the ability of PCA to extra cross-correlation between different process variables, with the ability of the orthonormal wavelets to separate deterministic features from stochastic ones, i.e., denoise data, and also its ability to approximately decorrelate autocorrelated data [16], [35]. A schematic illustration of the MSPCA algorithm is provided in Figure 2.

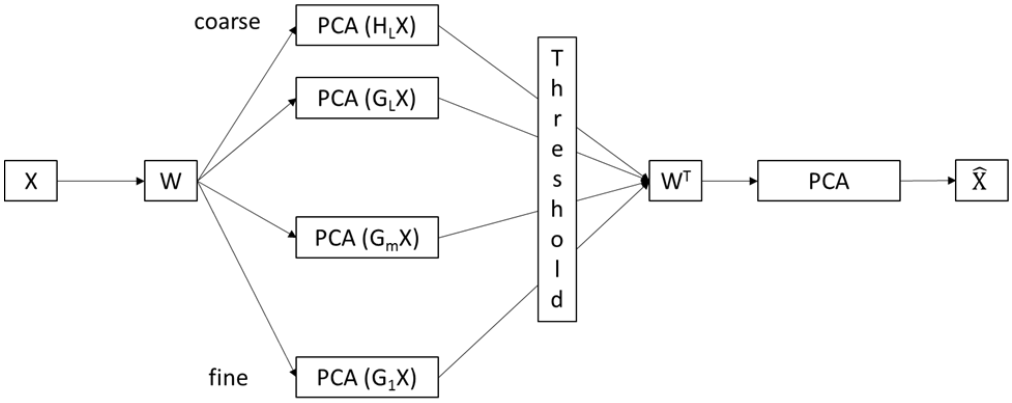

Figure 2. Multiscale PCA model.

The data matrix is first decomposed into multiple scales, after which PCA is carried out on all detail signals, and the final scaled signal. A training data matrix (of observations collected under normal operating conditions), is utilized in order to determine the thresholds at each scale, and these thresholds are applied on the wavelet coefficients obtained through decomposition of the testing data matrix. PCA is once again carried out after thresholding, in order to produce a final fault detection chart that utilizes the information at all scales. Application of the PCA model at different scales is advantageous as the wavelet coefficients (detail) at every scale satisfy the fundamental assumptions under which PCA performs best, i.e., low levels of noise, independence (uncorrelated), and normality [35], [40].

Most of the models used in this section model available training data, after which fault detection charts can then be applied in order to determine if subsequent testing data contain faults. Statistical quality control has seen the integration of hypothesis testing methods with effective process models in order to further enhance fault detection

performance. The following section provides an introduction to statistical hypothesis testing methods and how they have been utilized in order to carry out both fault detection and classification.

1.2. Statistical hypothesis testing methods

Hypothesis testing methods are recently being used more frequently as they bring in solid theoretical contributions to the area of statistical process monitoring [37]. Hypothesis testing is defined as the use of statistics to determine if a particular hypothesis is true or false [44]. For process monitoring or fault detection purposes, this would mean determining if a given observation falls under normal operating conditions, or is faulty.

Hypothesis testing is carried out by first establishing the value of a process parameter, e.g., mean or variance, for a particular set of observations collected under normal operating conditions, i.e., the null hypothesis. Statistical limits are obtained from the training data, which are then applied on process data obtained under test conditions to determine if the parameters are statistically different to normal operating conditions, i.e., alternate hypothesis.

The generalized likelihood ratio (GLR) technique is a hypothesis testing technique that has been utilized by different authors, and different versions and implementations will now be presented.

1.2.1. Generalized Likelihood Ratio (GLR) – Chi-square implementation (to monitor changes in mean)

The GLR technique seeks to maximize the detection probability for a given false alarm rate, and has been utilized for model-based fault detection purposes [29], [36]. An early version of the GLR chart used for model-based detection purposes can be found in literature, and focuses on detecting shifts in the mean [29].

Given an observation vector $y \in \mathbb{R}^n$ formed by one two possible Gaussian distributions:

$$\begin{aligned} H_0 &= \left\{ y \sim N\left(0, \sigma^2 I_n\right) \right\}, (\text{null hypothesis}), \\ H_1 &= \left\{ y \sim N\left(\theta, \sigma^2 I_n\right) \right\}, (\text{alternate hypothesis}) \end{aligned}, \tag{20}$$

where, θ and σ^2 are the mean and variations, i.e., parameters of the different distributions. Since the training data is standardized to zero-mean, unit variance, the mean of the null hypothesis is zero. The mean of the alternate hypothesis, θ, is unknown, and therefore has to predicted using its maximum likelihood estimate (MLE). The GLR decision function is defined as follows [36]:

$$\begin{aligned} T(y) &= 2\log \frac{\sup_{\theta \in \mathbb{R}} f_\theta(y)}{f_{\theta=0}(y)} = 2\log \left\{ \sup_{\theta} \exp \left\{ -\frac{\|y-\theta\|_2^2}{2\sigma^2} \right\} / \left\{ -\frac{\|y\|_2^2}{2\sigma^2} \right\} \right\} \\ &= \frac{1}{\sigma^2} \left\{ \min_{\theta} \left\| y - \hat{\theta} \right\|_2^2 + \|y\|_2^2 \right\} = \frac{1}{\sigma^2} \left\{ \left\| y - \hat{\theta} \right\|_2^2 + \|y\|_2^2 \right\} = \frac{1}{\sigma^2} \left\{ \|y\|_2^2 \right\} \end{aligned}, \tag{21}$$

where, $\hat{\theta} = \arg\min_{\theta} \|y-\theta\|_2^2 = y$ is the MLE of θ, the probability density function (PDF), of Y is $f_\theta(y) = \dfrac{1}{(2\pi)^{\frac{N}{2}} \sigma^N \exp\left\{ \|y-\theta\|_2^2 \right\}}$, and the Euclidian norm is $\| \cdot \|_2$.

Maximizing the likelihood function in the derivations shown above is equivalent to maximizing the natural logarithm, where the logarithmic function is monotonic [36]. As the noise is assumed to follow Gaussian distribution, the GLR statistic will follow a non-central chi-square distribution [36]:

$$T(y) = \frac{1}{\sigma^2}\left\{\|y\|_2^2\right\} \sim \chi_n^2, \tag{22}$$

with n representing the degrees of freedom (dof). This version of the GLR statistic computed the norm utilizing only the current observation so that it could be applied online, and therefore the GLR statistic follows a chi-square distribution with dof=1, χ_1^2.

Although, the GLR technique has shown improved performance, only the current observation is used in order to compute the GLR statistic. Many techniques have improved performance when process memory has been incorporated. This motivated the extension of the GLR to one that utilizes a moving-window scheme, and this will be described next.

1.2.1.1. Moving-Window GLR (MW-GLR)

The moving window GLR statistic is computed as follows [36]:

$$MW-GLR = 2\log\frac{f_\theta(Y)}{f_{\theta=0}(Y)}, \tag{23}$$

where, $Y = \left[\, y\left(i-\left(w-1\right)\right) \;\cdots\; \cdots\; y\left(i-1\right) y\left(i\right)\right]$, and *w* and *i* are the length of the moving window and the observation number, respectively. As with the GLR chart, the threshold for the MW-GLR chart needs to be computed, and this can also be done utilizing the distribution of the statistic.

The moment generating function is another means by which a particular distribution can be described. The moment generating function for a chi-square distribution with dof=1, can be represented as follows [36]:

$$M_{y_i}(t) = (1-2t)^{-\frac{r}{2}}, \tag{24}$$

where, r represents the dof of a chi-square distribution being described. The moment generating function for the MW-GLR statistic can now be derived as follows [36]:

$$\begin{aligned} M_{Y_i}(t) &= \prod_{i=1}^{w} M_{y_i}(t) \\ &= (1-2t)^{-\frac{r_1}{2}} \cdot (1-2t)^{-\frac{r_2}{2}} \cdot \ldots\ldots \cdot (1-2t)^{-\frac{r_w}{2}}. \\ &= (1-2t)^{-\frac{w}{2}} \end{aligned} \tag{25}$$

The derived expression demonstrates that the MW-GLR technique follows a chi-square distribution with dof equal to that of the length of the window being utilized, w [36].

Although, the above implementation of GLR has shown improved performance, it does not make complete use of the idea of parameter estimation utilizing maximum likelihood estimates, and it is also only designed to detect shifts in the mean. Reynolds developed a different algorithm for the implementation of the GLR technique, and has designed different versions depending on the type of the fault to be detected, i.e., a shift in the mean, a shift in the variance, or a one that is capable of simultaneously monitoring shifts in the mean and/or variance [13], [45], [46]. This implementation of the GLR technique will be described next.

1.2.2. Generalized Likelihood Ratio (GLR): General algorithm (applicable to different fault types)

This implementation of the GLR for different fault scenarios follows the following general procedure:

1. The null and alternate hypotheses are both defined for the given fault scenario, and the respective likelihood functions are subsequently derived.
2. For unknown parameters in the alternate hypothesis, the maximum likelihood estimates (MLEs) are computed, i.e., the mean or variance parameters.
3. According to statistical theory, the best possible detection rate for a given false alarm rate, is given by the log-likelihood ratio of the alternate hypothesis to the null hypothesis, and its maximum value and corresponding parameter values are obtained.

The null hypothesis for all cases, i.e., assuming no shift in the mean and variance is defined as follows [13]:

$$L\left(\infty, \mu_0 \mid x_1, x_2, ..., x_k\right) = \left(2\pi\right)^{-k/2} \left(\sigma_0^2\right)^{-k/2} \exp\left(-\frac{1}{2\sigma_0^2} \sum_{i=1}^{k} \left(x_i - \mu_0\right)^2 \right), \tag{26}$$

where, μ and σ^2 represent the mean and variance of the data, respectively.

1.2.2.1. GLR designed to detect a shift in the mean

The likelihood function of the alternate hypothesis for a shift in the mean from μ_0 to μ_1, at time τ is defined as follows [13]:

$$L\left(\tau,\mu_1,\sigma_0^2 \mid x_1,x_2,\ldots,x_k\right)=\left(2\pi\right)^{-k/2}\left(\sigma_0^2\right)^{-k/2} \exp\left(-\frac{1}{2\sigma_0^2}\left(\sum_{i=1}^{\tau}\left(x_i-\mu_0\right)^2+\sum_{i=\tau+1}^{k}\left(x_i-\mu_1\right)^2\right)\right). \quad (27)$$

As the magnitude of the mean value for a testing data set is unknown, its MLE has to be computed using the following equation [13]:

$$\hat{\mu}_{1,\tau,k}=\frac{1}{\left(k-\tau\right)}\sum_{i=\tau+1}^{k}x_i\,. \quad (28)$$

Substituting the MLE for the mean into the likelihood function for the alternate hypothesis, and taking the log-likelihood ratio of the alternate to the null hypothesis the following GLR statistic is derived [13]:

$$R_k=\max_{0\le\tau<k}\left(\frac{\left(k-\tau\right)}{2\sigma_0^2}\left(\hat{\mu}_{1,\tau,k}-\mu_0\right)^2\right). \quad (29)$$

Reynolds states that the all previous samples do not need to be used in order to maximize the detection rate, and a smaller window size may be used in order to decrease the computational demand of the GLR technique [13], [37].

1.2.2.2. GLR designed to detect a shift in the variance

The likelihood function of the alternate hypothesis for a shift in the mean from σ_0^2 to σ_1^2, at time τ is defined as follows [45]:

$$L\left(\tau,\mu_0,\sigma_1^2 \mid x_1,x_2,\ldots,x_k\right)=\left(2\pi\right)^{-k/2}\left(\sigma_1^2\right)^{-k/2}\exp\left(-\frac{1}{2\sigma_1^2}\sum_{i=\tau+1}^{k}\left(x_i-\mu_0\right)^2\right). \quad (30)$$

From a standpoint of quality control, an increase in the variance is of concern, as a larger variance would imply that the product quality is decreasing. As the magnitude of the variance value for a testing data set is unknown, its MLE has to be computed using the following equation [45]:

$$\hat{\sigma}_{1,\tau,k}^2=\max\left(\sigma_0^2,\frac{1}{\left(k-\tau\right)}\sum_{i=\tau+1}^{k}\left(x_i-\mu_0\right)^2\right). \quad (31)$$

Substituting the MLE for the variance into the likelihood function for the alternate hypothesis, and taking the log-likelihood ratio of the alternate to the null hypothesis the following GLR statistic is derived [45]:

$$R_k=\max_{0\le\tau<k}\left(\frac{\left(k-\tau\right)}{2}\left(\frac{\hat{\sigma}_{1,\tau,k}^2}{\sigma_0^2}-1-\ln\left(\frac{\hat{\sigma}_{1,\tau,k}^2}{\sigma_0^2}\right)\right)\right). \quad (32)$$

The GLR techniques described thus far have been developed and implemented in order to monitor a single parameter, i.e., the mean or the variance. However, for certain applications simultaneous monitoring of the mean and variance may be important. Reynolds developed such a method, which will be described next [46].

1.2.2.3. GLR designed to detect a shift in the mean and/or variance

The likelihood function of the alternate hypothesis that is designed to detect a either a shift in the mean from μ_0 to μ_1, and/or a shift in the variance from σ_0^2 to σ_1^2, at time τ is defined as follows [46]:

$$L\left(\tau,\mu_1,\sigma_1^2 \mid x_1,x_2,\ldots,x_k\right)=\left(2\pi\right)^{-k/2}\left(\sigma_0^2\right)^{-\tau/2}\left(\sigma_1^2\right)^{-(k-\tau)/2} \exp\left(-\frac{1}{2\sigma_0^2}\left(\sum_{i=1}^{\tau}\left(x_i-\mu_0\right)^2\right)-\frac{1}{2\sigma_1^2}\left(\sum_{i=\tau+1}^{k}\left(x_i-\mu_1\right)^2\right)\right). \quad (33)$$

The variance also needs to include the MLE for the mean as follows [46]:

$$S_{\tau,k}^2=\frac{1}{\left(k-\tau\right)}\sum_{i=\tau+1}^{k}\left(x_i-\hat{\mu}_{1,\tau,k}\right)^2. \quad (34)$$

As only an increase in the variance is of a concern, the MLE for the variance can be updated as follows [46]:

$$\hat{\sigma}_{1,\tau,k}^1=\max\left\{\sigma_0^2,S_{\tau,k}^2\right\}. \quad (35)$$

Substituting the MLEs for the mean and the variance into the likelihood function for the alternate hypothesis, and taking the log-likelihood ratio of the alternate to the null hypothesis the following GLR statistic is derived [46]:

$$R_k=\max_{0\le\tau<k}\left(\frac{\left(k-\tau\right)}{2}\left(\frac{S_{0,\tau,k}^2}{\sigma_0^2}-\frac{S_{\tau,k}^2}{\hat{\sigma}_{1,\tau,k}^2}-\ln\left(\frac{\hat{\sigma}_{1,\tau,k}^2}{\sigma_0^2}\right)\right)\right). \quad (36)$$

The techniques described thus far do not require pre-defined models obtained from fundamental principles, and rely solely on data collected under normal operating conditions, in order to establish a baseline of expected behavior. However, many chemical processes already have pre-defined models that they can utilized in order to formulate quantitative models, and state estimators such as the various Kalman filters can be utilized in order to continuously predict the value of given process variables and/or parameter online. These can also be utilized in order to predict if a process is deviating away from normal operating conditions. Most chemical processes are kept in check through the use

of various controllers, and even though a process may be experiencing drifts away from normal operating conditions, the controller can take measures in order to ensure that the desired set point is being met. Unfortunately, this could be at the expense of other factors, like increased utility cost in the case of a heat exchanger. Therefore, a method of determining if a process is deviating away from optimal operating conditions, while under control is required, i.e., deterioration in the process model itself. The following section introduces the different state and parameter estimations methods, which can be utilized in order to carry out the estimation of different process variables and parameters. A more detailed description of how these tools will be used be provided in Section 3.

1.3. State estimation methods

Several state estimation methods have been developed over time, from the Kalman filter which is applicable primarily to linear processes, to the Extended Kalman Filter (EKF) and Unscented Kalman Filter (UKF), which can be used to solve state estimation problems for nonlinear models [5], [47], [48]. Recently, the Particle Filter (PF) has also shown promise when applied to highly complex biological models, induction machine applications, and leak detection in pipelines [48]–[50]. For the purpose of this thesis, the EKF and UKF have shown sufficiently adequate performance and will be utilized in this work.

A given nonlinear state space model can be described as follows [48]:

$$\begin{aligned} \dot{x} &= g\left(x,u,\theta,w\right) \\ y &= l\left(x,u,\theta,\mathrm{v}\right) \end{aligned}, \tag{37}$$

where, $x \in \mathbb{R}^n$ is the state variable vector, $u \in \mathbb{R}^p$ is the input variable vector, $\theta \in \mathbb{R}^q$ is the unknown parameter vector, $y \in \mathbb{R}^m$ is the measurement variable vector, and g and l are nonlinear differentiable functions, $w \in \mathbb{R}^n$, and $v \in \mathbb{R}^m$, are the process and measurement noise, respectively. The process and measurement noise quantify the level of randomness in the process, and the variation in the collected measurements, respectively.

The discrete model can be obtained by discretizing the state space model [48]:

$$\begin{aligned} x_k &= f\left(x_{k-1}, u_{k-1}, \theta_{k-1}, w_{k-1}\right) \\ y_k &= h\left(x_k, u_k, \theta_k, v_k\right) \end{aligned}, \tag{38}$$

where, the state variables are described at time (*k*), using their values from the previous time step (*k-1*). The process and measurement noise have the following properties:

$$E\left[w_k\right] = 0,\ E\left[w_k w_k^T\right] = Q_k,\ \ E\left[v_k\right] = 0,\ \text{and}\ E\left[v_k v_k^T\right] = R_k. \tag{39}$$

As the parameter , θ_k, needs to be estimated along with the state vector, x_k, the parameter vector can be assumed to be defined by the following model [48]:

$$\theta_k = \theta_{k-1} + \gamma_{k-1}, \tag{40}$$

where, γ_{k-1} is white noise. In order to simultaneously estimate both the state and parameter vectors, a new state vector needs to be defined, where the parameter vector is augmented with the state vector [48]:

$$z_k = \begin{bmatrix} x_k \\ \theta_k \end{bmatrix} = \begin{bmatrix} f\left(x_{k-1}, u_{k-1}, \theta_{k-1}, w_{k-1}\right) \\ \theta_{k-1} + \gamma_{k-1} \end{bmatrix}. \tag{41}$$

Now defining the augmented noise vector [48]:

$$\varepsilon_{k-1} = \begin{bmatrix} w_{k-1} \\ \gamma_{k-1} \end{bmatrix}. \tag{42}$$

The nonlinear state space model can be rewritten as [48]:

$$\begin{aligned} z_k &= \Im\left(z_{k-1}, u_{k-1}, \varepsilon_{k-1}\right) \\ y_k &= \Re\left(z_k, u_k, v_k\right) \end{aligned}. \tag{43}$$

The objective of state estimation is to find an estimate for $\hat{z}_k$, for the state vector z_k such that the weighted covariance matrix of the estimation error is minimized, i.e., $E\left[\left(z_k - \hat{z}_k\right) M \left(z_k - \hat{z}_k\right)^T\right]$, where *M* is a symmetric nonnegative weight defining matrix. *M* is an identity matrix if all states are equally important, and this reduces the covariance matrix to $P = E\left[\left(z_k - \hat{z}_k\right)\left(z_k - \hat{z}_k\right)^T\right]$. The required minimization is accomplished by minimizing the following objective function [51]:

$$J = \frac{1}{2} Tr\left(E\left[\left(z_k - \hat{z}_k\right)\left(z_k - \hat{z}_k\right)^T\right]\right). \tag{44}$$

Minimizing the objective function the Extended Kalman Filter (EKF), and Unscented Kalman Filter (UKF), estimate the state vector z_k using a two-step algorithm, that involves a prediction step and estimation or update step.

1.3.1. Extended Kalman Filter (EKF)

For the EKF algorithm the two steps are as follows.

1.3.1.1. Prediction step for EKF

It is a prediction of the augment state vector and measurement vector using their values from the previous time step using a nonlinear model [52]:

$$\begin{aligned} \hat{z}_{k|k-1} &= \Im\left(z_{k-1|k-1}, u_{k-1}\right) \\ \hat{y}_k &= \Re\left(z_{k|k}, u_k\right) \end{aligned} . \tag{45}$$

1.3.1.2. Estimation step for EKF

An update to the augmented state vector is then made after obtaining values of the measurement vector, y_k, as follows [52]:

$$\begin{aligned} P_{k|k-1} &= A_{k-1} P_{k-1|k-1} A_{k-1}^T + G_{k-1} Q G_{k-1}^T \\ K_k &= P_{k|k-1} C_k^T \left(C_k P_{k|k-1} C_k^T + H_k R H_k^T\right)^{-1} \\ P_{k|k} &= \left(I - K_k C_k\right) P_{k|k-1} \\ \hat{z}_{k|k} &= \hat{z}_{k|k-1} + K_k \left(y_k - \hat{y}_k\right) \end{aligned} , \tag{46}$$

where, $A_{k-1} \approx \left.\frac{\partial \Im}{\partial z}\right|_{\hat{z}_{k-1}}$, $C_{k-1} \approx \left.\frac{\partial \Re}{\partial z}\right|_{\hat{z}_{k|k-1}}$, $G_{k-1} \approx \left.\frac{\partial \Im}{\partial \varepsilon}\right|_{\varepsilon_{k-1}}$, $H_{k-1} \approx \left.\frac{\partial \Re}{\partial v}\right|_{v_k}$ are the matrices of the linearized model at every time step.

One disadvantage of the EKF is that it functions my approximating the mean and covariance of the nonlinear state vector by linearizing the nonlinear model, and therefore

may not be able to provide an accurate approximation. The unscented Kalman filter was developed in order to overcome to limitation.

1.3.2. Unscented Kalman Filter (UKF)

The unscented Kalman filter (UKF) functions by relying on an unscented transformation, which is a method that was developed in order to calculate the statistics of a random variable that undergoes a nonlinear mapping [53]. This is accomplished by first defining sigma vectors of the state, and then propagating them through the nonlinear model [54]. The mean and covariance matrix can now be approximated as the weighted sample mean and covariance of the transformed sigma vectors. Improving the estimation of the mean and covariance of the state vector subsequently enhances the estimation accuracy of the UKF algorithm. The UKF algorithm is implemented as follows.

Let $z \in R^n$ be a random variable with mean $\bar{z}$ and covariance P. If $y = f(z)$ the mean and covariance can now be computed through the following steps [54]:

1. Define $(2n+1)$ sigma points, Z_i:

$$\begin{aligned} z_0 &= \bar{z} \\ z_i &= \bar{z} + \left(\sqrt{(n+\lambda)P}\right)_i \qquad i = 1,...,n \\ z_i &= \bar{z} - \left(\sqrt{(n+\lambda)P}\right)_i \qquad i = 1,...,2n \end{aligned} \quad , \tag{47}$$

   where, λ is the scaling parameter.

2. Propagate all the sigma points through the nonlinear function, i.e., $Y_i = f(Z_i)$

3. Estimate the mean and covariance matrix as:

$$\bar{y} = \sum W_i Y_i, \quad P_y = \sum W_i \left(Y_i - \bar{y}\right)\left(Y_i - \bar{y}\right)^T . \tag{48}$$

Like the EKF algorithm, the UKF algorithm is also carried out through a prediction step and an update step.

1.3.2.1. Prediction step for UKF

As with the EKF algorithm, it is a prediction of the augment state vector and measurement vector using their values from the previous time step using a nonlinear model using the transformed sigma vector [54]:

$$\begin{aligned} & z_{k|k-1} = \Im\left(z_{k-1}, u_{k-1}\right) \\ & \text{Define} \quad z_{k|k-1,i} \qquad i = 0,...,2n \ \left(\text{sigma points}\right) \\ & \qquad Y_{k|k-1} = \Re\left(z_{k|k-1,i}, u_{k-1}, v_{k-1}\right) \\ & \qquad \hat{y}_k = \sum_i W_i Y_{k|k-1,i} \end{aligned} . \tag{49}$$

1.3.2.2. Update step for UKF

Once again an update to the augmented state vector is made after obtaining values of the measurement vector [54]:

$$\begin{aligned} & P_{k,y} = \sum_i W_i \left[Y_{k|k-1,i} - \hat{y}_k\right]\left[Y_{k|k-1,i} - \hat{y}_k\right]^T \\ & P_{k,z,y} = \sum_i W_i \left[Z_{k|k-1,i} - z_{k|k-1}\right]\left[Y_{k|k-1,i} - \hat{y}_k\right]^T \\ & z_{k|k} = z_{k|k-1} + K_k\left(y_k - \hat{y}_k\right) \\ & K_k = P_{k,z,y} P_{k,y}^{-1} \end{aligned} . \tag{50}$$

This subsection has demonstrated how state and parameter estimation methods can be implemented once a nonlinear model is available, and measurements have been collected from a given process. An example of how these techniques can be utilized in order predict process drifts and determine equipment wellness will be provided in Section 3.

1.4. Research objectives

The main objectives of this work are threefold:

- Development of improved fault detection and classification algorithms by successfully integrating different process monitoring models and techniques, and presentation of their applications.
- Development of a straightforward algorithm that can be utilized in order to track process degradation (despite being under control) in multiple operating regimes through the utilization of different state and parameter techniques. The novelty, ease of implementation, and practical applicability of the developed algorithm will be demonstrated through both simulated synthetic data, and real data from a heat exchanger.
- Literature review of existing leak detection and localization techniques, with a focus on subsea and arctic conditions, to guide the design and development of an experimental laboratory set up that can be utilized in order to study fluid behavior in pipeline, particularly in the event of leaks.

2. STATISTICAL PROCESS MONITORING ALGORITHMS FOR FAULT DETECTION AND CLASSIFICATION *

The previous section presented many conventional fault detection algorithms described in literature, that are often used in practice. Since an objective of this work is to develop improved fault detection and classification algorithms by successfully integrating different process monitoring models and techniques, this section will present algorithms that were developed as part of this objective and explain their novelty. [1]

2.1. Multiscale PCA-based Generalized Likelihood Ratio (GLR) algorithms

Two MSPCA-based GLR algorithms were developed through the course of this work. The first, an MSPCA-based moving-window (MW) GLR fault detection algorithm sought to combine the advantages of the MSPCA model, with the detection capabilities of the GLR technique. The second, an improved MSPCA-based GLR fault detection algorithm sought to address deficiencies in the original model that was developed.

[1] Part of this chapter is reprinted with permission from "Process monitoring using PCA-based GLR methods: A comparative study" by M. Ziyan Sheriff, M Nazmul Karim, Hazem N Nounou, Mohamed N Nounou, 2018. Journal of Computational Science, 27, 227-246, Copyright 2018 by Elsevier.

2.1.1. Multiscale PCA-based Moving-Window (MW) Generalized Likelihood Ratio (GLR) algorithm

The MSPCA-based MW-GLR fault detection algorithm that was developed sought to extract the advantages of the MSPCA model, and its ability to handle data that deviate from fundamental assumptions of conventional process models, and also integrate the superior fault detection capabilities of the GLR chart. As the initial work of the GLR chart used for process monitoring purposes focused only on shifts in the process mean, only this type of fault was examined in this work. In addition to integrating the MSPCA model with the GLR fault detection technique, the initial GLR technique that utilizes only a single observation in order to evaluate the GLR statistic at a given time instant, was extended to a moving window technique. The theoretical derivation of the resulting distribution of the MW-GLR statistic was also presented. The resulting detection statistic for the MW-GLR technique shows that it equals the norm of the residuals in a given window, and this is equivalent to applying a mean filter on the squares of the residuals.

A schematic illustration of the developed algorithm is presented in Figure 3. The MSPCA model is utilized in order to model data that may violate fundamental assumptions of conventional models, i.e., deviate away from normality, be autocorrelated, and contain high levels of noise. The MW-GLR chart is then applied on the residuals from the MSPCA model, in order to detect faults. The performance of the developed MSPCA-based MW-GLR technique was evaluated using a simulated synthetic example, and the Tennessee Eastman process [10], [36], [55]. In order to maintain conciseness of this work,

the results for the Tennessee Eastman process are not included, but are available in literature [36].

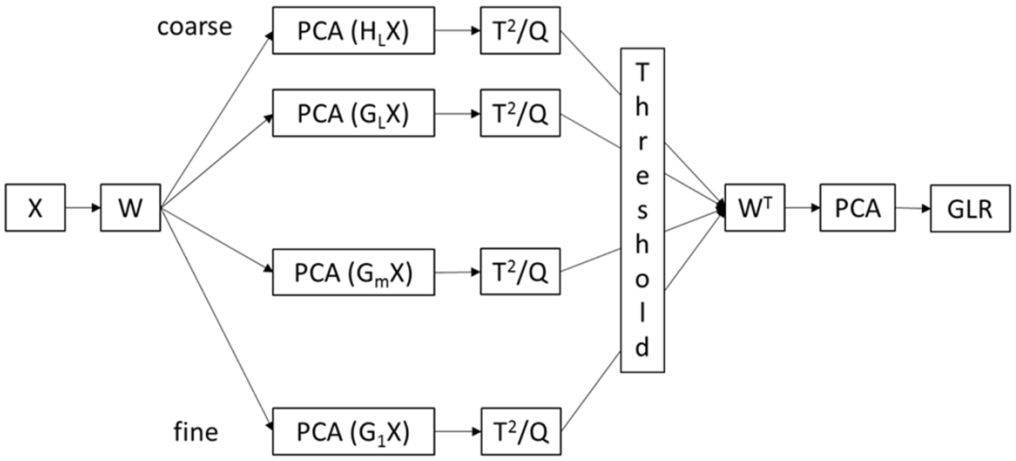

Figure 3. MSPCA-based MW-GLR algorithm.

The simulated example utilized the same model to generate data that was used in the original MPSCA paper [35]. The model is composed of four variables, where the first two variables are generated using independent normal distributions, and the third and fourth variables are summations and difference of the first two variables, respectively, as follows [35]:

$$\begin{aligned}\tilde{x}_1(t) &= N(0,1)\\ \tilde{x}_2(t) &= N(0,1)\\ \tilde{x}_3(t) &= \tilde{x}_1(t)+\tilde{x}_2(t)\\ \tilde{x}_4(t) &= \tilde{x}_1(t)-\tilde{x}_2(t)\end{aligned}. \tag{51}$$

The data matrix, $\tilde{\mathrm{X}}$, is then contaminated with white noise, uncorrelated Gaussian error of zero mean and unit variance as follows [35].

$$\mathrm{X}(t) = \tilde{\mathrm{X}}(t) + 0.2N(0,1). \tag{52}$$

For the simulated synthetic example, two different fault sizes were examined, added between observations 1001:1300 (highlighted in light blue in all figures). In order to keep the presentation of the results concise in this section, only one fault, i.e., a fault of magnitude 0.3, will be discussed. More details on the simulation results can be found in published work [36]. The results for the conventional and multiscale PCA charts, along with the MSPCA-based MW-GLR chart are provided. Published work also examines additional charts as well [36]. A fault magnitude of 0.3 is sufficiently small that the conventional PCA-based techniques T^2 and Q fail as seen in Figure 4 (a) and Figure 5 (a), respectively. Although, the MSPCA-based Q chart is able to perform better with a slightly lower missed detection rate, it is unable to detection a majority of the fault as seen in Figure 5 (b).

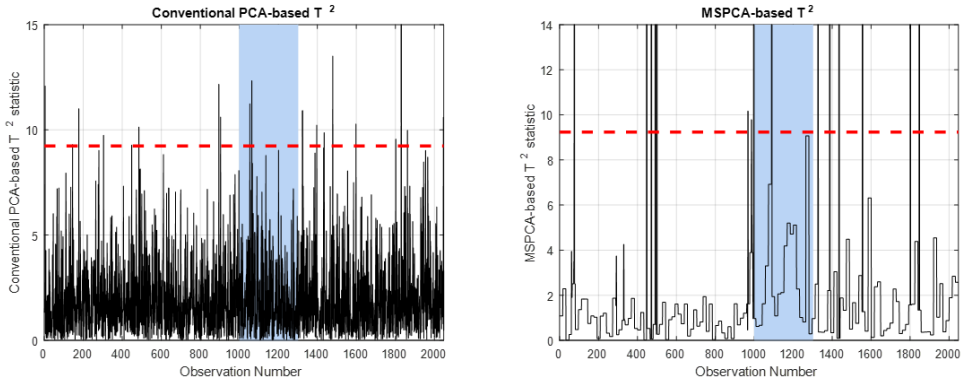

Figure 4. Monitoring a fault of magnitude 0.3 using PCA and MSPCA-based T^2 charts.

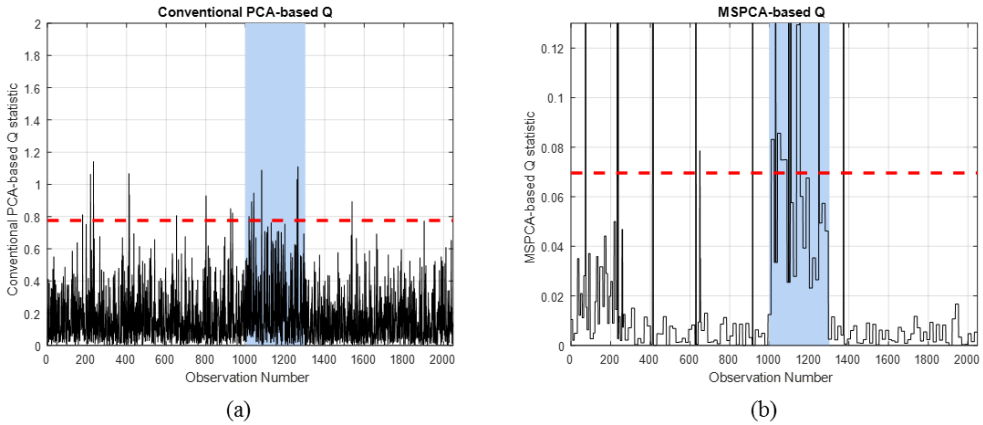

Figure 5. Monitoring a fault of magnitude 0.3 using PCA and MSPCA-based Q charts.

Examining the MSPCA-based MW-GLR chart for two different window lengths show that the technique is able to significantly lower the missed detection rate, especially for a longer window length of 50 as shown in Figure 6 (b).

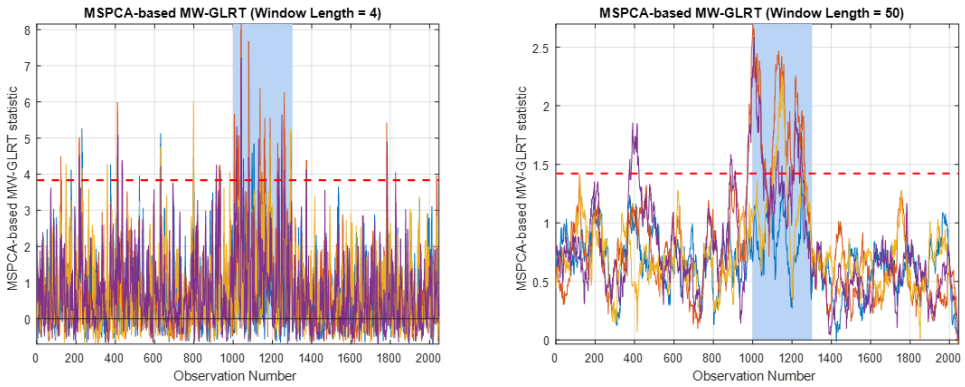

(a) (b)

Figure 6. Monitoring a fault magnitude of 0.3 using MSPCA-based MW-GLR charts.

The results for the given examples are presented in Table 1. The results show that the MSPCA-based MW-GLR chart is able to provide the lowest missed detection rate when compared to the other conventional fault detection techniques.

Table 1. Summary of fault detection results - Simulated synthetic example (monitoring a fault of magnitude 0.3).

	Missed Detection Rate (%)	**False Alarm Rate (%)**	**ARL_1**
Conventional PCA-based T^2	99.7477	0.1889	131.3441
MSPCA-based T^2	99.6412	0.3169	138.3850
Conventional PCA-based Q	97.3838	0.7939	37.3126
MSPCA-based Q	89.0601	1.4075	50.8664
MSPCA-based MW-GLR (window length = 4)	84.6234	3.9759	13.8600
MSPCA-based MW-GLR (window length = 50)	27.6300	5.4000	8.0200

2.1.2. Improved Multiscale PCA-based GLR fault detection algorithm

The MSPCA model utilized in developed algorithm and presented in published work thus far constructs the PCA model on every scale and applies Q statistic in order to monitor characteristics. This is the same procedure followed by Bakshi [35]. However, recent work has shown that the GLR chart is able to provide better results over the Q chart in the time domain, therefore applying the GLR chart instead of the Q chart on every scale should produce improved fault detection results [11], [37].

A schematic illustration of the developed algorithm is presented in Figure 7. The new algorithm that was developed, i.e., the Improved Multiscale PCA-based GLR algorithm is advantageous due to the following design features:

- The Improved MSPCA-based GLR technique does not require extensive trial-and-error in the selection of the window length for different applications and fault sizes, as the generalized implementation of the GLR technique used a fixed window size when compared to the chi-square implementation. This increases the range of applicability of the new algorithm.
- Better noise feature separation is obtained on every scale by applying GLR on residuals from the PCA model instead of T^2 and Q charts, thereby improving the detection on every scale.
- The generalized implementation of the GLR provides the opportunity for different fault types to be monitored, i.e., sustained shifts in the mean, sustained shifts in the variance, slow drifts etc. as demonstrated by the authors in [37].

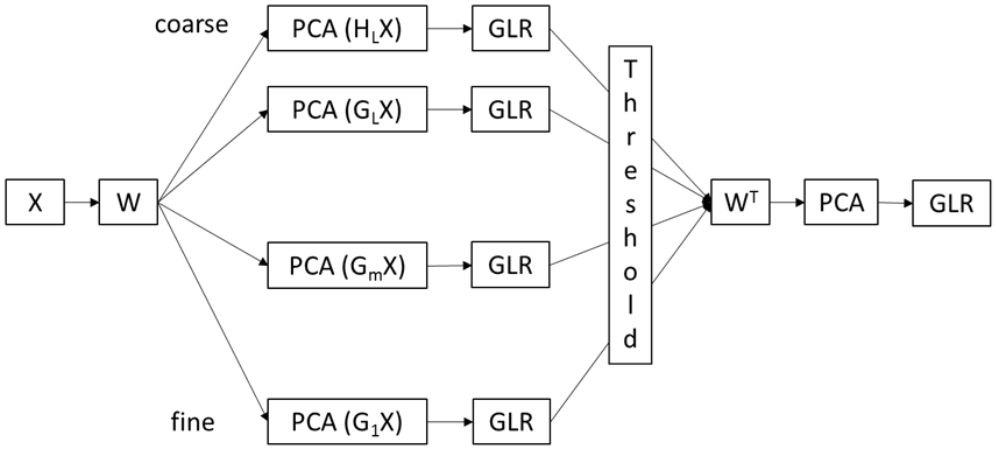

Figure 7. Improved MSPCA-based GLR algorithm.

The effectiveness of the developed algorithm was assessed by applying the Improved MSPCA-based GLR technique on the same simulated synthetic example utilized in Section 2.1.1. A summary of a Monte-Carlo simulation of 1000 realizations is presented in Table 2.

Table 2. Summary of fault detection results (revised) - Simulated synthetic example (monitoring a fault of magnitude 0.3).

	Missed Detections (%)	**False Alarms (%)**	**ARL_1**
MSPCA-based MW-GLR	27.63	5.40	8.02
Improved MSPCA-based GLR	10.63	5.21	5.01

From the results it can be observed that the Improved MSPCA-based GLR algorithm is able to provide a significantly lower missed detection rate, and lower ARL_1 value, when compared to the previously developed MSPCA-based GLR algorithm, thus motivating its application in practice.

2.2. Monitoring using PCA-based GLR algorithms – A comparative review

Although the chi-square implementation of the GLR chart show reasonable results, only shifts in the mean were considered as the type of fault present [36]. In reality process can experience a wide variety of fault types. Reynolds has developed versions of the GLR technique that are capable of monitoring shifts in just the variance, and simultaneous shifts in the mean and/or variance [13], [45], [46]. However, most of Reynolds work focused on

the out-of-control average run length (ARL_1) [13]. Depending on the application, it might be necessary to examine the performance of different GLR techniques keeping the missed detection rate, and false alarm rate in mind as well. Therefore, a comprehensive review of different fault scenarios, and the performance of the different GLR charts was required.

This was accomplished by developing different PCA-based GLR charts, that utilized PCA in order to model the data, after which the different GLR techniques were applied in order to examine their performance under different fault scenarios. The performance was first assessed utilizing data from a simulated synthetic model, and the following three fault scenarios were examined:

- A shift in the mean, with no shift in the variance.
- A shift in the variance, with no shift in the mean.
- A simultaneous shift in both the mean and variance.

From the results it was observed that the GLR charts designed for specific purposes, i.e., to just detect a shift in the mean, or to just detect a shift in the variance, were able to outperform the GLR designed to simultaneously monitor both shifts in the mean and variance. Their superior performance can be attributed to the fact that only a single parameter needed to be estimated when maximizing the GLR statistic [37].

The simulated model used to demonstrate these results is the same as what was used in the previous section [35], [37]. 2000 observations of training data are generated using the model, and another 2000 observations are generated as testing data. The different fault types described earlier are generated using the testing data, and the fault is added between observations 1001:2000. The faulty region is highlighted in light blue in all

figures. The GLR charts designed to monitor different types of faults were applied on residuals from a PCA model.

2.2.1. Scenario I – A shift in the mean, with no shift in the variance

For a scenario where only a shift in the mean was expected, a fault of size unity was utilized as the shift in the mean for demonstrative purposes. Examining the conventional PCA-based charts, we can see that the PCA-based T^2 (see Figure 8 (a)) is unable to detect most of this fault, while the PCA-based Q chart (see Figure 8 (b)) is able to do significantly better and detect most of the fault.

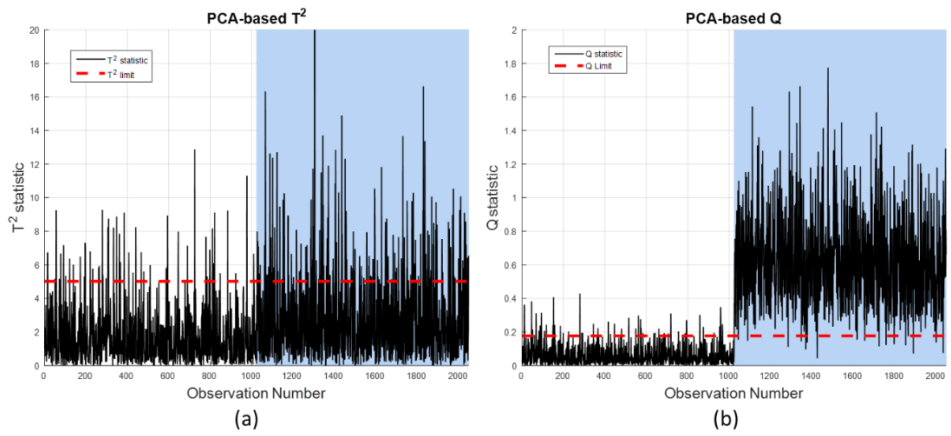

Figure 8. Scenario I - Conventional PCA-based charts (T^2 and Q) (Reprinted with permission from [37]).

From the PCA-based GLR designed specifically to detect a particular fault type we can see that the GLR designed to detect a shift in the mean is able to flag most of the

fault (see Figure 9 (a)), while the GLR chart designed to detect a shift in the variance is unable to detect this fault (see Figure 9 (b)).

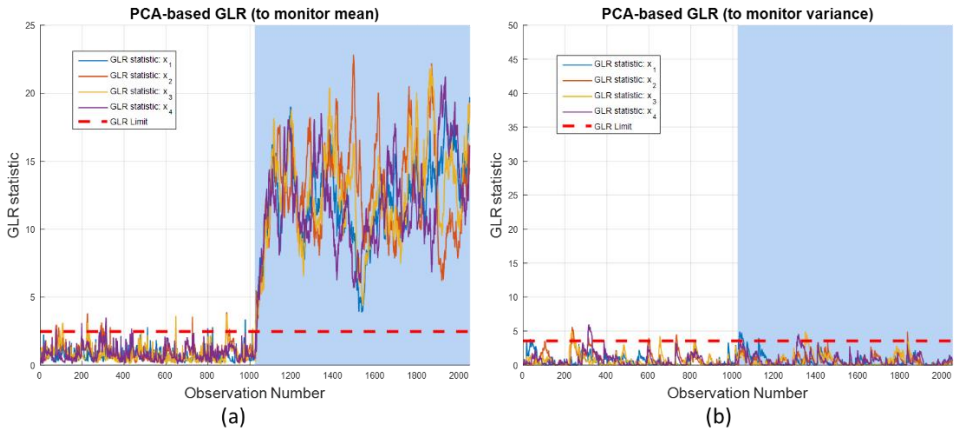

Figure 9. Scenario I - PCA-based GLR charts designed specifically to detect particular fault types (Reprinted with permission from [37]).

From the PCA-based GLR chart designed to simultaneously monitor a shift in the mean and/or variance, we can see that the cart is able to detect most of the fault (see Figure 10). However, upon further inspection many missed detections can be observed.

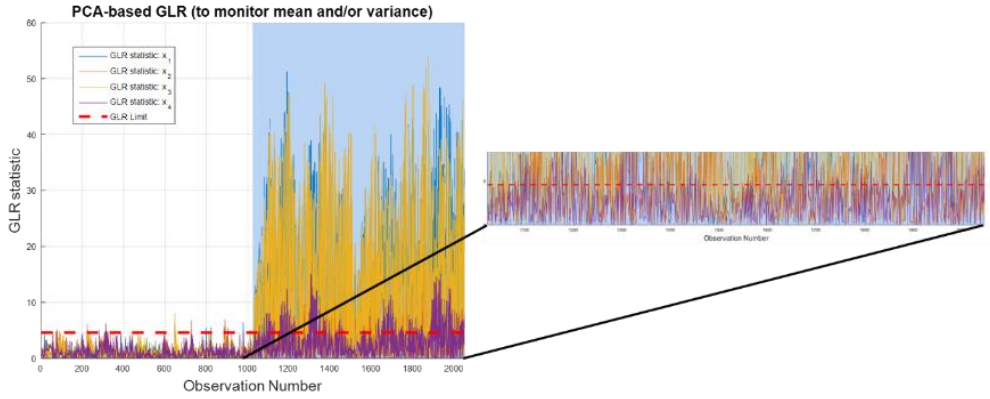

Figure 10. Scenario I - PCA-based GLR chart designed to simultaneously monitor a shift in the mean and/or variance (Reprinted with permission from [37]).

The fault detection results for Scenario I are summarized in Table 3, and they show that the in order for a process expected to only experience a shift in the mean, the PCA-based GLR chart designed specifically to detect a shift in the mean is able to outperform all other fault detection charts with the lowest missed detection rates.

Table 3. Summary of fault detection results - Scenario I (Reprinted with permission from [37]).

	Missed Detections (%)	**False Alarms (%)**	**ARL_1**
Conventional PCA-based T^2	80.05	5.02	5.01
Conventional PCA-based Q	1.49	5.06	4.52
Conventional PCA-based GLR (to monitor mean)	0.41	5.04	4.55
Conventional PCA-based GLR (to monitor variance)	94.16	5.06	94.82
Conventional PCA-based GLR (to monitor mean and/or variance)	29.10	5.07	4.64

2.2.2. Scenario II – A shift in the variance, with no shift in the mean

For a scenario where only a shift in the variance was expected, an increase in the standard deviation from 1 to 2 was utilized for demonstrative purposes. Examining the conventional PCA-based charts, we can see that both the PCA-based T^2 (see Figure 11 (a)) and Q (see Figure 11 (b)) charts are unable to efficiently detection most of the fault as there are many missed detections.

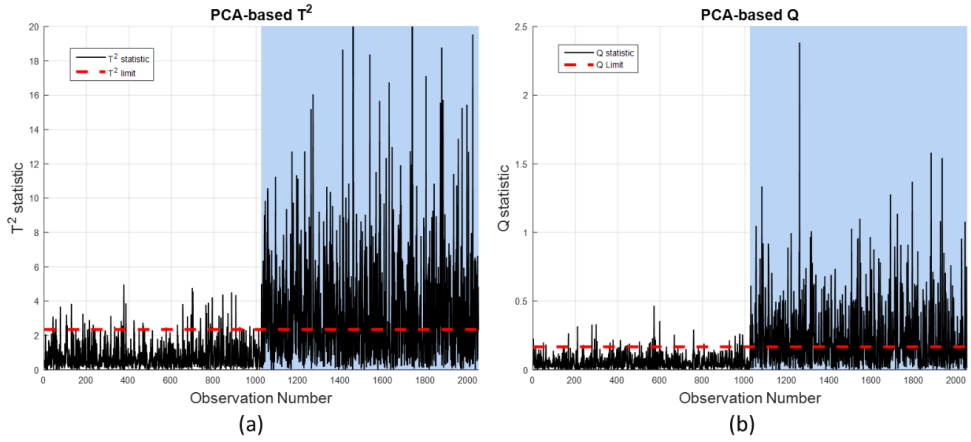

Figure 11. Scenario II - Conventional PCA-based charts (T^2 and Q) (Reprinted with permission from [37]).

From the PCA-based GLR designed specifically to detect a particular fault type we can see that the GLR designed to detect a shift in the variance is able to flag most of the fault (see Figure 12 (b)), while the GLR chart designed to detect a shift in the mean is unable to detect a majority of this fault (see Figure 12 (a)).

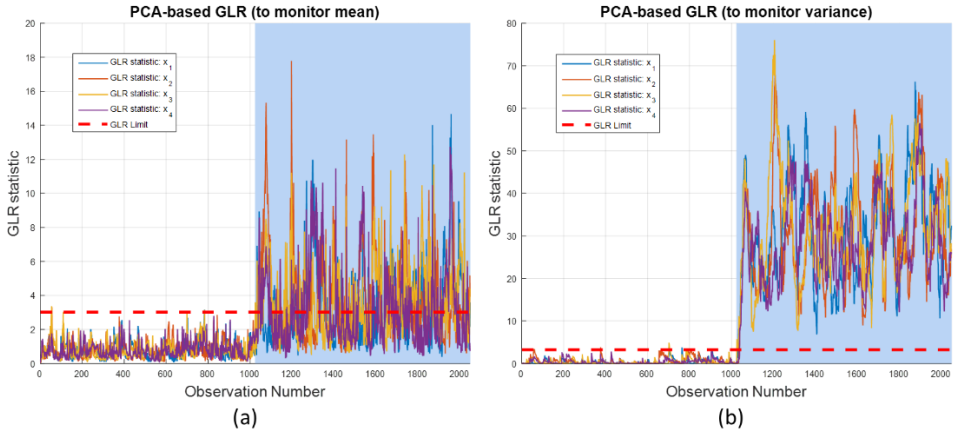

Figure 12. Scenario II - PCA-based GLR charts designed specifically to detect particular fault types (Reprinted with permission from [37]).

From the PCA-based GLR chart designed to simultaneously monitor a shift in the mean and/or variance, we can see that the cart is able to detect most of the fault (see Figure 13). However, once again upon further inspection we can observe that there are many missed detections.

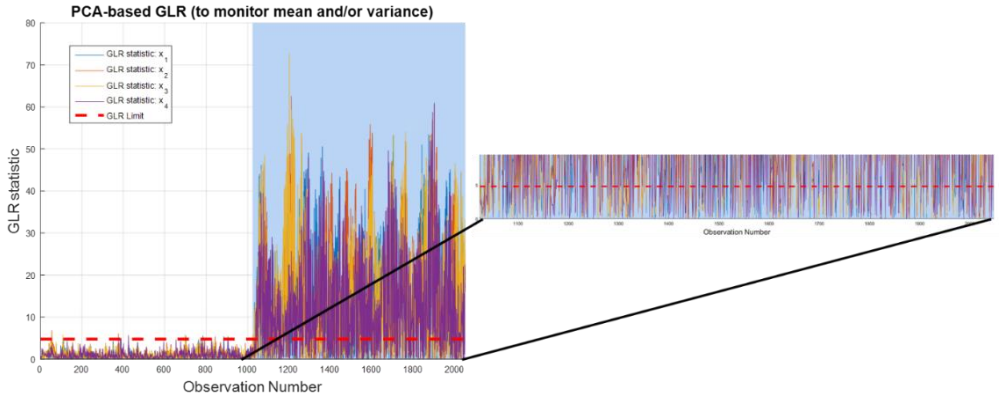

Figure 13. Scenario II - PCA-based GLR chart designed to simultaneously monitor a shift in the mean and/or variance (Reprinted with permission from [37]).

The fault detection results for Scenario II are summarized in Table 4, and they show that the in order for a process expected to only experience a shift in the variance, the PCA-based GLR chart designed specifically to detect a shift in the variance is able to outperform all other fault detection charts, with the lowest missed detection rate.

Table 4. Summary of fault detection results - Scenario II (Reprinted with permission from [37]).

	Missed Detections (%)	**False Alarms (%)**	**ARL_1**
Conventional PCA-based T^2	52.68	5.06	4.21
Conventional PCA-based Q	52.64	5.05	3.31
Conventional PCA-based GLR (to monitor mean)	14.79	5.04	3.34
Conventional PCA-based GLR (to monitor variance)	0.25	5.06	2.94
Conventional PCA-based GLR (to monitor mean and/or variance)	18.09	5.07	3.61

2.2.3. Scenario III – A simultaneous shift in the mean and variance

For a scenario where both a shift in the mean and variance were expected, a fault size of unity for shift in the mean, and an increase in the standard deviation from 1 to 2 was utilized for demonstrative purposes. Examining the conventional PCA-based charts, we can see that the PCA-based Q chart (see Figure 14 (b)) is able to perform better than the PCA-based T^2 chart (see Figure 14 (a)).

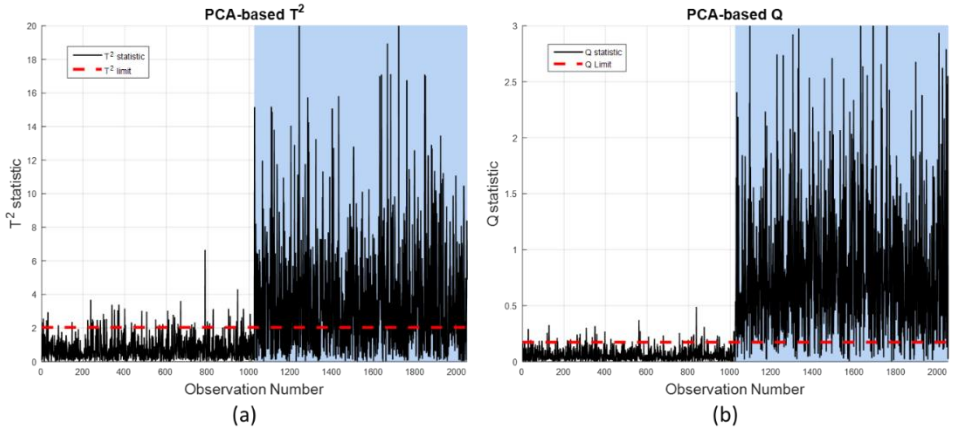

Figure 14. Scenario III - Conventional PCA-based charts (T^2 and Q) (Reprinted with permission from [37]).

For the PCA-based GLR chart designed specifically to monitor either a shift in the mean or a shift in the variance, it can be observed that both GLR charts are able to detect the shift (see Figure 15).

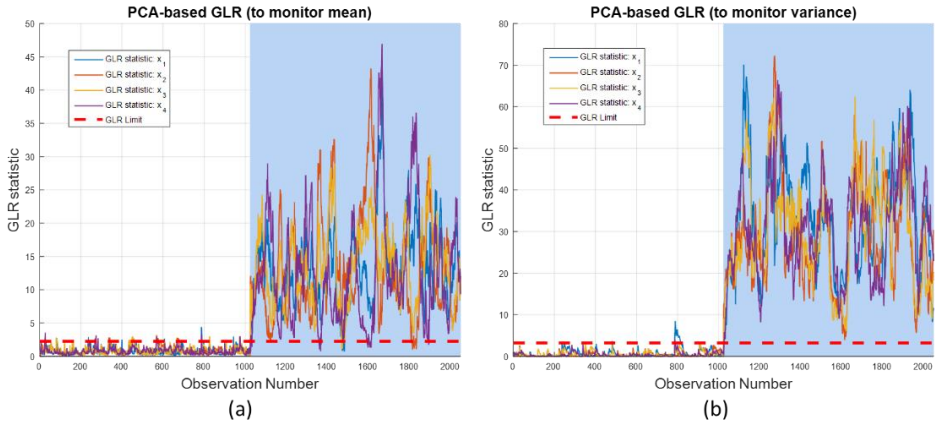

Figure 15. Scenario III - PCA-based GLR charts designed specifically to detect particular fault types (Reprinted with permission from [37]).

However, when observing the PCA-based GLR chart designed to specifically simultaneously monitor shifts in the mean and variance (see Figure 16), we observe the same trend as in Scenarios I and II, where missed detections are present.

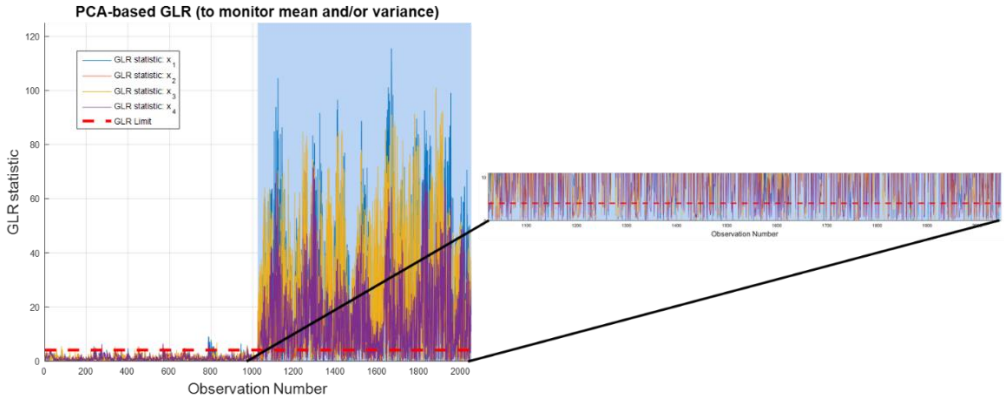

Figure 16. Scenario III - PCA-based GLR chart designed to simultaneously monitor a shift in the mean and/or variance (Reprinted with permission from [37]).

The fault detection results for Scenario III are summarized in Table 5, and they show that the in order for a process expected to experience both shifts in the mean and variance, the PCA-based GLR charts designed to specifically monitor one parameter, either the mean or variance, both need to be implemented in parallel, as they are both able to provide significantly lower missed detection rates than the PCA-based GLR chart designed to simultaneously monitor both parameters at the same time. This can be attributed to the fact that the simultaneously monitoring requires the computation of two maximum likelihood estimations, i.e., two parameters, meaning that the optimum solution might not be obtained.

Table 5. Summary of fault detection results - Scenario III (Reprinted with permission from [37]).

	Missed Detections (%)	**False Alarms (%)**	**ARL_1**
Conventional PCA-based T^2	45.53	5.03	2.84
Conventional PCA-based Q	8.98	5.05	2.19
Conventional PCA-based GLR (to monitor mean)	0.18	5.09	2.13
Conventional PCA-based GLR (to monitor variance)	0.18	5.03	2.13
Conventional PCA-based GLR (to monitor mean and/or variance)	13.85	5.01	2.13

2.2.4. Application to the Tennessee Eastman process

The performance of the PCA-based GLR chart was also evaluated utilizing the Tennessee Eastman process, and these results will be highlighted next. The Tennessee Eastman process is a benchmark process that has been utilized by many to evaluate the performance of different fault detection algorithms [10], [55]–[57]. The process consists of five process units: reactor, condenser, stripper, compressor, and separator, as shown in Figure 17.

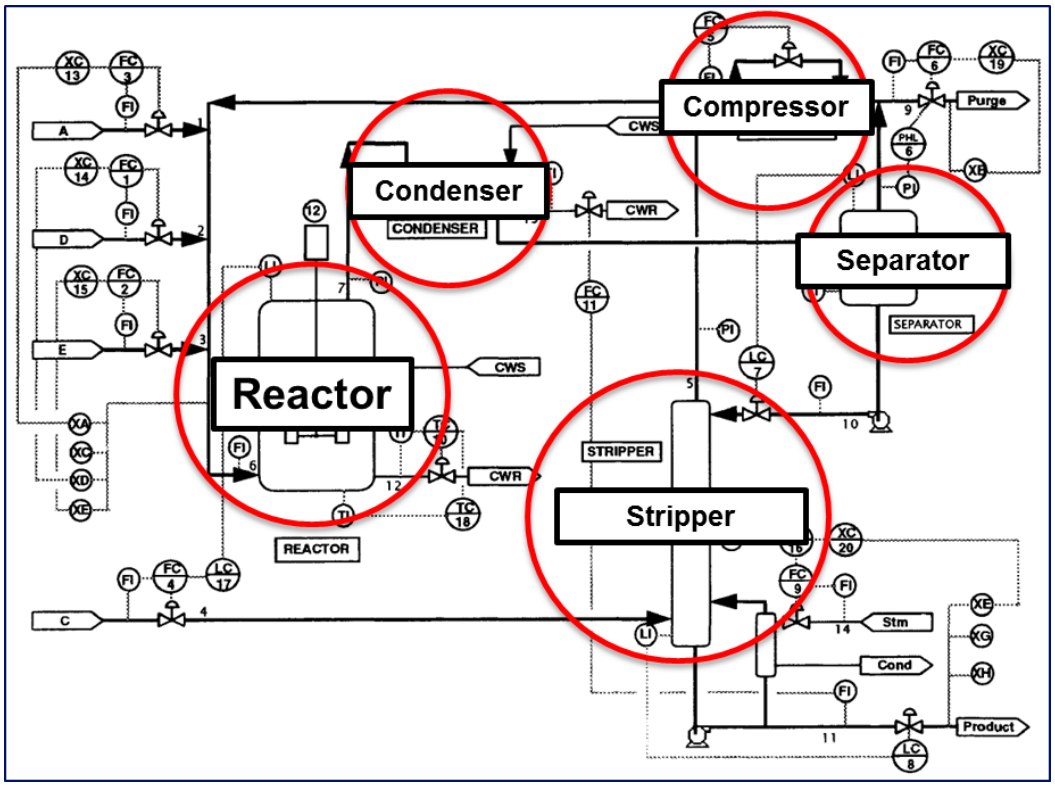

Figure 17. Tennessee Eastman process flow diagram (Reprinted with permission from [37]).

Process data from the Tennessee Eastman process model is available for training and testing purposes [58]. A large bank of faults has been utilized in order to examine the performance of various techniques [10], [58]. For this particular example, in order to demonstrate the practical applicability of the different PCA-based GLR charts, one of the faults will be examined, i.e., a step fault in the mean of the condenser cooling water inlet temperature (IDV 5). This fault was selected as conventional techniques are unable to detect most of this fault. As the previous example demonstrated that the PCA-based GLR charts designed specifically to monitor the different parameters, i.e., the mean, and the variance, need to be implemented in parallel, this will be followed for Tennessee Eastman process example.

The training data is composed of 800 samples collected under normal operating condition, representing 8 hours of operation. The fault starts after 8 hours of normal operation, and is sustained for the remainder of the testing data set, from observations 801 to 2000, i.e., hours 8-20. The faulty region is shaded in light blue in all figures.

From the conventional PCA-based charts (see Figure 18) we can see that both the T^2 and Q charts are unable to efficiently detect most of the fault. From the PCA-based GLR charts we can observe that the GLR chart designed specifically to detect a shift in the mean (see Figure 19 (a)) is able to detect most of the fault, while GLR chart designed to detect a shift in the variance (see Figure 19 (b)) is unable to efficiently detect most of the fault.

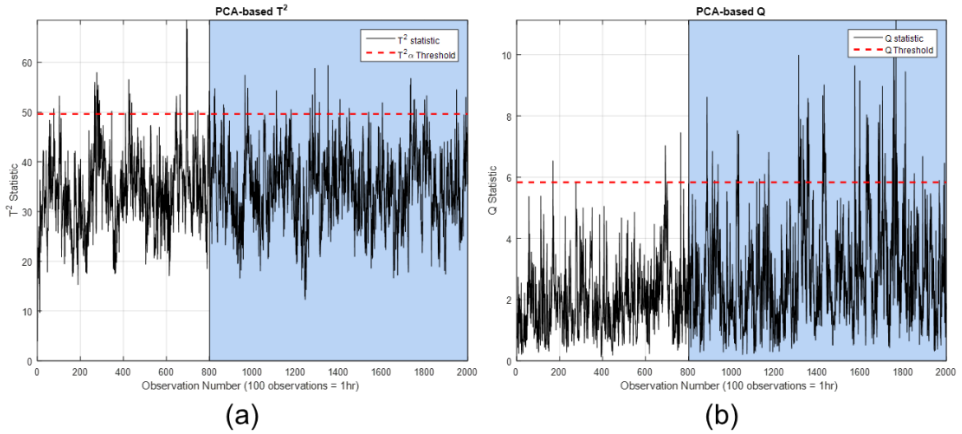

Figure 18. IDV(5): Shift in the mean - Conventional PCA-based charts (Reprinted with permission from [37]).

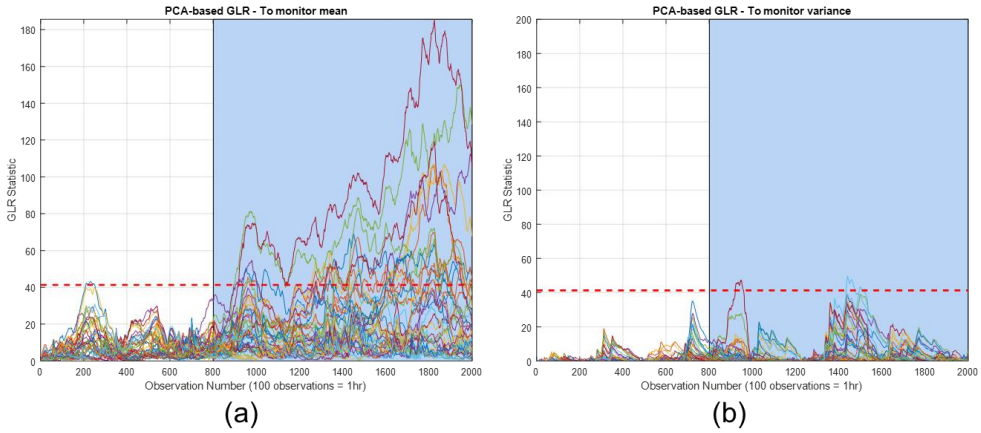

Figure 19. IDV(5): Shift in the mean - PCA-based GLR charts designed specifically to detect particular fault types (Reprinted with permission from [37]).

Table 6 summaries the fault detection results for the Tennessee Eastman process. We can observe that the PCA-based GLR chart designed specifically to detect a shift in

the mean in able to provide the significantly lower missed detection rates that then rest of the charts. Although, the PCA-based T^2 is able to provide a low ARL_1 value, that can be attributed to random noise, as most of the fault cannot be detected by the PCA-based T^2. These results also show that using both PCA-based GLR charts in parallel allows the process engineering to determine what class of fault has occurred, i.e., a shift in the mean, or a shift in the variance.

Table 6. Summary of fault detection results: IDV(5): Shift in the mean (Reprinted with permission from [37]).

	Missed Detections (%)	**False Alarms (%)**	**ARL_1**
T^2	97.58	3.75	1.00
Q	92.75	0.50	86.00
GLR (to monitor mean)	7.92	5.00	96.00
GLR (to monitor variance)	70.92	6.38	84.00

Both illustrative examples presented in this section demonstrate that in order to detect a particular type of fault the GLR chart designed specifically to detect that fault needs to be utilized. If a process is expected to experience different types of faults GLR

charts designed to detect each type faults need to be implemented and run in parallel, rather than a GLR chart designed to simultaneously track multiple parameters. When tracking changes in multiple parameters simultaneously, values of these parameters have to be estimated and computed simultaneously, thereby making it harder to maximize the GLR statistic. This could lead poorer fault detection and classification results.

Although results presented in this section are promising, the algorithms presented thus far are primarily for data that are approximately linear. In practice, industrial processes may be nonlinear and complex. The following section presents an example of how a nonlinear model can be used in order to carry out effective detection for nonlinear data.

2.3. Application of Kernel Principal Component Analysis (KPCA) to chemical processes

Although PCA has been extended to handle data from nonlinear models, there was limited application to chemical processes. Therefore, a goal of this work was to demonstrate the applicability of KPCA to a nonlinear chemical process, i.e., a continuous stirred tank reactor (CSTR), to demonstrate its effectiveness in detecting different process faults [59].

The dynamic model for the CSTR that was utilized in order to generate nonlinear data is defined as follows [60]:

$$\frac{\partial C_A}{\partial t} = \frac{F}{V}\left(C_{A_0} - C_A\right) - k_0 e^{-E/RT} C_A$$
$$\frac{\partial T}{\partial t} = \frac{F}{V}\left(T_0 - T\right) + \frac{\left(-\Delta H\right)}{\rho C_p} e^{-E/RT} C_A - \frac{q}{V \rho C_p}, \tag{54}$$
$$q = \frac{a F_c^{b+1}}{F_c + \left(\frac{a F_c^b}{2 \rho_c C_{pc}}\right)}\left(T - T_{c_{in}}\right)$$

where, F, V, k_0, and E represent the flow rate, reactor volume, reaction rate constant, and activation energy, respectively. The temperature and concentration of the different fluids are given by T and C, respectively. ΔH, ρ, and C_p represent the heat of reaction, densities, and heat transfer coefficients, respectively.

The training data set is composed of four process variables. The first two process variables are the flow rates of the coolant and feed, respectively. The third and fourth process variables are the outlet concentration and temperature, respectively. Dynamic data was then generated using the CSTR model. Zero mean Gaussian noise with a signal to noise ratio (SNR) of 20 was then added to the data. The training data used to train the KPCA model is shown in Figure 20. A fault of 3σ was then added to the temperature and concentration variables at 3 locations: 101:150, 251:350, and 401:450 in the testing data, and this is shown in Figure 21.

Comparing the conventional and kernel PCA-based Q statistic, it can be observed that the KPCA-based Q statistic (see Figure 22 (b)) is able to provide significantly lower missed detection rates than the conventional PCA based Q statistic (see Figure 22 (a)). The improved results of the KPCA-based Q charts can be attributed to the kernel techniques being able to effectively capture the nonlinearity of the data in the

hyperdimensional feature space, thus demonstrating the practical applicability of the kernel techniques for nonlinear chemical processes.

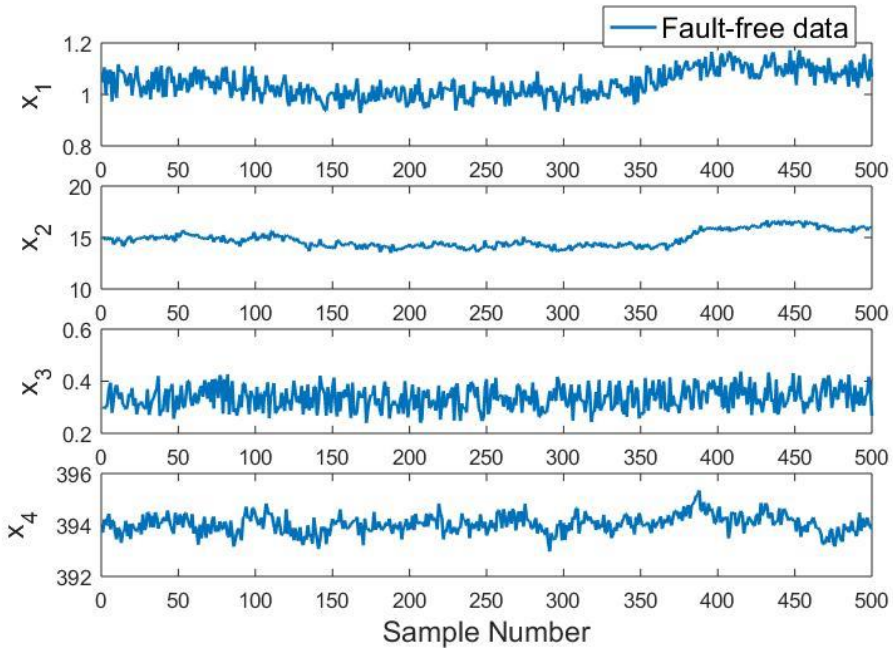

Figure 20. CSTR model: Training data.

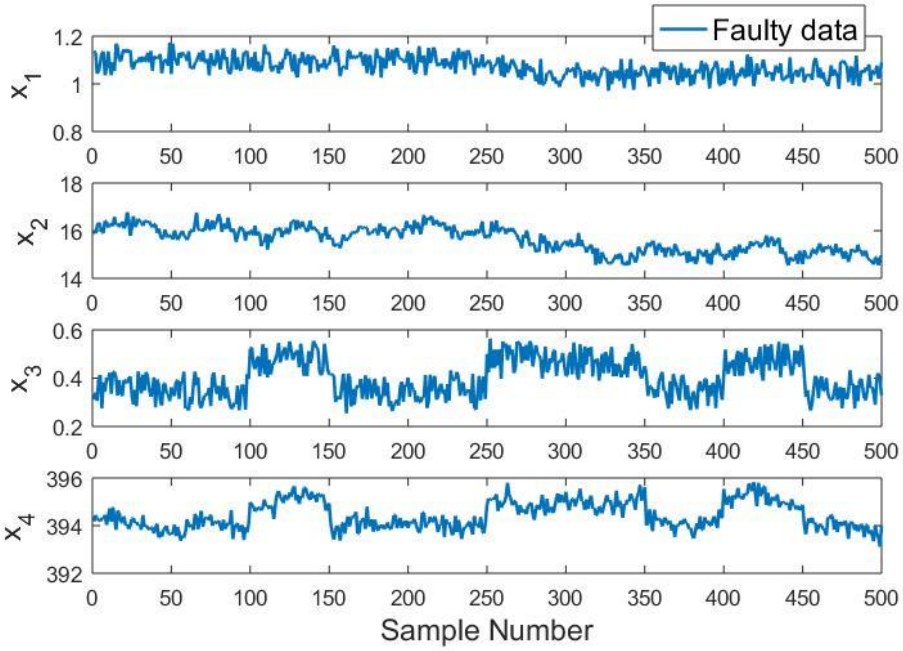

Figure 21. CSTR model: Testing data.

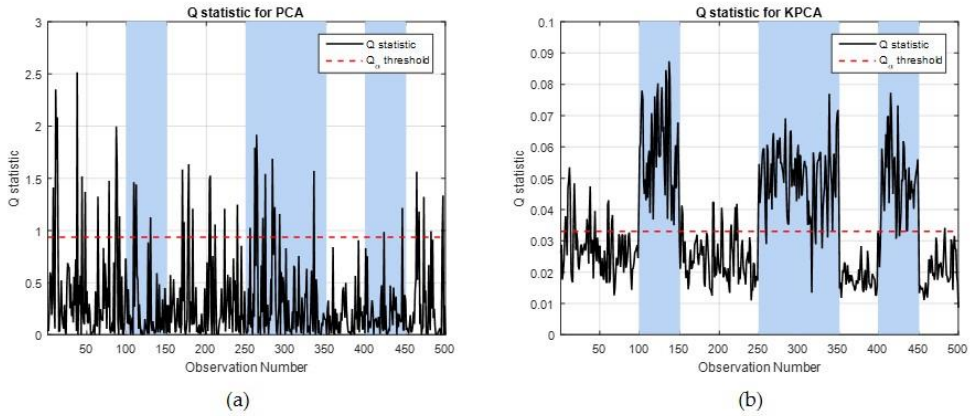

Figure 22. Conventional and kernel PCA charts (CSTR).

This section has presented numerous data-based process monitoring methods, that improved fault detection and classification performance. Additional algorithms that were developed through the course of this work, but that were not included or discussed can be found in literature [61]–[66]. In practice different processes may experience degradation in the process model itself, i.e., process drifts whose existence and impact can be tough to ascertain when operating under control, such as the case of fouling in a heat exchanger operating continuously under control. Since heat exchangers and other process units are designed to function under different operating conditions (or regimes), this adds additional complexity to monitoring. The following section develops a novel dynamic contour-based monitoring scheme in order to track equipment degradation in multiple operation regimes.

3. TRACKING EQUIPMENT DEGRADATION IN MULTIPLE OPERATING REGIMES USING A DYNAMIC MODEL-BASED MONITORING SCHEME

Several process industries require monitoring and control in order to ensure that quality variables of different streams are adhering to strict limits. This is essential in order to maintain product quality and safe operation, while being economically feasible. Monitoring is carried out in two phases: fault detection and diagnosis, during which faults are initially flagged, and then classified. A broad number of monitoring techniques are available, and these can be categorized using different schemes. Isermann highlights the importance of model-based methods for fault detection and diagnosis, and provides a review on these techniques [47], [67]. The authors in [4], [5] further classify model-based techniques into quantitative model-based techniques and qualitative-model based techniques. However, they also highlight the importance of developing models based on process history and available data, i.e., data-based models [6].

Although processes operate at steady state for long periods of time, they are dynamic in nature, and operating regimes can change depending on the operating conditions. Many authors have explored the classification of operating regimes for various applications [68], [69]. Unfortunately, it is often assumed that there is no degradation in the process model itself, i.e., possible degradation in the equipment is neglected.

In practice many processes operate under control in order to ensure that deviations in quality variables are managed, despite fluctuations in the input or disturbance variables, so that the physical properties of these streams can adhere to strict production standards.

Therefore, when equipment experiences degradation that leads to drifts in the process model, these controllers continuously adjust levels of the manipulated variable in order to ensure that desired set-points of the controlled (quality) variables are being achieved. Increased levels of manipulated variable lead to increased operating costs even when production standards are being satisfied, implying that the process is operating at sub-par conditions. Monitoring only the output variables is insufficient, as these remain unchanged despite changes in the process model. Model parameters often cannot be directly measured in practice, e.g., overall heat transfer coefficient to track fouling in heat exchangers. It is therefore essential to develop an efficient algorithm and means to monitor process drifts, including the model parameters as well. Hence, a primary objective of this work is to develop such an algorithm, capable of tracking equipment degradation by monitoring changes in the process model in multiple operating regimes.

Equipment degradation, more commonly referred to as condition monitoring, has been a popular independent topic of research. Various fault detection and diagnosis methods have been employed by numerous authors in order to detect degradation in model conditions for a wide variety of applications, e.g., electrical machines, agricultural machinery, gas turbines, hydropower plants [70]–[73]. Literature has mainly focused on equipment health, and often neglects to simultaneously monitor overall plant dynamics (including operating and related costs). This further validates the need for an integrated method capable of simultaneously tracking both deviations in the process model (equipment degradation) and drifts in the operating conditions/regimes, as they are invariably linked. Therefore, a second objective of this work is to ensure that the

developed algorithm is able to provide a process engineer with a simple algorithm to monitor both equipment degradation and process drifts online, while enabling decision-making with respect to the urgency of maintenance, and cost involved with operating under sub-par conditions. This work will demonstrate how a novel model-based algorithm, that integrates state estimation techniques with a contour profile can be utilized to achieve the proposed goals. In 1982 A conservative estimate of the cost of fouling in heat exchangers in the US was predicted to be close to $180 million [74]. This cost was projected to be closer to $14 billion per year in 2014 [75]. Therefore, a third objective of this work is to apply the developed algorithm to track fouling in heat exchangers, and reduce related economic losses through early detection and maintenance [76].

The remainder of this section is organized as follows. Section 3.1 provides a critical review of existing fault detection and diagnosis methods to monitor changes in the operating regime, and equipment degradation. Section 3.2 discusses the development of the proposed model-based algorithm, including design aspects and features. In Section 3.3 the proposed algorithm is applied on two illustrative examples, including one that utilizes real data from a double-pipe heat exchanger to demonstrate its practical applicability when tracking fouling online for a continuous process. Concluding remarks and future directions for this work are also presented with the illustrative examples.

3.1. Existing fault detection and diagnosis methods

Fault detection and diagnosis methods to monitor changes in the operating regime, and equipment degradation have shown broad interest. Unfortunately, these tasks have been examined independently. This section will review popular existing methods for both.

3.1.1. Monitoring changes in operating regimes

Although the goal of most industrial process is to operate at steady state to ensure streams and process variables adhere to expected standards, these processes are inherently dynamic in nature. Therefore, most processes will have multiple operating modes or regimes, and classification of these regimes by their features or properties is of interest.

In chemical processes, multiple operating conditions often result in different values for the output variables. For a given application, if a certain set of operating conditions is desired, then other operating conditions are often considered to be faulty. For these cases it would be essential to efficiently classify process data belonging to different operating conditions. The authors in [77] utilize Hidden Markov Model (HMM) and a Back-Propagation Neural Network (BPNN) in order to carry out classification of abnormal operating conditions. HMM and BPNN are both data-based techniques that can draw on vast amounts of available plant data to identify whether a process is operating under normal or abhorrent conditions. Potential disadvantages of these models are their requirement for large amounts of data and general model complexity when it comes to model training, which make their implementation tricky in practice.

The authors in [69], [78], [79] provide a detailed guide on how to utilize an operating regime based approach for nonlinear modeling and control for chemical, biochemical and petroleum applications. However, their main contribution is the partitioning of different operating regimes based on how the fundamental principles and models vary in each regime, i.e., thermodynamics, kinetics, physics etc. The goal is to then utilize the models in each regime to design better controllers. Unfortunately, the authors neglect to incorporate possible equipment degradation in their modeling work, which is essential for many chemical processes.

Automatic control of the slag regime in a blast-furnace smelting process is an example of a process that requires control strategies to be adjusted in order to ensure that material and energy resources are efficiently utilized in different operating regimes [80]. Additionally, classification work using self-organizing maps have been utilized by authors to identify multiple regimes for semiconductor applications [68]. Alternatively, Gaussian mixture models (GMM) have also been used in order to classify data from multiple regimes [81]. Unfortunately, for both SOM and GMM to be reliable the authors acknowledge that there needs to be necessary and sufficient data to obtain reliable classification results. Once classification has been carried out, models such as PCA may be utilized in each regime in order to carry out regime-specific monitoring [36], [37], [82]–[85].

The authors in [86] provide a fault detection and isolation scheme based on an adaptive filter to monitor a hydraulic process with multiple operating models. However, the authors assume that the dynamic behavior of the system at different operating points

can be approximated by a set of multiple linear time invariant (LTI) models) so that an adaptive linear Kalman filter for fault detection and isolation can be applied. Chemical processes may be nonlinear in nature, therefore, nonlinear versions of the Kalman filter such as the extended Kalman filter (EKF) and unscented Kalman filter (UKF) that are able to handle the non-linearity in a given process should be utilized instead [48]. Although the authors include the degradation of a pump as one of their fault cases, they are mainly concerned with fault detection and isolation, and fail to evaluate the potential economic losses incurred by operating at sub-par conditions.

Similar work has been completed in order to design multi-linear fault detection methods that account for the transition region between operating regimes including model-based methods that utilize parity space [87], [88]. Although reasonable results are obtained, the authors state that model tuning is required for each of the sub models, adding increased complexity. Additional work that attempts to monitor processes during the transition phase between different operating regimes is available is literature [89]–[92].

3.1.2. Monitoring equipment degradation / Condition monitoring

Equipment degradation or condition monitoring has been a topic of interest for a wide range of industrial applications. Regular maintenance is required in order to improve the life cycle of existing equipment, and to decrease capital costs [76]. Regular maintenance also ensures that the efficiency of process equipment is being maintained, thereby decreasing operating costs. A few different applications of condition monitoring are presented in this section.

In mechanical applications, model-based techniques such as Artificial Neural Networks (ANNs) have been applied to predict film thickness levels in spur gears using acoustic emission data. These methods provides an indication of tooth wear and tear of the gears [93]. However, this work focuses only on estimation accuracy, and does not provide an insight into a potential maintenance schedule. More recently acoustic emission data has been used to develop damage indicators based on power spectral entropy (PSE) for strain-hardening cementitious composites [94]. Iintegrating similar indicators with continuous chemical processes could prove advantageous.

Probabilistic approaches for condition monitoring have also been developed for other mechanical applications such as gas turbines [73]. However, the authors state that the quality of statistical data that is received determines the effectiveness of the approach. Qualitative methods have also been applied for gas turbine condition monitoring, where health of the individual components are examined [95]. However, the introduction of a metric to quantify the urgency of maintenance could prove beneficial. More recently nonlinear state estimation methods have been employed in order to examine the turbine blade health, and has demonstrated conceptual simplicity and high accuracy, with clear physical interpretation [14].

For a hydropower plant application the authors in [72] developed a condition monitoring and fault diagnosis method based on Support Vector Machines (SVM), a supervised learning method. Unfortunately, fault diagnosis mainly focused on sensor failure, rather than model degradation, i.e., process unit malfunction.

Similar conclusions are made in condition monitoring literature for agricultural machinery, where unsupervised learning methods, such as SOM and ANN have been utilized for steady state data [71]. The authors in [71] identify condition monitoring for dynamic data, and the potential development and use of hybrid diagnostic models as two future research ideas.

The authors in [70] examine the feasibility of using unsupervised learning methods, e.g., ANN, for electrical applications, such as those with multiple transducer inputs. Although they are capable of providing improved results over feature maps that have been utilized, there are two notable disadvantages, i.e., decision ambiguities at the boundaries of different regions, and the amount of data required for model training.

The literature surveyed thus far examining techniques that monitor changes in the operating regime and equipment degradation provide the following notable conclusions:

- State estimation methods have shown promise in tracking changes in operating regimes as well as equipment degradation. They are conceptually simple, highly accurate, and easy to physically interpret.
- Although there is work that aims to quantify equipment degradation through damage indicators, there is a lack of literature that examines the economic impact of operating at sub-optimal operating conditions, i.e., in the presence of equipment or model degradation.
- Due to the abundance of monitoring techniques available, a technique that combines efficiency and simplicity could prove to be an effective solution.

3.2. Model-based equipment degradation monitoring algorithm

In order to proceed with the design and development of an effective monitoring algorithm its purpose needs to be clearly defined. Motivating factors behind the design of the algorithm are initially discussed. The proposed monitoring algorithm is then presented, including how contours can be utilized in order to carry out monitoring of equipment degradation in multiple operating regimes.

3.2.1. Design discussion

Design and development of the algorithm was guided by the following needs and requirements:

- An algorithm capable of identifying equipment degradation despite changes in the input and/or desired set-points, i.e., different operating regimes.
- A user-friendly algorithm enabling easy implementation and comprehension for process engineers, to enhance and simplify maintenance decisions.
- An algorithm capable of identifying the economic impact of operating in different regimes, with and without degraded equipment.

From the literature surveyed for continuous processes, monitoring of changes using the linear and nonlinear state estimation techniques have shown promise. Therefore, state estimation techniques should be incorporated in the developed algorithm.

Methods that utilize classification and clustering methods to indicate where data lies, i.e., for different operating regimes, often use a graphical representation to do so.

Therefore, a graphical representation such as a contour profile could prove an efficient method to identify the operating point, degree of degradation, and respective cost.

3.2.2. Monitoring algorithm

The algorithm developed in this work is implemented in three phases: design variable definition, contour profile generation, and dynamic contour-based monitoring.

- **Design variable definition** – The details for this stage vary depending on the process and specific equipment being monitored. In this stage the process model is identified, along with the possible model parameter(s) that can be utilized in order to track equipment degradation, e.g., overall heat transfer coefficient in a heat exchanger.
- **Contour profile generation** – In this stage contour profiles are constructed by running the process at different steady states for different values of the design variables, i.e., varying degrees of degradation, and/or input conditions. This produces a profile like the one illustrated in Figure 23.
- **Dynamic contour-based monitoring** – In this stage dynamic data and measurements are collected and fed into the state estimation algorithm, in order to determine the exact operating point on the contour profile. The process engineer can utilize the contour to determine if the process equipment requires maintenance, and if process drifts need to be addressed or corrected based on economic, environmental or safety costs.

3.2.3. Dynamic process monitoring through contour profiles

An example of the contour profile described in the contour profile generation phase is illustrated in Figure 23. The contour profile is constructed utilizing information gathered from multiple steady state runs at varying degrees of model degradation. A nominal operating point can be defined as a point of low relative cost, while the regime around this nominal operating point can be defined as the nominal operating regime. The regions outside the nominal operating regime can be denoted as sub-par and undesirable operation regimes, respectively. The cut-offs for the different regimes can be defined and adjusted by the process engineer and will be application dependent.

Most industrial processes are designed to operate at steady state for long periods of time, although they must be able to operate at different steady states as and when required. Therefore, during continuous operation it is essential to determine the exact operating point, and this can be accomplished through state estimation techniques.

It is important to note that the parameter choices for either axis of the contour profile would depend entirely on the application. For example, for a continuous stirred tank reactor (CSTR) that operates with a catalyst and contains a cooling jacket, the process has two main model parameters that can experience change or degradation, i.e., possible degradation in catalyst quality, and possible decrease in efficiency of the cooling jacket through fouling.

Similarly, if a process engineer is required to monitor only one process unit, e.g., a heat exchanger, one model parameter could monitor the decrease in efficiency of the heat exchanger, while the second parameter could be the input parameter, e.g., one of the

inlet flow rates to the heat exchanger. Alternatively, if the process engineer needs to operate the heat exchanger at a different set-point (outlet temperature of one of the streams), an additional contour profile can be generated and made available, in order to carry out monitoring due to the introduction of the third parameter. This could also be represented as a 3-dimensional surface plot. However, in order to illustrate the applicability of the developed algorithm while maintaining its simplicity this work will focus on 2-dimensional contour profiles. Future work will demonstrate the applicability of the algorithm for more complex industrial applications. As should be noted through the two examples of applications described thus far, there is a broad potential for monitoring of different dynamic chemical processes, and the design of the contour profiles depends entirely on the concerned application.

The goal of the contour is to evaluate the cost with regards to operating at a particular point. Determination of the operating point on the contour profile is provided by state estimation, during the dynamic contour-based monitoring stage. The cost does not necessarily have to be a monetary value, i.e., the operating cost, but other factors such as environmental or safety factors could also be evaluated using these profiles. Safety limits may also be integrated and added to the operating cost contours in order to identify if a process is operating under safe conditions, e.g., the inlet temperatures of streams to a given process unit do not exceed the temperatures that the equipment can handle.

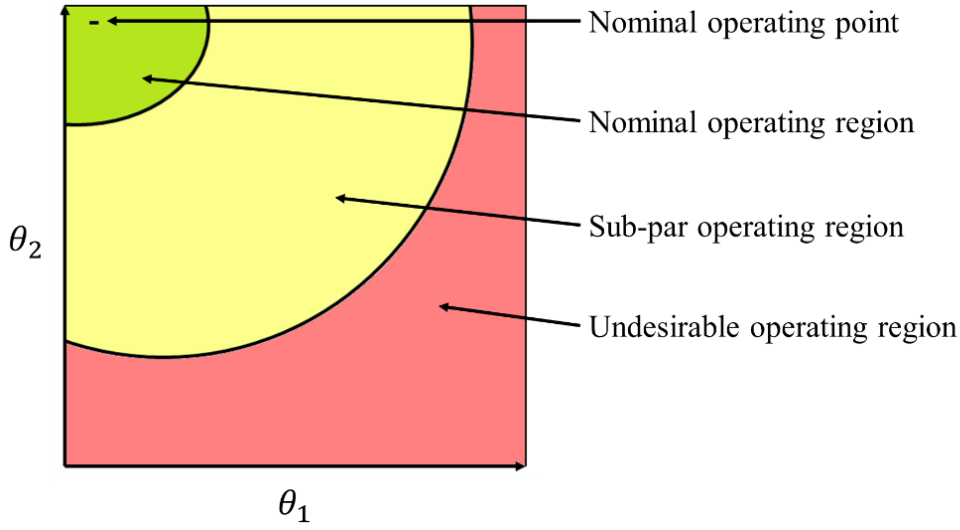

Figure 23. Illustration of cost contour profile.

Although the algorithm presented in this work has broad applicability, its practical implementation will be studied using the example of monitoring fouling in heat exchangers. Therefore, it is essential to provide a summary of current state of the art methods to monitor fouling in heat exchangers. A primary area of active research is the modeling of fouling, that seeks to verify and validate the type of fouling deposition in heat exchangers [96]–[99]. Such models aid in the development of computational fluid dynamic (CFD) models that can study changes in flow behavior when fouling is present [100], [101]. Unfortunately, in practice it is possible for a heat exchanger to experience different types of fouling [102]. Therefore, a more general procedure to monitor equipment degradation (fouling) such as the algorithm proposed in this work is preferred to eliminate rigidity in the modeling of fouling. Heuristic models are often developed and utilized by process industries [103], [104]. Such models require experienced process

engineers with knowledge of the process to help design these algorithms, thereby decreasing the range of practical applicability. The authors in [105] propose a dynamic thermo-hydraulic model to track fouling in multiple operating regimes. Although promising, this method is limited in application to only heat exchangers, and assumes that all measurements and physical properties are available. Our proposed algorithm is broadly applicable, capable of monitoring degradation in different types of process equipment. The developed algorithm can also function in the event that physical properties are unavailable (or unmeasurable) due to the use of state and parameter estimation techniques, making it particularly novel and advantageous.

Assessment of the proposed algorithm is required in order to encourage its application in practice, and this will be examined and evaluated in the next section through two illustrative examples that seek to study fouling in heat exchangers.

3.3. Illustrative examples

In this section, the performance of the developed monitoring algorithm will be assessed. The algorithm will first be applied on data from a simulated synthetic model of a heat exchanger in Simulink, and then on real data from a double-pipe heat exchanger to monitor model degradation, i.e., fouling in a heat exchanger. The dynamic model of a heat exchanger is obtained from the energy balance for the hot and cold streams, which is nonlinear and denoted as follows [106]:

$$\begin{aligned}\frac{dT_{h,o}}{dt} &= \frac{\dot{m}_h\left(T_{h,i}-T_{h,o}\right)}{\rho_h V_h} - \frac{UA}{\rho_h V_h C_{p,h}}\left(\Delta T_{lm}\right)\\ \frac{dT_{c,o}}{dt} &= \frac{\dot{m}_c\left(T_{c,i}-T_{c,o}\right)}{\rho_c V_c} + \frac{UA}{\rho_c V_c C_{p,c}}\left(\Delta T_{lm}\right)\end{aligned}, \tag{54}$$

where, $T_{h,o}$, $T_{h,i}$, $T_{c,o}$, and $T_{c,i}$ represent the outlet and inlet temperatures of the hot and cold streams, respectively. $\dot{m}$ and ρ denote the mass flow rates and densities of the respective streams, while *V*, *A*, *U*, and ΔT_{lm}, represent the volume of each side of the heat exchanger, the heat transfer area, overall heat transfer coefficient, and log-mean temperature, respectively.

The heat exchangers in both illustrate examples were designed as counter-flow, and hence the log-mean temperature difference (ΔT_{lm}) is defined as follows [106]:

$$\Delta T_{lm} = \frac{\left(T_{h,i}-T_{c,o}\right)-\left(T_{h,o}-T_{c,i}\right)}{\log\left(\frac{\left(T_{h,i}-T_{c,o}\right)}{\left(T_{h,o}-T_{c,i}\right)}\right)}. \tag{55}$$

3.3.1. Simulated synthetic example: Simulink

The heat exchanger simulated in this section is available in literature [107]. It is a shell-and-tube floating-head heat exchanger, that utilizes cooling water as the utility (available at 21.1 ^{o}C). Pressurized gas, with properties equivalent to air, needs to be cooled from 65.6 ^{o}C to 37.8 ^{o}C. The heat exchanger is expected to handle loads of approximately 9072 kg/hr. More details are available in the text [107]. Since the overall heat transfer coefficient (*U*) provides an indicator of the efficiency of the heat exchanger, and conversely its state of degradation, it will be one of the model parameters in the contour

profile. It should be noted that a decrease in the overall heat transfer coefficient indicates degradation in performance. As the outlet temperature of the hot stream is fixed (according to the problem definition), and the manipulated variable is the cooling utility, the inlet flow rate of the hot stream can be used as the second parameter on the contour profile. A proportional-integral-derivative (PID) controller is setup in Simulink in order to ensure that the process is operating under control, with the outlet temperature of the hot stream as the controlled variable, and the cooling utility as the manipulated variable.

A contour profile is then constructed utilizing information gathered from multiple steady state simulations at varying degrees of degradation and varying inlet flow rates of the hot stream, and is illustrated in Figure 24. As operating cost is of primary interest in the examples presented in this work it should be noted that the flow rate of utility required directly corresponds to the operating cost. The utility is generally provided at a fixed rate from suppliers, and can be directly multiplied using total required utility in order to determine the actual operating cost. If the heat exchanger is operating at inlet flow rate of approximately 2250 kg/hr for the hot stream, assuming there is no fouling, i.e., 335.8 W/m^2K, the required utility is expected to be approximately 4224 kg/hr. This may be identified as the nominal operating point for this particular inlet flow rate. Assuming there are no changes in the inlet flow rate of the hot stream, if the equipment undergoes degradation, when the next contour is intercepted the required cooling utility increases to 5597 kg/hr, which is a 33% increase in the cooling utility from the nominal operating point. Similarly, once again assuming that there are no changes in the inlet flow rate of the hot stream, if the equipment undergoes further degradation, when the next two contours

are intercepted the required cooling utility increases to 6971 kg/hr, and 8344 kg/hr, respectively. These contours correspond to an increase in cooling utility of approximately 66%, and 100% from the nominal operating point. If implemented in practice, the process engineer can utilize the 33% and 66% increase in the cooling utility as two warning signals for equipment maintenance, while the 100% increase in the cooling utility can serve as a definite signal for required maintenance. These limits can be set by the process engineer depending on the application and their knowledge of the process.

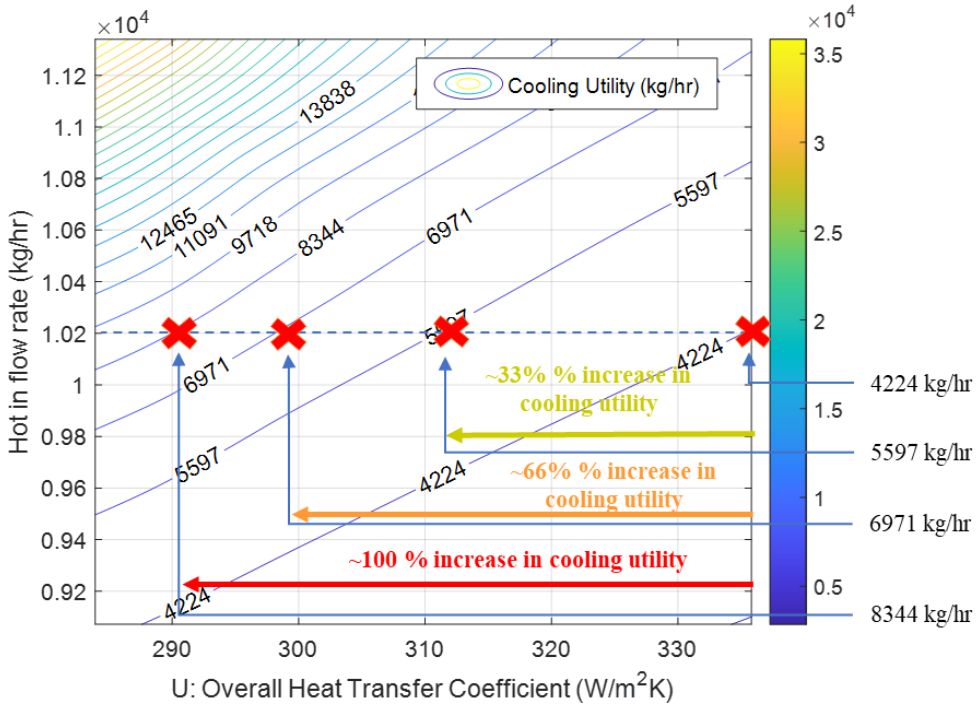

Figure 24. Contour profile - Operating cost (simulated heat exchanger illustration).

Dynamic data is required in order to test the prediction capabilities of the state and parameter estimation methods during the dynamic testing phase. A simulated heat exchanger operating under control can be used in order to obtained dynamic sensor measurements of the physical parameters of the different streams being monitored, i.e., temperature and mass flow rates. The inlet temperature of the hot stream is still assumed to be 65.6 ^{o}C, while the cooling utility is available at 21.1 ^{o}C. The desired outlet temperature of the hot stream is still 37.8 ^{o}C.

For the dynamic simulation the heat exchanger is expected to start with an inlet flow rate of 9072 kg/hr for the hot stream, with the overall heat transfer coefficient at 335.8 W/m^{2}K. In the simulated model a ramp function with a gradient of -5.68 (W/m^{2}K)/hr is introduced after the third hour. In reality fouling might not necessarily influence the overall heat transfer coefficient through a negative ramp function, and this will be explored further in the example using real data in the following section. Additionally, in order to test the estimation capabilities a ramp function with a gradient of +45.4 (kg/hr)/hr is introduced to the inlet flow rate of the hot stream (the input variable) after the sixth hour.

The state and parameter estimation results for the dynamic simulation are presented in Figure 25 and Figure 26, respectively. As Simulink provides measurements that are noise-free, Gaussian noise of zero-mean, unit variance is added in order to replicate real data as shown in Figure 25 (a). The state estimation results show that both estimation methods EKF and UKF are able to accurately predict the states in Figure 25 (b), and (c), respectively. Due to the efficiency of the heat exchanger decreasing from the third hour as it experiences degradation, it is expected that the outlet temperature of the

cold stream decreases. The flow rate of the manipulated variable, i.e., mass flow rate of the cold stream is adjusted by the controller in order to ensure that the outlet temperature of the hot stream is being met. The outlet temperature of the cold stream will decrease due the decreased residence time in the heat exchanger caused by the increased flow rate of the coolant.

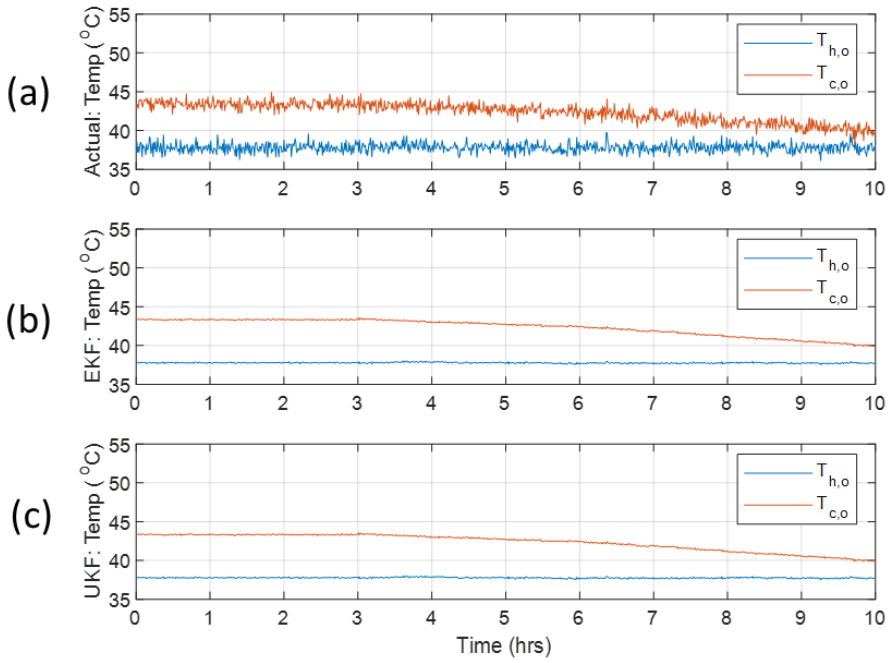

Figure 25. State estimation (simulated heat exchanger).

Figure 26 (a) provides the true values of the overall heat transfer coefficient utilized by the model during the simulation. The parameter estimation results show that both estimation methods EKF and UKF are able to accurately predict the change in the parameter (*U*), using only the measurable values, i.e., temperatures and flow rates being

fed into the estimation algorithm. It should be noted that in reality it could take much longer for a process to experience fouling, and the accuracy of the parameter estimation in this illustrative example for short time periods is encouraging.

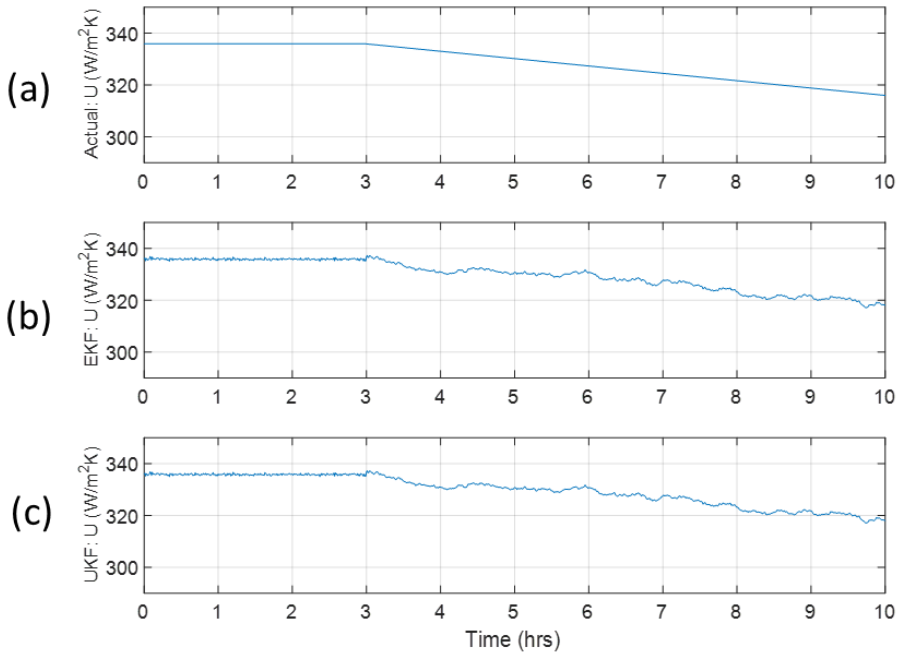

Figure 26. Parameter estimation (simulated heat exchanger).

Progression of this particular dynamic simulation on the contour profile is illustrated in Figure 27. In this particular case, the nominal operating point required a cooling utility of 2824 kg/hr, which increases to 3421 kg/hr by the end of the simulation as the process experiences both degradation (through fouling), and a change in the input (increase in the inlet flow rate of the hot stream). If no corrective action is taken the

efficiency of the heat exchanger would decrease further, crossing multiple contour lines, clearly identifying an increase in the required cooling utility due to fouling.

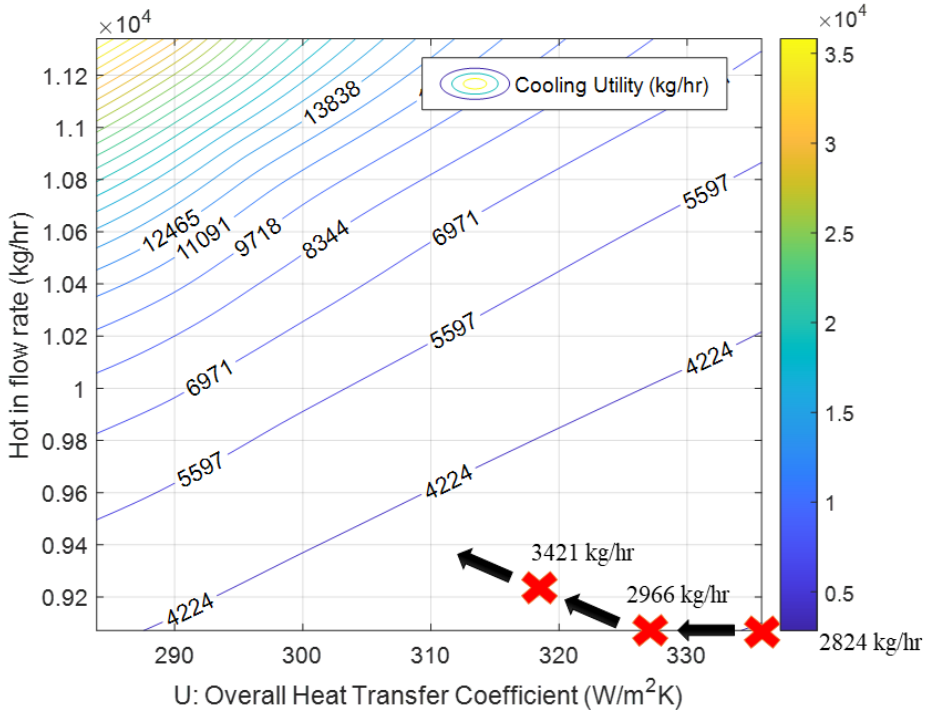

Figure 27. Contour profile - Operating cost (simulated heat exchanger in practice).

Although this illustrative example has demonstrated how the proposed algorithm can be implemented to efficiently track equipment degradation in multiple operating regimes, it needs to be applied on real data in order to assess its practical applicability and determine if any modifications of the algorithm are required.

3.3.2. Practical application – Double-pipe heat exchanger

In order to demonstrate the practical applicability of the developed algorithm a U-tube double-pipe heat exchanger available at Texas A&M University at Qatar was utilized. For this case, the outlet temperature of the cold stream needed to be maintained at 25 ^{o}C, with heating utility available at 40 ^{o}C. A proportional-integral (PI) controller ensures that the process is operating under control, with the outlet temperature of the cold stream as the controlled variable, but with the heating utility as the manipulated variable in this case. It should be noted that the PI controller was adequately tuned prior to conducting the experiment.

In practice fouling could take weeks, months or years. Unfortunately, in order to overcome this limitation and to replicate fouling and its impact, heat shrink tubes were used to coat the outside of the inner tube of the available U-tube double pipe heat exchanger.

It should be noted that the applicability of the model presented in Equation (56) for the U-tube double-pipe heat exchanger was confirmed by feeding in the estimated parameter values obtained from experimental data into a model constructed in Simulink. The outlet temperatures that were obtained from this simulation were in the same range as the experimental data, thus confirming model validity.

Utilizing data collected from multiple steady state experimental runs, the contour profile illustrated in Figure 28 is obtained. It should be noted that three levels of fouling were examined:

- Minimum fouling (no coating with heat shrink tube).
- Medium fouling (with quarter length of the U-tube coated with heat shrink).
- Maximum fouling (with half length of the U-tube coated with heat shrink tube).

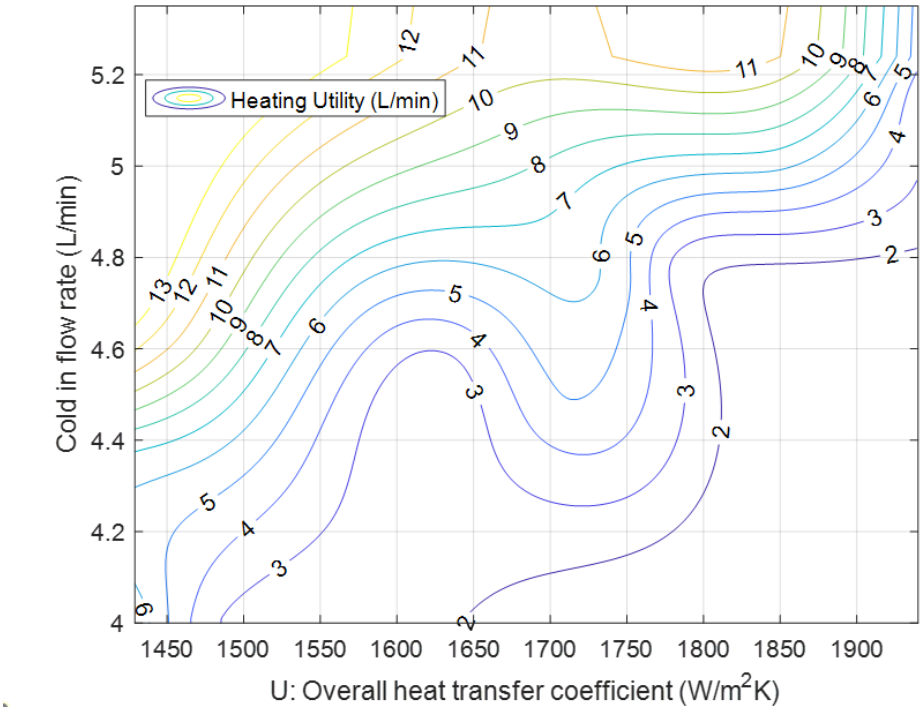

Figure 28. Contour profile - Operating cost (heat exchanger real data with U).

A few observations and conclusions can be made from Figure 28. The contours are not as smooth as those obtained in the simulated example (see Figure 24). This can be attributed to a few reasons. First, due to limitations with equipment it is only possible to obtain a limited number of levels of fouling i.e., three. Second, it should be noted that in the simulated example it was assumed that there was no limitation on the maximum flow

rate of the coolant. In practice, it would be necessary to incorporate these limitations. Most importantly, Figure 28 illustrates that rough contours are obtained, with large variability in the overall heat transfer coefficient. This can be attributed to the fact that the overall heat transfer coefficient is not only influenced by fouling that might be present, but also the convective heat transfer coefficient of the two fluids. The variation in the convective heat transfer coefficient is primarily due to varying bulk velocities of both streams (for different input conditions). Therefore, it might be necessary to modify the model parameter used to directly track the equipment degradation. Decoupling the convective heat transfer coefficient from the overall heat transfer coefficient may enable smoother contours to be obtained.

The state and parameter estimation results for the dynamic data are presented in Figure 29 and Figure 30, respectively. The true measurement values of the two outlet streams are shown in Figure 29 (a). The state estimation results show that both estimation methods, EKF and UKF, are able to accurately predict the states as seen in Figure 29 (b), and (c), respectively. Due to the efficiency of the heat exchanger decreasing as the level of fouling increases, it is expected that the outlet temperature of the hot stream increases. The flow rate of the manipulated variable (mass flow rate of the hot stream) is adjusted by the controller in order to ensure that the outlet temperature of the cold stream (the controlled variable) is being meant. The outlet temperature of the hot stream will decrease due the decreased residence time in the heat exchanger caused by the increased flow rate of the heating utility.

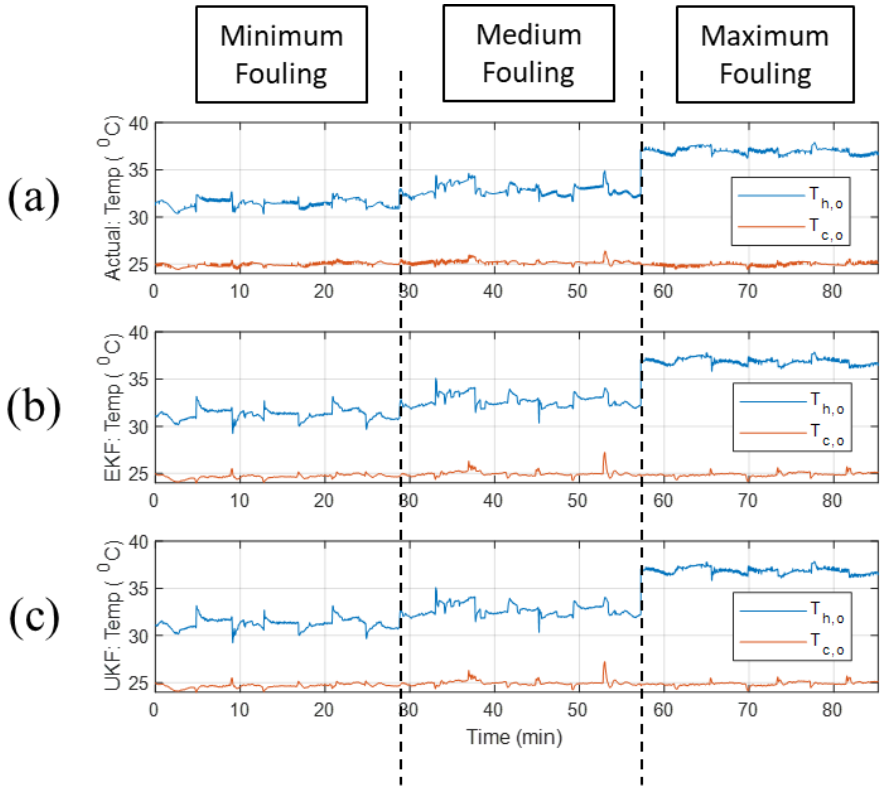

Figure 29. State estimation (heat exchanger real data).

Unlike the simulated example the true value of the overall heat transfer coefficient is unknown. The parameter estimation results in Figure 30 show that both estimation methods, EKF and UKF, are able to predict the change in the parameter (U) using only the measurable variables, i.e., temperatures and flow rates of the heat exchanger, being fed into the estimation algorithm. Although, it can be observed that the maximum value of the overall heat transfer coefficient decreases with an increase in the level of fouling, large fluctuations in the overall heat transfer coefficient can also be observed. As discussed previously, this can be attributed to the change in the input condition and subsequently the manipulated variable, i.e., changes in the flow rate of the heating utility required due to

changes in input condition (inlet flow rate of the cold stream) every 4 minutes, which influence the convective heat transfer coefficients of the fluids. This in turn causes changes in the overall heat transfer coefficient. Therefore, it might be necessary to modify the model parameter used to directly track the equipment degradation. Decoupling the convective heat transfer coefficient from the overall heat transfer coefficient appears to be a logical first step in order to improve the estimation of the level of fouling.

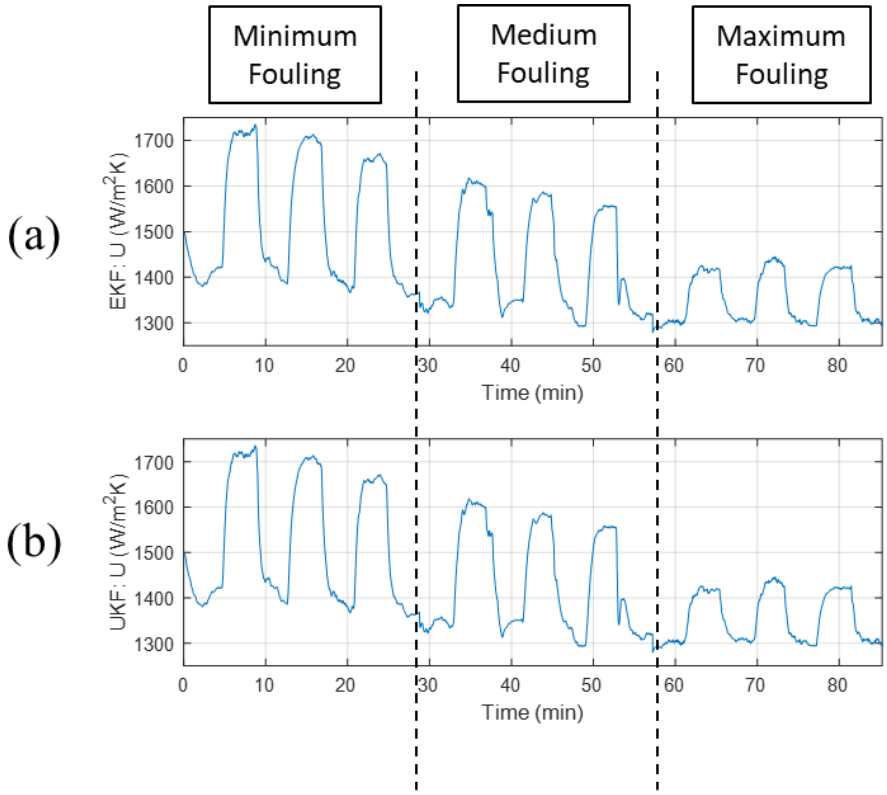

Figure 30. Parameter estimation - U (heat exchanger real data).

Due to the large variation in the overall heat coefficient seen in the contour profile (see Figure 28) and the parameter estimation results (see Figure 30) it can be assumed that

an average process engineer might have difficulty interpreting the results to monitor equipment degradation in real time. Therefore, the proposed model parameter needs to be changed to one capable of monitoring the equipment degradation more effectively.

As previously noted, the overall heat transfer coefficient has a number of contributing factors, which can thus be broken down further as shown [106]:

$$U_o = \frac{1}{\left(\frac{A_o}{A_i h_i} + \frac{A_o \ln\left(D_o / D_i\right)}{2\pi kL} + \frac{1}{h_o} + R_f \right)}, \tag{56}$$

where, U_o, h_o, h_i, are the overall heat transfer coefficient, and the convective heat transfer coefficients of the fluid in the outer and inner tubes, respectively. D_o and D_i denoted the outer and inner diameters of the tube's heat exchange area, while k, L, and R_f represent the thermal conductivity of the heat exchanger material, length of heat exchange area, and fouling resistance, respectively. The values of most parameters are known, or can be computed as in the case of the convective heat transfer coefficients, and the only unknown is the fouling resistance. Therefore, the model parameter that could appropriately quantify the degradation in performance of the heat exchanger is the fouling resistance.

Seider-Tate equations have been utilized in order to design heat exchangers in multiple industries for the last few decades, and were employed in this work to compute the convective heat transfer coefficients (h) of the two fluids experiencing turbulent flow [108]:

$$h = \frac{k}{D}\left[1.20\left[0.027\,\mathrm{Re}^{0.8}\,\mathrm{Pr}^{1/3}\left(\frac{\mu}{\mu_w} \right)^{0.14} \right] \right], \tag{57}$$

where, k, μ, and D denote the thermal conductivity and dynamic viscosity of the fluid (in bulk and at the wall (w)), and characteristic diameter, respectively. Re and Pr are the Reynolds and Prandtl numbers, respectively.

Using the steady state experimental runs that were available, the contour profile illustrated in Figure 31 is obtained. It can now be noted that the contours are much smoother, as the two model parameters have been decoupled (no correlation to one another). The contours show that an increase in the level of fouling requires more heating utility in general, while an increase in the inlet flow rate of the cold stream requires an increase in the heating utility.

The state estimation results are identical to those shown in Figure 29. Furthermore, the parameter estimation results in Figure 31 show that both estimation methods, EKF and UKF, are able to predict the change in the parameter (R_f), using only the measurable variables, i.e., temperatures and flow rates being fed into the estimation algorithm. These results are much simpler to interpret for the process engineer, as they can clearly track model degradation by monitoring the trend in the fouling resistance. Figure 32 clearly demonstrates that the value of the fouling factor is approximately 0.0002 m^2K/W in the case of minimal fouling, which increases to 0.0003 m^2K/W, and 0.0004 m^2K/W for the cases of medium and maximum fouling, respectively. These values are consistent with those available in literature [106]. The impact of fouling can clearly be interpreted from the contour profile in Figure 31 as well. For a step change in the inlet flow rate of the cold stream from 4 L/min to 5.2 L/min in the case of minimum fouling, the required heating utility increases from approximately 2 L/min to 6 L/min (see (1) in Figure 31). For the

same step change in the cold in flow rate from 4 L/min to 5.2 L/min the case of maximum fouling, the required heating utility increases from approximately 4 L/min to over 13 L/min (see (2) in Figure 31). This highlights the significant increase in demand in heating utility caused by the presence of fouling. Designation of warning lines on the contour plot is recommended, to inform process engineers on site about the urgency of maintenance. This allows potential increased operational costs to be addressed before they become a burden on the plant. e.g., two warning contours lines for maintenance can be set at 7 L/min and 10 L/min of required heating utility, while essential maintenance can be signaled at 13 L/min of required heating utility.

Once again, it should be noted that in reality it could take much longer for a process to experience fouling, but the accuracy of parameter estimation for short time periods is extremely encouraging.

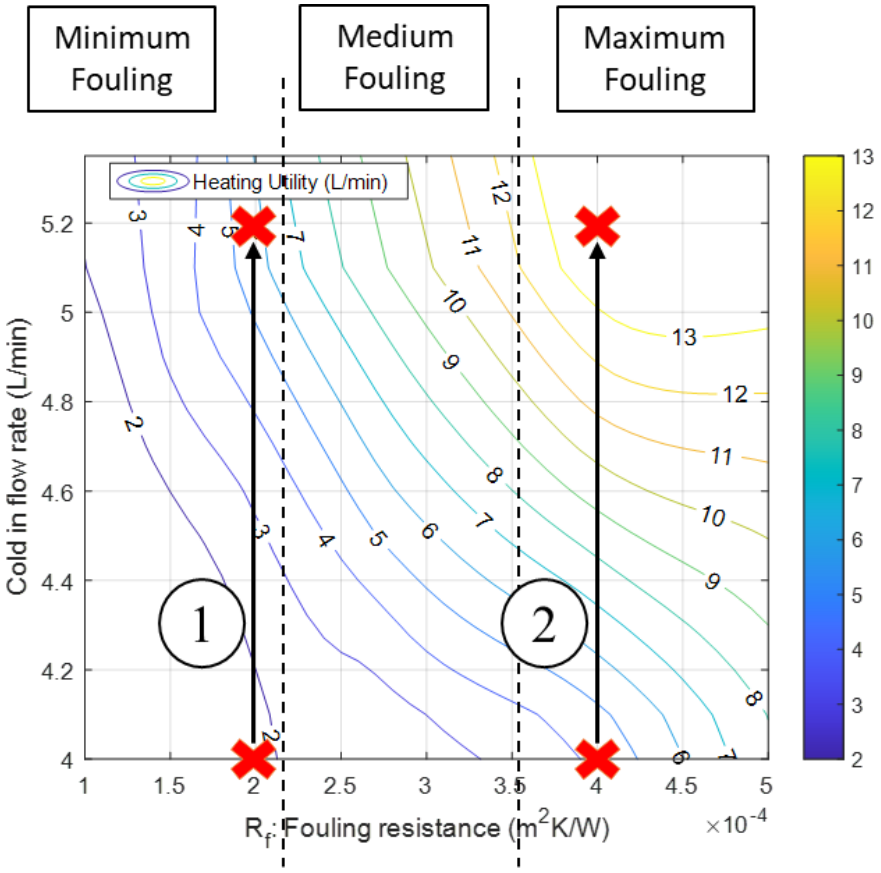

Figure 31. Contour profile - Operating cost (heat exchanger real data with R_f).

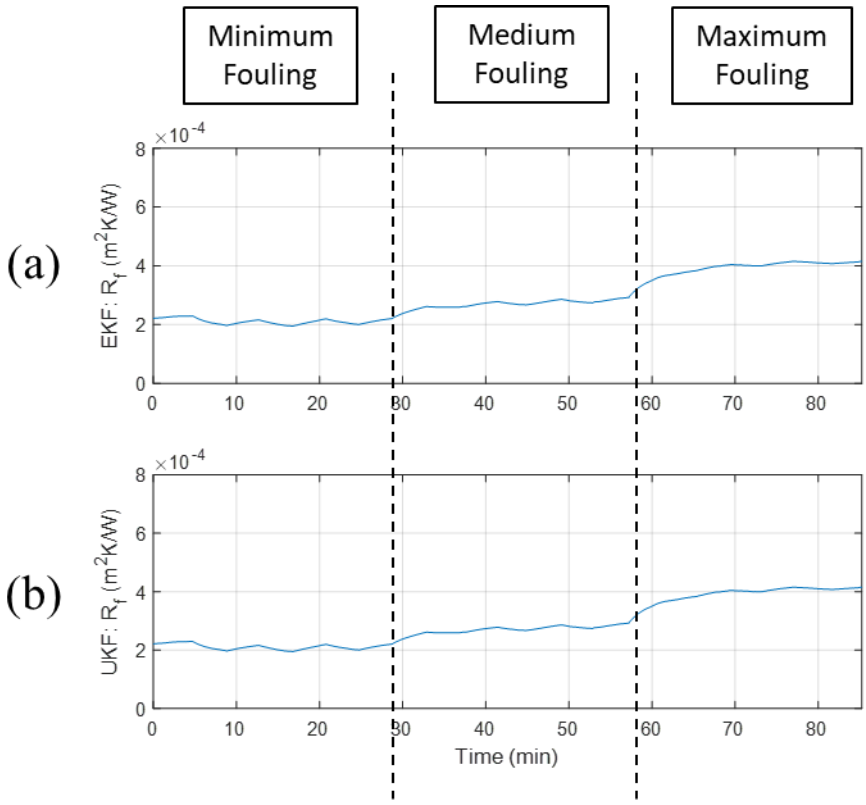

Figure 32. Parameter estimation - R_f (heat exchanger real data).

The illustrative examples presented in this section highlight the practical applicability of the proposed technique. The double-pipe heat exchanger demonstrates the need for the process engineer to have an understanding of the process before selecting the model parameter to monitor and quantify the degradation in the process model.

In this section, a model-based algorithm was developed in order to track equipment degradation in multiple operating regimes was proposed. This was accomplished by using state and parameter estimation to track the exact state of the process and degradation experienced by the process model by monitoring the model parameters. This information can then be utilized to determine the operating point on the cost contour profile, and to

also determine if continued operation is justified. Furthermore, as demonstrated Section 3.3.1, the contour lines can be utilized by the process engineer in order to determine the urgency of equipment maintenance. The performance of the developed algorithm was assessed and evaluated using two illustrative examples, using simulated data, and real data from a double-pipe heat exchanger. The examples demonstrate the practical applicability of the developed algorithm and highlights the importance of picking the correct model parameters to monitor process drifts and model degradation. The novelty of the developed algorithm is threefold. First, it provides the process engineer with a simple chart to track equipment degradation in multiple operating regimes while the process is operating under control by monitoring changes in the model parameters. Second, it provides a numerical value for the cost associated with the current operating point, and the recommended corrective action that would be required in order to bring the process back to a more desirable operating region. Third, this work has demonstrated the potential to mitigate extensive losses due to fouling in heat exchangers faced industries in the US, and the rest of the world.

Although the results presented in this section are promising, there is room for further work. The physical parameters of the fluids in this work were assumed to be constant. For other processes and applications, it is possible that the temperature ranges are larger, which leads to larger differences in the values of the physical parameters. Therefore, improving the accuracy of underlying model is one direction for future work. Additionally, there are a number of applications and equipment that have two model parameters that can experience degradation over time. This increases the model

complexity, which can require three-dimensional plots to interpret the current state of the process, operating regime and equipment degradation. Therefore, exploring such models and applications is a direction for future work.

This section has presented a means of tracking equipment degradation in multiple operating regimes using computationally efficient monitoring methods. Chronic leak detection, i.e., small pipeline leaks, can lead to significant releases of greenhouse gases resulting in substantial environmental pollution, as well as substantial economic and reputational losses to the manufacturing and pipeline transportation industries. The following section critically examines existing leak detection and localization literature, in order to guide the design and development of an experimental setup that can be used to study fluid behavior in the event of a leak. Since industrial processes provide an abundance of sensor measurements, an additional objective in the study of fluid behavior in pipelines is to examine if redundant pressure sensor measurements can be used to predict flow rates from different operating conditions, in the absence or malfunctioning of a flow meter.

4. LEAK DETECTION: COMPREHENSIVE REVIEW, EXPERIMENTAL DESIGN AND CLASSIFICATION OF SENSOR DATA*

Detection of leaks from transportation pipelines has been an existing problem for several decades. Leaks from small cracks or pinholes are termed chronic leaks, as they can go unnoticed for extended periods of time, leading to both economic loss and environmental damage. Literature lacks a comprehensive review of chronic leaks, particular under arctic and subsea conditions. Therefore, an objective of this section is the review of existing leak detection technology, especially under these conditions. Once promising methods for future work have been identified, a second objective of this section is the design and development of an experimental leak detection setup that can be used to study leak detection behavior before extension to multiphase flow under harsh conditions. A third objective is the study of fluid behavior in pipelines is to examine if redundant pressure sensor measurements can be used to predict flow rates from different operating conditions, in the absence or malfunctioning of a flow meter.

[2] Part of this chapter is reprinted with permission from "Chronic leak detection for single and multiphase flow: A critical review on onshore and offshore subsea and arctic conditions" by Niresh Behari, M. Ziyan Sheriff, M. Azizur Rahman, Mohamed Nounou, Ibrahim Hassan, Hazem Nounou, 2020. Journal of Natural Gas Science and Engineering, 81, 103460, Copyright 2020 by Elsevier.

4.1. Review of Leak Detection Techniques with Critical Analysis on Subsea and Arctic Conditions 2

4.1.1. Introduction

Chronic or small pipeline leaks can be a significant contributor to Greenhouse Gas (GHG) emissions resulting in global warming, and environmental pollution [109]. If these leaks go unattended and are not addressed within prescribed time limits, the pipeline fracture can propagate causing large scale environmental releases, fires or explosions [15]. For offshore deep water or arctic conditions chronic leaks need to be repaired in the shortest possible time possible due to the large-scale environmental impact and potential for the leak to escalate to a catastrophic rupture.

Leak detection methods in pipelines can be broadly classified into three categories: methods based on signal processing, methods based on state estimation, and methods based on knowledge, as illustrated in Figure 33. Methods based on signal processing involve analysis of the different types of measurements collected from different sensors. Methods based on state estimation generally utilize dynamic pipeline models in order to compute and monitor the different states, e.g., flow rates, and pressures, to determine if a leak has occurred. Knowledge based methods utilize the abundant data collected from numerous sensors to distinguish normal (no-leak) conditions from various faulty (leak) scenarios and conditions

A primary objective of this section is the critical analysis of the current state of leak detection technology, especially under subsea and arctic conditions. A detailed introduction to leak detection for both single phase and multiphase flow is provided, after which promising methods that warrant further exploration are highlighted.

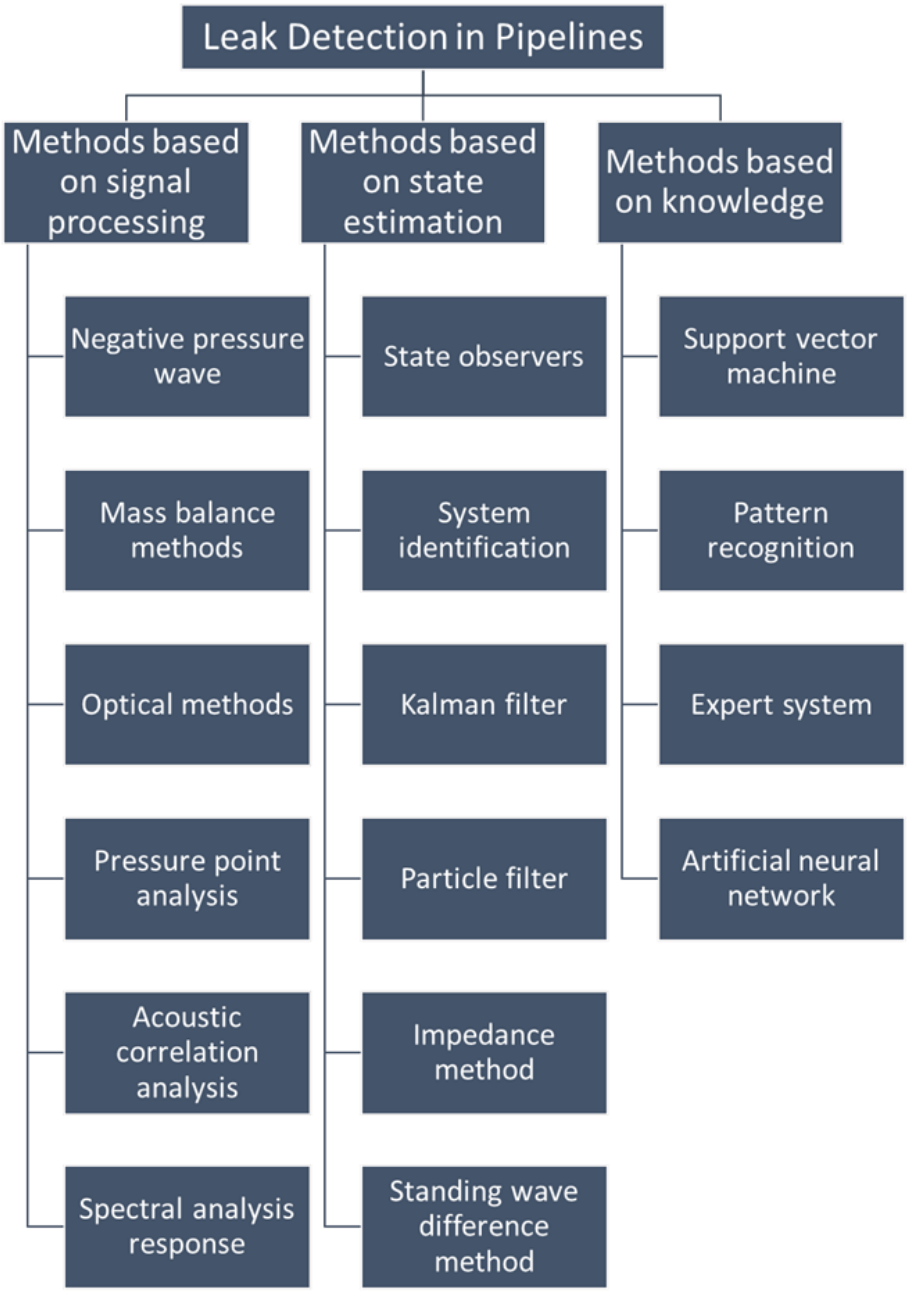

Figure 33. Leak Detection Techniques - Common Classification Hierarchy (Reprinted with permission from [110]).

4.1.2. Overview of existing leak detection techniques

Any process equipment has a given life cycle, after which maintenance is required. Off-shore (subsea) pipelines may also experience damage or decrease in strength over time. Leaks from these subsea pipelines can result in different oil and gas fluids contaminating the environment, leading to undesired economic and environmental losses. Therefore, early detection and localization of such leaks is critical to maintain process safety, and minimize economic losses. Leak detection methods based on signal processing methods were some of the earliest monitoring techniques developed for detection and localizations purposes, and a few of the more popular techniques will be discussed next.

4.1.2.1. Methods based on signal processing

4.1.2.1.1. Negative pressure wave

During the event of a leak in a pipeline, the liquid density experiences a sharp drop at the leak point due to both loss of fluid medium and a drop in the pressure. This pressure wave spreads from the leak point to locations across the pipeline segment. Once the pressure reaches the end of a pipeline, the negative pressure wave will be noticed first through the station inlet pressure, and then through the station outlet pressure. Since leaks occur at different locations, different time differences can be noted when the negative pressure wave is captured [111]. Therefore, utilizing the time difference when both sides of the pipe detect the negative pressure wave, along the length of the pipeline and wave velocity, the leak location can thus be determined. Unfortunately, this technique mainly

detects abrupt leaks. Slow or chronic leaks may be difficult to detect, as a clear negative pressure wave may not be generated in these cases [112]. Using pressure waves for leak detection is also reported to be impractical for long-range pipelines [113].

Many authors have applied filtering techniques such as wavelet filtering, and moving average filter to smoothen, i.e., filter out noise from the signal obtained before carrying out leak detection [114]–[116]. High false alarm rates are observed when the leak is small, i.e., smaller than 0.5% of the nominal flow value [117]. The authors in [118] aim to tackle the issue of high false alarms experienced by this technique by supplementing the negative pressure wave method, with measurements of flow taken at the extreme ends of the pipe. The differences in flow signal can also be utilized to determine if a leak has occurred. The authors use wavelet transform to extract significant features from the negative pressure wave, and reduce the false alarm rate. One performance index used to evaluate capability of a given leak detection and localization technique is the smallest detectable leakage flow rate (SDLFR), and the authors in [119] state that the leakage position, pressures at inlet and outlet, flow rate, density, wave speed in the pipeline, and precision of the instruments are all factors that affect the SDLFR.

4.1.2.1.2. Mass balance methods

The mass balance method utilized to detect leaks is based on fundamental principles. In the event of a leak, the mass balance equation shows a systematic deviation. However, the line pack term can experience large variance. The authors [120] discuss the importance of the packing term, and explain that since the packing term is tied to the wave

velocity, it is poorly defined in the transient stage thus causing the increased variance. Other authors have also tried to conduct leak detection during absence of recorded feed rates, but have stated that leak detection accuracy is an issue that needs to be addressed [121]. The mass balance method is therefore not as effective in practice, especially during transient operational stages. Since this method is sensitive to pipeline dynamics and arbitrary disturbances, high false alarms can occur, making the utilization of this technique impractical. Most of the work related to mass balance methods have only focused on single phase liquid systems.

4.1.2.1.3. Optical methods

Optical methods for leak detection and localization can be categorized into active and passive methods. Active methods require the use of a radiation source to illuminate the area of concern, while passive methods do not require such a source. The advantage of optical methods is their portability, and ability to carry out remote detection and localization. Active methods include light detection and ranging (LIDAR), diode laser absorption, millimeter wave radar, and backscatter imaging [122]–[125]. Passive methods include thermal imaging, multi-spectral imaging, and gas filter correlation radiometry [126]–[128]. Optical fiber can be used to monitor physical and chemical properties. However, the authors in [129] state that applying this method might be tricky for existing pipelines, as a few pipelines might need to be dug up, to place the optical fiber sensors and cables. The authors also state that high cost, and stability over time of the fiber chemical coating are causes for concern when implementing this technique.

4.1.2.1.4. Pressure point analysis (PPA)

PPA is one of the more popular leak detection and diagnosis methods [130]. The PPA method functions by monitoring pipeline pressure at a single point on the pipeline, and comparing it to previous pressure measurements by examining the running statistical trend. The PPA method only requires pressure signals from one or more points, and can be combined with selective filtering and software thresholds to determine whether there is a leak by examining successive measurements. PPA is advantageous as it is cost effective and easy to maintain, and can detect small or chronic leaks [111], [130], [131]. It is important to note that it might be difficult to diagnose the fault point using this method.

4.1.2.1.5. Acoustic correlation analysis

This method utilizes the sound waves generated by the presence of leak as the signal source. Acoustic sensors need to be installed along the length of the pipeline to pick up the sound of the leak point. Signal processing technology is then used to detect and localize the leak point [132], [133]. This method is able to detect small leaks, and has the advantage of both high detection and localization accuracy as well. The authors in [134] apply acoustic correlation analysis to a pipeline network, and state that this method distinguishes between different features in the pipeline, e.g., bends, leaks etc., with fewer sensors than more traditional methods. Most of the work that uses acoustic correlation analysis has been for single phase liquid systems. The authors in [113] demonstrate the

use of acoustic correlation methods pipeline in a vapor-soil environment, and state the acoustic method is only good for lower flow rates, as higher flow rates are contaminated with too much noise. The authors in [112] carry out an evaluation of acoustic and mass balance methods, to assess their performance at a multiphase laboratory, however, only using water as the working fluid. The authors conclude that the acoustic method is quick, and able to locate the leak precisely provided that the leak is abrupt enough, while the mass balance method, quantifies the leak flow rate and detects any progressive leaks. Unfortunately, this method is not recommended for pipeline transport in the oil and gas industry, as subsea pipelines may operate at high flow rates, and will be contaminated with too much noise to make this technique effective.

4.1.2.1.6. Spectral analysis response

When a leak occurs, it generates leak signals such as ultrasonic waves. Examination and extracting characteristic parameters of these leak signals for further analysis, allows the user to derive a relationship between the ultrasonic spectrum and leak parameters. The parameters can include the aperture of the leak point, the inner pressure of the pipeline that can be used in order to judge the state of the leak point, which in turn enhance the accuracy of detection. These methods are usually based on Fast Fourier Transform (FTT) [135], [136]. The accuracy of this method depends very highly on the eigenvalue problem, which can be addressed using a filter diagonalization method (FDM) [137]–[139]. Spectral analysis generates large amounts of data, limiting the ability of this technique to be applied in real time [140].

Most of the methods thus far focus on utilizing measurements collected from different sensors, along with the application of different analytical techniques to detect and localize faults. Methods based on other model-based methods will now be discussed.

4.1.2.2. Methods based on state estimation

4.1.2.2.1. State observers

For state estimation methods that use observers, the equations for pressure and flow are initially set up. Two pressure extremes are used as inputs, and algorithms are then developed to carry out leak detection and localization using the error signal that measures the difference between the measured and observed values [141]. The authors in [141] utilize a Luenberger type observer, and examine two different cases, one with oil as the fluid, and another with gas. Both cases only included a single phase. Unfortunately, this method assumes that two pressure extremes are not affected by the size of the leak and can only be used in the event of small leaks. Therefore, an effective leak detection technique needs to have a broader working range, and capable of a wide range of leak sizes.

4.1.2.2.2. System identification

This method functions by comparing the actual values from the pipeline with a model to determine if a leak has occurred [111]. Both fault-free and fault sensitive models are constructed. For the fault sensitive models, correlation analysis is used to determine if a leak has occurred, and for the fault free model, algorithms are introduced to localize the

fault. Similar to the method used in state observers, this method also assumes that leak size does not affect both pressure extremes, which is not ideal as effective leak detection techniques need to have broader working ranges.

4.1.2.2.3. Kalman filter

The Kalman filter method requires discrete state space models of flow and pressure to be set up [8]. The pressure and flow at the either end of the pipeline (start and end) are used as inputs, and the pipeline is divided into multiple sections, and three states are monitored (flow, pressure, and amount of leakage) for each section [142]. A suitable criterion is utilized to detect and localize a leak. This method requires that the mean and variance of the process noise be determined in advance, and is therefore sensitive to unexpected disturbances. There is also a link between the number of sections utilized and the degree of the detection and localization.

4.1.2.2.4. Particle filter

A shortcoming of the traditional Kalman filter methods, such as the Extended Kalman Filter (EKF), is that they require the nonlinear pipeline model to be linearized. However, these transformations are only reliable if it is possible for the error propagation to be approximated by a linear function, which does not work for gas pipeline model. Fortunately, the particle filter is a sequential Monte Carlo method that is based on point mass, i.e., particle, representation of the probability density functions, and can utilized to estimate state in both non-Gaussian and nonlinear systems without the need for

linearization [50]. The authors in [50] demonstrate how an adaptive particle filter algorithm can be applied to detect and isolate faults for a model where time-varying parameter estimation is required. The algorithm is able to detect small leaks as well.

4.1.2.2.5. Impedance methods

The hydraulic impedance is the ratio of head fluctuation to discharge, while the characteristic impedance is defined using the pipe parameters and the propagation constant. When the friction in the pipe is neglected, the final pipe impedance in the presence of a leak is a function of the hydraulic impedance. The leak point position can then be determined by calculating the hydraulic impedance at different points where a leak can be detected [143]. This method is often used for linear pipelines, as the calculation of characteristic impedance may encounter many uncertainties for more complex structures.

4.1.2.2.6. Standing wave difference methods (SWDM)

SWDM is a method that has been used for water transmission in pipelines. An oscillator is used to create sinusoidal excitation at one end of pipeline and measure the head and discharge simultaneously [144]. Every discontinuity of pipeline impedance, which is the ratio between head fluctuation and discharge causes the reflection of incident waves, which create residual standing waves. The distance between the site of the excitation, and discontinuity of pipeline is calculated by examining the respective resonance frequencies. More studies are required for different situations, e.g., with

multiphase flow, unsteady friction, as the pressure response diagrams adds complexity to the model.

Most of the techniques introduced thus far have focused on developing and applying models based on fundamental principles, in detect and localize leaks. Fortunately, over recent decades due to the abundance of continuous measurements collected from different types of sensors, artificial intelligence methods, i.e., those based on machine learning, popularly known as knowledge based methods were developed to monitor pipeline leaks, and a few of these is described next.

4.1.2.3. Methods based on knowledge

4.1.2.3.1. Support vector machine (SVM)

The goal of SVM is to monitor the available parameters values at a number of sensors along the length of the pipeline, to determine if they have deviated from their normal values [131], [145]. The SVM is trained using data collected from leaks of varying sizes at different locations.

4.1.2.3.2. Pattern recognition

This method involves extracting the transient features and recognizing the patterns produced by negative pressure waves during a leak in the pipeline [146]. The features and patterns produced different pumps and valves in the process, is different to those of a leak, and therefore it is easy to classify normal operation to a periods of leaks. This method is also said to provide lower missed detection rates and false alarms. The authors in [147]

demonstrate how the pattern recognition can be utilized to detect leaks in a municipal water supply network, using cluster analysis, and fuzzy pattern recognition.

4.1.2.3.3. Expert system

This system is based on a complex nonlinear distributed parameter control system [148], [149]. The method tries to combine all known data on the process, leak events, and determines when a leak is present. Known data may include experience knowledge, leak patterns, the leak mechanism model, and laws of physics. A breadth search is done to identify the most severe phenomenon, after which a depth-first search is done, completing qualitative diagnosis using experience knowledge to find out when a leak has occurred.

4.1.2.3.4. Artificial Neural Network (ANN)

Another well-known knowledge based technique is ANN. The authors in [150] combine an observer-based method with ANN using a real time transient model (RTTM) composed of partial differential equations, to detect leaks in pipelines. However, they state that this technique is not suitable for multiphase flows, due to their complexity.

A majority of the techniques described thus far were initially designed in to detect leaks in systems that experienced chronic leaks. A discussion on multiphase flow leak detection will now be provided.

4.1.3. Discussion on multiphase flow leak detection

A wide majority of current literature available analyzes leak detection for systems that contain single phase flow. The earliest work that provides a comprehensive review of the different techniques, and also discusses if they are capable of detecting leaks in systems that contain multiphase flow was provided in [151].

4.1.3.1. Concerns associated with multiphase flow

With the increase in the transport lines due to an increase in deep water activities, leak detection in subsea pipelines is an important research area. Multiphase flow contains several issues that make it significantly harder to detect leaks than flowlines that only contain single phase flow. With multiphase flow, density differences between the different phases cause phase separation and different shear stresses on the wall of the pipe, and these flowlines also experience an expansion of the compressible gas phase resulting in a decrease in the pressure. Multiphase flow also experiences an exchange of mass between the different phases. Different flow patterns emerge from the different phases, and understanding the flow pattern is critical to understanding and predicting the pressure gradient along the length of the pipeline.

Fluids produced at the reservoirs, like those in the Gulf of Mexico are subject to an array of conditions. These include multiphase pipelines with high gas-to-oil ratios (GOR), brine, hydrogen sulfide, carbon dioxide, hydrates, paraffin, asphaltene, and sand as well. These variables make it tough to model and study pipelines that experience multiphase flow [152].

4.1.3.2. Extension of single-phase techniques to multiphase flow

The authors in [151] claim that the range of leak sizes detectable by pressure drop and mass balance methods is greatly reduced as the system is highly flow pattern dependent for multiphase flowlines. The report states that leak detection using ultrasonic flow meters in multiphase flowlines is limited to higher gas volume fractions. Multiphase flowlines that utilize vapor-monitoring systems detect leaks, however, these are limited to shallow water depths, and may be unsuitable for subsea flowlines. Multiphase flowlines that utilize mass balance methods are not able to detect and localize leaks, while RTTM and PPA methods seem to perform sufficient well for multiphase flowlines [151]. A recent literature review states that leak monitoring using fiber-optic cables might be the best option currently available. However, they do state that it might not be fiscally conceivable or realistic to expect installation on all pipelines [152].

A demonstration of how a mechanistic model can be developed for leak detection purposes using pressure traverse calculations using the change in inlet pressure, and a change in the outlet flow rate is available [153]. Beggs and Brill's correlations can be utilized to decipher complicated gas-oil two flow mechanism in subsea pipelines. The paper states that outlet flow rate provides a better indicator of a leak than the inlet flow rate, however, the inlet pressure provided better performance with increasing gas compressibility [153]. Gas compressibility studies are also included, and the paper concludes that leaks that occur further upstream, and with larger leak openings are easier to detect using either metric [153].

The authors conclude that for multiphase flowlines there is a need for larger scale experiments, and the use of pressure and temperatures sensors through fiber optic cables for multiphase flowlines shows promise [151]. This conclusion is similar to that reached by the authors in [152] where a hybrid system for through the use of fiber optic cables and computational pipeline monitoring (CPM) may be the most effective method of monitoring leaks in subsea pipelines.

Several conclusions can be made from the works discussed thus far. The selection of the best leak detection technique is application dependent. Multiple authors state that leak detection using fiber optic cables shows promise, but state that installing these along the entire length of the pipeline might not be feasible. Therefore, selection of fiber optic density, i.e., locations to place these fiber optic cables is an area that needs to be investigated further, to ensure reliability in results, while being as cost effective as possible. Reliability in results can be further improved by implementing hybrid monitoring systems. E.g., pressure and temperature measurements and similar data collected through fiber optic cables can be combined with multivariate statistical models and techniques such as PCA, to determine if a process has deviated from normal operating conditions. Akinsete demonstrates how a hybrid model based on real time transient monitoring (RTTM) methods can be combined with intelligence methods based on Big Data analytics in order to detect leaks of 0.1% of nominal flow within two hours [154]. Similarly, Fidaner demonstrates how fiber optic measurements can be combined with neural networks and wavelet transform in order to monitor and analyze multiphase data in real time by calculating flow rates and flow patterns in a wellbores [155]. Worsley compares the leak

detection performance of multiple hybrid methods for both single and multiphase flow, but does highlight the requirement for more testing in the field [156].

4.1.4. Potential methods for multiphase flow leak detection and localization

From a broad overview of existing leak detection and localization technology, several key issues can be identified. Additionally, the development and implementation of a pipeline repair strategy for subsea conditions (more than 3000 m) or in sub-zero temperature arctic conditions near ice formations is challenging. Therefore, it is critical to detect small hydrocarbon leaks in the shortest possible time using effective leak detection and localizations systems. A comprehensive review of recent technologies that show potential for leak detection and localization for metallic pipeline leaks include the following:

- Fiber optic cable including distributed temperature sensing (DTS), distributed acoustic sensing (DAS), and distributed strain sensing (DSS).
- Negative or dynamic pressure wave technology with effective signal to noise ratio (SNR), or statistical methods.
- Real time transient monitoring (RTTM), with sequential probability ratio testing (SPRT).
- Subsea vapor monitoring chronic leak detection.
- CFD modeling supporting leak detection technology.

The three types of fiber optic cable leak detection and localization technology have mainly been applied to pilot experiments and new pipelines, and [157] highlight key risks using DTS or DAS for arctic or subsea conditions. Dynamic pressure wave methods rely on customized SNR filters, and characterize the type of flow, environmental properties, and pipe damping properties [157]. SPRT and RTTM is used for complex pipeline networks for any type of flow conditions and is suited for onshore and offshore applications.

Large or catastrophic leaks greater than 10 mm can be detected using dynamic pressure sensing, whereas medium to small leaks between 4 to 8mm is suited to RTTM and SPRT leak detection and location technology [157]. Pipeline leaks greater than 4 mm for onshore, arctic and subsea conditions were investigated by [157]–[159]. However, there is no published field data available which fully addresses chronic leaks less than 3 mm. The literature shows that no field studies describing complex pipeline networks is available, which uses fiber optic leak detection technology to address deep water pipeline leaks for depths greater than 3000m or in arctic conditions.

The capital expenditure (CAPEX) for fiber optic leak detection and location is high compared to existing leak detection systems, and risk is higher since there are key installation risks related to amplification or repeater units required for strengthening of the reflected light signal as well as provision for maintenance of the pipeline when the fiber optic cables are installed. Additional installation costs for larger pipe bridges are required due to spacing requirements of the fiber optic cable. Dynamic pressure wave technology is ideal to monitor low hazard pipelines e.g. safe water transport and monitoring of large

to medium scaled leaks. SPRT and RTTM has similar accuracy at lower risk compared to fiber optic DTS and is a cheaper alternative to retrofit existing pipeline networks however there is uncertainty for locating or detecting leaks less than 3 mm for deep water conditions greater than 3000 m or arctic conditions.

4.1.5. Concluding remarks on leak detection for multiphase flowlines

The authors conclude that for multiphase flowlines there is a need for larger scale experiments, and the report does state that the use of pressure and temperatures sensors through fiber optic cables for multiphase flowlines shows promise [151]. This conclusion is similar to that reached by the authors in [152] where a hybrid system for through the use of fiber optic cables and computational pipeline monitoring (CPM) may be the most effective method of monitoring leaks in subsea pipelines.

A number of conclusions can be made from the literature examined thus far. The selection of the best leak detection technique is application dependent. Multiple authors state that leak detection using fiber optic cables shows promise, but state that installing these along the entire length of the pipeline might not be feasible. Therefore, selection of fiber optic density, i.e., locations to place these fiber optic cables is an area that needs to be investigated further, to ensure reliability in results, while being as cost effective as possible. Reliability in results can be further improved by implementing hybrid monitoring systems. E.g., pressure and temperature measurements and similar data collected through fiber optic cables can be combined with multivariate statistical models and techniques

such as PCA, in order to determine if a process has deviated from normal operating conditions.

Although the use of fiber optic sensors does show a lot of promise in the area of multiphase flow leak detection, due to limited project budget a simpler low-cost alternative that serves a similar purpose is required. The next section covers design and development of an experimental setup detailing equipment selection, piping and instrumentation diagram (P&ID) and budget.

4.2. Design and Development of Leak Detection Setup

A primary objective of this section was to utilize literature review to guide the design and development of a leak detection setup that could be used to study flow behavior in the event of leaks. The long-term goal of this project is to utilize the experimental leak detection setup as a preliminary tool in assessing applicability of any developed algorithm to transportation pipelines in subsea or arctic conditions. This section presents the experimental design, i.e., equipment selection, piping and instrumentation diagram (P&ID), and budget.

4.2.1. Experimental Design – Equipment Selection

This section will detail the experimental design procedure explaining the reasoning behind the selection of the different components.

4.2.1.1. Pipeline

Pressure drop calculations for a series of different pipeline diameters need to be assessed in order to determine the dimensions of the pipeline to be used.

Pressure drop calculations for the following conditions will be examined:

- Three operating pressures: 2 bar, 3 bar, and 4 bar.
- Four pipeline inner-diameters: 0.5 in, 0.75 in, 1 in, 2 in.
- Two volumetric flow rates: 5 L/s, 10 L/s.

It is important to note that the pipeline inner diameters were selected for preliminary analysis. The final pipeline inner and outer diameters that will be selected will vary depending on the availability in Qatar, and also after analysis of the different scenarios as shown in Section 4.2.1.1.1. The Reynolds number for the above scenarios vary from ~63000 to ~254000 as will be demonstrated shortly.

4.2.1.1.1. Choice of pipeline length

The pressure drop will be measured across a length of 1 meter. The length of the pipeline is directly proportional to the expected pressure drop, i.e., a longer length will correspond to a higher pressure drop. A length of 2 meters was initially proposed, however, due to space limitations in the laboratory, this size was reduced to 1 meter. The total length of the setup is expected to be approximately 4 meters, and this will be further discussed in further detail in Section 4.2.2.

4.2.1.1.2. Differential pressure transducer availability

The choice of the differential pressure transducer has to be carried out in parallel to the selection of the pipeline dimensions, as the dimensions of the pipeline will need to be adjusted in order to fit within the ranges of the differential pressure transducers that are available for use. A list of the available differential pressure transducers and their ranges are provided in Table 7 in both bar and Pascal.

Table 7. List of available differential pressure transducers.

Ranges						Choice
0	25	mbar	0	2500	Pa	A
0	70	mbar	0	7000	Pa	B
0	170	mbar	0	17000	Pa	C
350		mbar	35000		Pa	D
1		bar	100000		Pa	E
2		bar	200000		Pa	F
3.5		bar	350000		Pa	G
7		bar	700000		Pa	H
10		bar	1000000		Pa	I
17.5		bar	1750000		Pa	J
35		bar	3500000		Pa	K
50		bar	5000000		Pa	L
70		bar	7000000		Pa	M

The expected pressure drop for 3 different operating pressures: 2 bar, 3 bar, and 4 bar, are shown in Table 8,

Table 9, and Table 10, respectively. A smooth pipeline was assumed for the friction factor. For each operating pressure range, three different pipeline diameters are examined: 0.5 inch, 0.75 inch, and 1 inch. Calculations for 2 inch pipelines were also carried out. However, since the expected pressure drop is too low for detection by available differential pressure sensors, these results were not included. For each pipeline diameter two different volumetric flow rates were examined as shown. For each scenario at each operating pressure, a match to suitable differential pressure transducer shown in Table 7 was made.

Table 8. Differential pressure calculations (Operating pressure: 2 bar).

Volumetric Flow Rate (L/s)	5	10	5	10	5	10
Reynolds Number	63397	126794	42265	84529	31698	63397
Development Length (m)	0.3529	0.3961	0.4947	0.5553	0.6287	0.7057
Operating Pressure (bar)	2					
Air Density (kg/m3)	2.3384					
Diameter (in)	0.50		0.75		1.00	
Mass Flow Rate (kg/hr)	42.09	84.18	42.09	84.18	42.09	84.18
Fluid velocity (m/s)	39.47	78.94	17.54	35.08	9.87	19.74
Friction factor	0.031					
Differential pressure (Pa)	4446	17785	586	2342	139	556
Sensor Choice	B	D	A	A/B	A	A

Table 9. Differential pressure calculations (Operating pressure: 3 bar).

Volumetric Flow Rate (L/s)	5	10	5	10	5	10
Reynolds Number	95095	190191	63397	126794	47548	95095
Development Length (m)	0.3775	0.4238	0.5293	0.5941	0.6727	0.7551
Operating Pressure (bar)	3					
Air Density (kg/m3)	3.5077					
Diameter (in)	0.50		0.75		1.00	
Mass Flow Rate (kg/hr)	63.14	126.28	63.14	126.28	63.14	126.28
Fluid velocity (m/s)	39.47	78.94	17.54	35.08	9.87	19.74
Friction factor	0.031					
Differential pressure (Pa)	6669	26678	878	3513	208	834
Sensor Choice	B/C	D	A	B	A	A

Table 10. Differential pressure calculations (Operating pressure: 4 bar).

Volumetric Flow Rate (L/s)	5	10	5	10	5	10
Reynolds Number	126794	253587	84529	169058	63397	126794
Development Length (m)	0.3961	0.4446	0.5553	0.6233	0.7057	0.7921
Operating Pressure (bar)	4					
Air Density (kg/m3)	4.6769					
Diameter (in)	0.50		0.75		1.00	
Mass Flow Rate (kg/hr)	84.18	168.37	84.18	168.37	84.18	168.37
Fluid velocity (m/s)	39.47	78.94	17.54	35.08	9.87	19.74
Friction factor	0.031					
Differential pressure (Pa)	8893	35571	1171	4684	278	1112
Sensor Choice	C	E	A	B	A	A

From these results we can observe that a 1 inch pipeline might be too large, as the expected pressure drop values are on the lower end for low flow rates. For a 0.5 inch pipeline a wide range of differential pressure drops are expected for the different flow rates, meaning that multiple differential pressure transducers might need to be purchased. However, for the 0.75 inch pipe, 2-3 differential pressure transducer would cover most of the proposed volumetric flow rates. Therefore, a pipeline diameter closer to 0.75 inches (inner diameter) would seem a reasonable choice to proceed.

4.2.1.1.3. Selection of pipeline and material

Different materials of pipeline exist: brass, copper, stainless steel. In order to obtain results that might be relatable to subsea conditions, stainless steel needs to be selected. Swagelok provides a different pipeline tubing options, and was examined to see if a suitable match could be obtained.

After examining pipeline tubing available from suppliers in Doha, Qatar, a revision in the proposed pipeline inner diameter was made from 0.75 to 0.62 inch. A pipeline of 0.75 inch outer diameter, with tube wall thickness 0.065 inch can be sourced locally in Qatar, and the resulting pipeline inner diameter is 0.62 inches obtained using the following equation:

$$\text{Pipeline Inner Diameter} = \text{Pipeline Outer Diameter} - 2\left(\text{Tube Wall Thickness}\right). \quad (58)$$

Taking into consideration the revised pipeline diameters, the pressure drop calculations were reassessed at operating pressure 2 bar, 3 bar, and 4 bar, and are presented in Table 11, Table 12, and Table 13, respectively.

Table 11. Revised differential pressure calculations (Operating pressure: 2 bar).

Volumetric Flow Rate (L/s)	5	10
Reynolds Number	51126	102253
Development Length (m)	0.4221	0.4738
Operating Pressure (bar)	2	
Air Density (kg/m3)	2.3384	
Diameter (in)	0.62	
Mass Flow Rate (kg/hr)	42.09	84.18
Fluid velocity (m/s)	25.67	51.34
Friction factor	0.031	
Differential pressure (Pa)	1517	6067
Sensor Choice	A	B

Table 12. Revised differential pressure calculations (Operating pressure: 3 bar).

Volumetric Flow Rate (L/s)	5	10
Reynolds Number	76690	153379
Development Length (m)	0.4516	0.5070
Operating Pressure (bar)	3	
Air Density (kg/m3)	3.5077	
Diameter (in)	0.62	
Mass Flow Rate (kg/hr)	63.14	126.28
Fluid velocity (m/s)	25.68	51.34
Friction factor	0.031	
Differential pressure (Pa)	2275	9100
Sensor Choice	A	C

Table 13. Revised differential pressure calculations (Operating pressure: 4 bar).

Volumetric Flow Rate (L/s)	5	10
Reynolds Number	102243	204506
Development Length (m)	0.4738	0.5319
Operating Pressure (bar)	4	
Air Density (kg/m3)	4.6769	
Diameter (in)	0.62	
Mass Flow Rate (kg/hr)	84.18	168.37
Fluid velocity (m/s)	25.67	51.34
Friction factor	0.031	
Differential pressure (Pa)	3033	12133
Sensor Choice	B	C

4.2.1.2. Choice of differential pressure transducer

From the revised pressure drop calculations a decision to purchase choice B for the differential pressure sensor was made using Table 7. Choice B covers a working pressure range of 0 to 7000 Pa, which will cover experimental runs for up to around 10 L/s at 2 bar operating pressure, and a lower flow rates for the higher operating pressures. From literature the difference in pressure drop between no leak and leak condition is around 20-25%, and this was taken into account when deciding which differential pressure

transducer to purchase [160]. The product detail of the selected differential pressure transducer is presented in Table 14.

Table 14. Differential pressure transducer choice.

Product	Differential pressure transducer
Model	PXM409-070HDWUUSBH (Omega)
Range	0 to 70 mbar
Accuracy	± 0.08 %
Instrument Design Pressure	35 bar

4.2.1.3. Choice of dynamic pressure transducer

In addition to the differential pressure measurements, obtaining dynamic pressure measurements on either side of the pipeline leak is of interest, in order to examine if these readings can also be utilized in order to determine if a micro-leak has occurred. Dynamic pressure sensors take high frequency pressure measurements (in the range of kHz). The product detail of the selected dynamic pressure transducer is presented in Table 15.

Table 15. Dynamic pressure transducer choice.

Product	Dynamic pressure transducer
Model	UPS-HSR-B02P5-N (Stork Solutions)
Range	-1 to 2.5 bar
Accuracy	0.15 % FS
Instrument Design Pressure	5 bar

4.2.1.4. Leak modeling: Choice of needle valve

A decision was made to model the leak using a safe high-precision regulating stem tip needle valve. This should allow the engineer running the apparatus to adjust the leak size as desired. Since Swagelok was chosen for tubing, the needle valve was selected from the same company, in order to make it easier to find appropriate fittings to connect the needle valve to the rest of the setup. The needle valve model selected was a "Stainless Steel Integral Bonnet Needle Valve", Swagelok Part Number: SS-18RM8-F8. Appropriate fittings were also selected. In order to safely dispose of the compressed gas venting through this needle valve flexible piping will be utilized.

4.2.1.5. Choice of pressure regulator with general purpose filter and oil filter

The compressed air available in the laboratories at Texas A&M University at Qatar is contaminated with oil particulates due to the compressors being used. Therefore, an oil filter is required in order to eliminate the presence of these oil particulates, so that the

results that are obtained from the experimental setup are not adversely affected. Most oil filters are generally combined with a general purpose filter. Certain vendors provide a combined unit that includes both filters and a pressure regulator as well. Incorporating a pressure regulator with the setup should enable us to obtain different operating pressures.

The following units were purchased:

- Model Number: B84G-6AK-AD1-RMG
    - This is a general purpose filter (5 micron) with a pressure regulator.
- Model Number: F84C-6AD-ADO
    - This is the oil removal filter.
- Model Number: 840014-51KIT
    - This is a quick clamp required to connect the general purpose filter with regulator and the oil removal filter units.

4.2.1.6. Choice of flow and temperature sensor

As it is necessary to determine the density of the gas flowing through the set up, and also to obtain the flow rates to provide a quantitative analysis, flow sensors are required. Instead of having multiple units that measure the temperature and flow throughout the setup, it is possible to have one sensor that measures both. The flow sensor measures the fluid velocity, which can be used to determine the volume flowing through, as the dimensions of the tubing are known.

This sensor will be connected to the rest of the rest up using a cross union and other relevant fittings. The opposite port of this cross union will have a pressure gauge in

order to determine the pressure at that particular point, so that the density of the gas can be calculated.

Two flow and temperature sensors will be installed, one at the start of the pipeline, in order to determine the initial velocity, and a second one at the end of the pipeline in order to determine the final velocity, and flow rate, in order to examine if the leak volume can be identified using the difference between the two volumetric flows. The product detail of the selected dynamic pressure transducer is presented in Table 16.

Table 16. Choice of flow and temperature sensor.

Product	Flow and temperature sensor
Model	FMA1003 (Omega)
Range	0-50.8 m/s (velocity) & -40-121^{o}C (temperature)
Accuracy	1.5% FS (velocity) & 0.5% FS (temperature)
Instrument Design Pressure	4.13 bar

4.2.1.7. Choice of pressure gauges

In order to compute the density at the start of the pipeline, in addition to the flow and temperature sensor, a pressure gauge is also required. As with the flow sensor, two pressure gauges will be installed, one at the start of the pipeline, and one at the end of the pipeline. The product detail of the analog pressure gauge is presented in Table 17.

Table 17. Choice of analog pressure gauge.

Product	Pressure gauge (analog)
Model	PGC-25B-[*] (Omega)
Range	0 to 60 psi
Accuracy	3% (over first and last 10% of range), 2% over remainder
Instrument Design Pressure	6.20 bar

Additionally, digital pressure gauges was purchased. The product detail of the selected dynamic pressure transducer is presented in Table 18.

Table 18. Choice of digital pressure gauge.

Product	Pressure gauge (digital)
Model	DPG8001-60 (Omega)
Range	0 to 60 psi
Accuracy	0.25% FS terminal point
Instrument Design Pressure	33 bar

4.2.1.8. Choice of additional needle valves for pressure build up and flow management

A needle valve after the pressure regulator is required in order to control the amount flowing through the pipeline. A valve at the end of the pipeline is required in order to build up pressure in the pipeline. Therefore, two additional needles will be purchased in order to accommodate these requests. The model for these needle valves is Swagelok Part Number: SS-18RS12.

4.2.2. Piping and Instrumentation Diagram (P&ID)

The proposed experimental setup is 4.3 m in length, with 0.62 in inner diameter, and 0.75 in outer diameters for most of the flowline. The pipeline and most fittings are stainless steel Swagelok components.

The compressed air supply in the laboratory at Texas A&M University at Qatar will be connected to the developed pipeline utilizing flexible piping. A pressure relief valve will be installed right after the tap from the building supply, set at 7.1 bar. The first unit at the start of the pipeline will be the pressure regulator, with the general-purpose filter, and oil filter. Another pressure relief will be installed right after this combination unit, set at 2.2 bar. This will be followed by a needle valve to adjust the flow rate of the compressed air through the pipeline. After 90 cm a flow/temperature sensor and a pressure gauge will be connected to the flowline using a cross union. After a development length of 90 cm, a dynamic pressure sensor will be utilized to collect high frequency pressure measurements. The differential pressure drop across the proposed length of pipeline (1 m) will be measured using a high frequency differential pressure sensor. Midway through the 1m length, a needle valve will be connected to the setup using a T-union, in order to model the leak and control the amount leaking from the pipeline. The current plan is to quantify the leak using a bubble flow meter, but other options are also being investigated. When the bubble flow meter is not in use, flexible piping will most like be used in order to vent the leaked gas to the fume hood. An additional dynamic pressure sensor will be connected to the pipeline in order to take measurements after the differential pressure sensor. This will be followed by a second temperature/flow sensor with a pressure gauge connected to

the pipeline using a cross union. The final component on the pipeline will be a second needle valve, in order to build up pressure if and when required. A short length of pipeline will then be available at the end of the pipeline before being connected to flexible piping in order to return the compressed air to the fume hood for safety. The piping and instrumentation diagram (P&ID) and general arrangement drawing for the experimental leak detection setup are provided in Figure 34 and Figure 35, respectively.

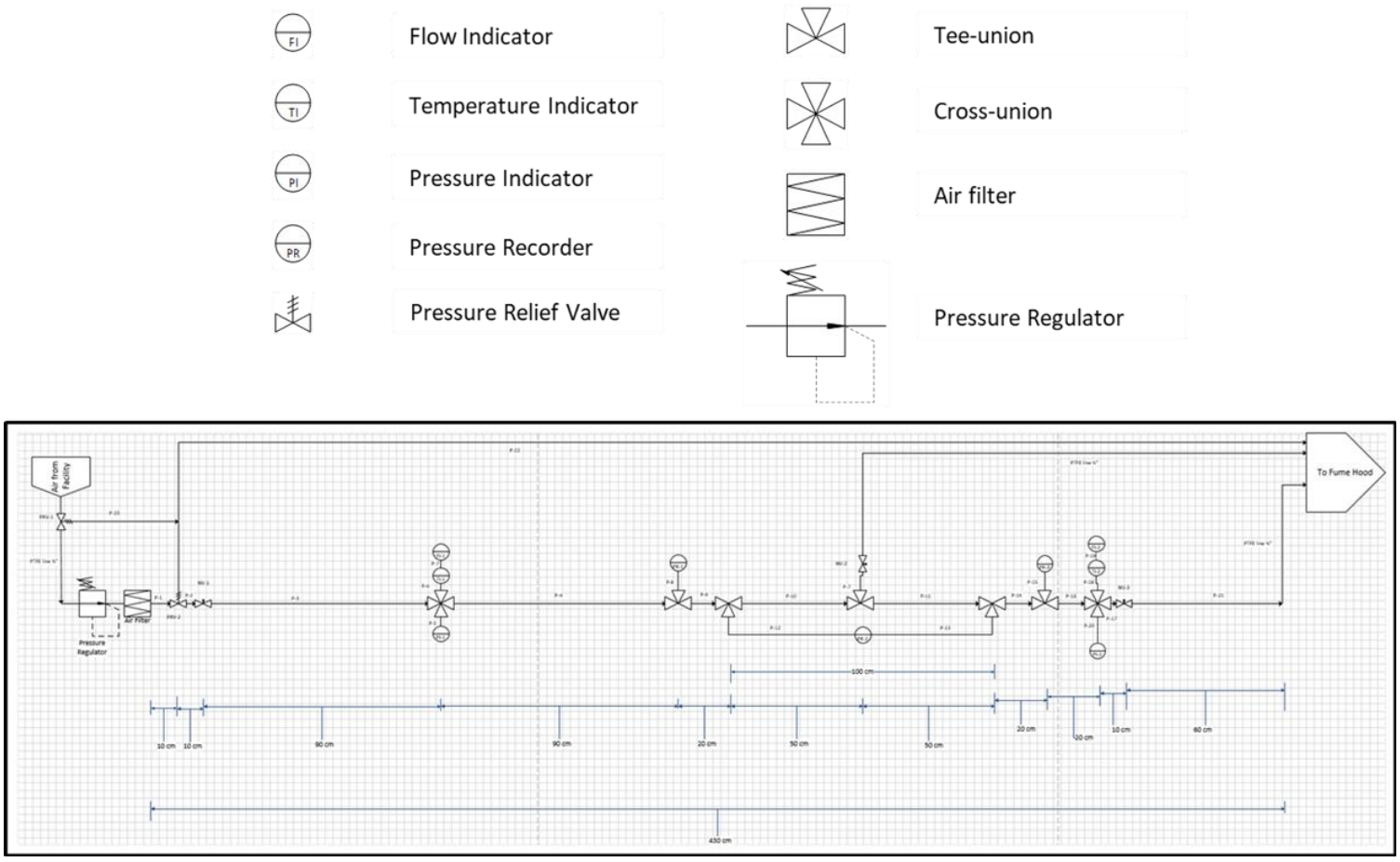

Figure 34. Piping and instrumentation diagram (P&ID) - Experimental leak detection setup.

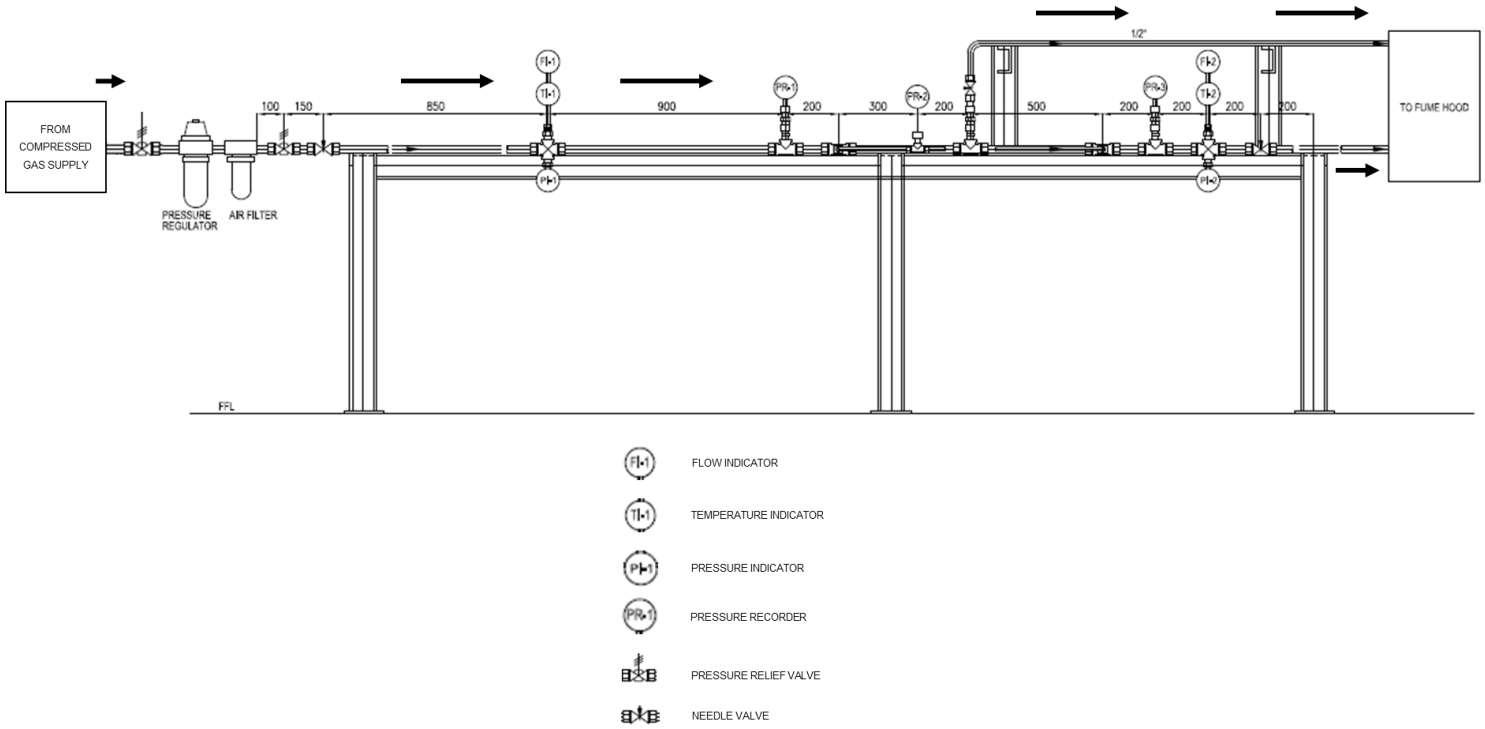

Figure 35. General arrangement drawing - Experimental leak detection setup.

4.2.3. Budgeting and expenses

The previous sections listed the different components and the required arrangement. A budget is required in order to illustrate how much such a project would cost.

4.2.3.1. Total estimated budget

Table 19 provides a budget breakdown of the total budget. It should be noted that transportation and import costs have not been included, and therefore an approximate buffer of around 30% might be required. It is also possible that additional fittings may be required, and flexible piping also needs to be purchased. Therefore, the total actual budget could be closer to **~$12000**.

Table 19. Budget breakdown of total estimated budget.

Setup	**Cost (USD)**
Dynamic pressure setup	1413.86
Differential pressure setup	1497.26
Needle valve setup (leak)	388.55
Tubing (2 6m length pipelines)	1049.86
Temperature / flow meter setup	3239.40
Pressure regulator with filters setup	750.00
Additional needle valves (for flow control / pressure build up)	800.00
Total (without transport/duty)	**9138.93**

As the setup is still under construction, the following section presents a study on flow behavior carried out using data obtained from an existing multiphase flow-loop.

4.3. Classification of sensor measurements from non-Newtonian fluids using batch and continuous analysis of data

Due to technological advancements, industrial processes and transportation pipelines are able to collect an abundance of data from sensors. Although the abundant availability of data is beneficial, interpreting these measurements and using them for process monitoring purposes is essential in order to ensure fluid characteristics are being

maintained within expected limits. Statistical process monitoring methods provide an increasingly reliable means of achieving this goal [18].

Like all equipment, sensors can fail over time, and therefore it is crucial for measures to be in place to ensure that processes are being efficiently monitored. For example, redundancy can be created, and measurements from differential pressure sensors can be utilized in order to track changes in flow rate, in the absence or malfunction of a flow meter. However, these sensors can often be masked by noise, making it difficult to classify the flow rate. Therefore, one objective of this work is to investigate the possibility of using only differential pressure measurements to classify non-Newtonian fluids despite noisy sensor measurements. The classification will be carried out using batch and online data analysis methods.

In order to examine if differential pressure measurements from two different batches, i.e., flow rates, have significant differences in the mean and/or variance, different statistical tests can be employed. The two-sample t-test has often been used in order to test for differences in the mean, while F-test for equality of variances has been used to test for differences in variance [44]. For the case of online analysis of data from continuous processes, a number of monitoring charts are available, and for this work the generalized likelihood ratio (GLR) and exponential likelihood ratio (ELR) charts were chosen as they have shown promising detection and classification capabilities in recent literature [13], [36], [37], [45], [161].

The multiphase laboratory at Texas A&M University at Qatar contains a multiphase flow-loop, capable of running fluids under a number of different conditions:

single phase, multi-phase, and at inclinations as well, in order to replicate actual drilling scenarios [162]. The flow-loop contains a number of different sensors that allow flow rates, temperatures, and pressures to be measured.

The classification of measurements will be carried out in two parts: treating the measurements from different flowrates as data from different batches, and treating the measurements as online data from a continuous process with transitions also available from one flow rate to the next. The non-Newtonian fluid is Flowzan biopolymer which is frequently used in oil and gas field drilling and production operations [163].

The remainder of this section is structured as follows. A brief introduction to methods used to classify the differential pressure measurements using batch and continuous analytical methods is initially provided. Illustrative examples using non-Newtonian fluid Flowzan are the presented, including a discussion on the results and findings. Concluding remarks are then presented.

4.3.1. Statistical tests to classify data using batch analysis and continuous analysis

4.3.1.1. Statistical tests for batch analysis

For the first case, where differential pressure measurements are obtained from different batches, two tests will be utilized. The two-sample t-test is a well-established test that compares two population means to establish if they are significantly different, while the F-test for equality of variances is used in order to determine if two populations have significantly different variances [44].

For a case where the null hypothesis is defined as $H_0 = \mu_1 - \mu_2 = \Delta_0$, where a test statistic is required to determine if there is a significant difference in the population means the two-sample t-test can be used [44]:

$$T_0^* = \frac{\bar{X}_1 - \bar{X}_1 - \Delta_0}{\sqrt{\frac{S_1^2}{n_1} + \frac{S_2^2}{n_2}}}, \tag{59}$$

where, $\bar{X}$, S^2, and *n* represent the sample mean, sample variance, and sample size, respectively. Similarly, the F-test for equality of variance can be utilized in order to determine if two populations have significantly different variances [44]:

$$F = \frac{s_1^2}{s_2^2}. \tag{60}$$

For both tests thresholds available in literature are used to determine if the null hypothesis is rejected, i.e., there is a significant difference in the mean or variance.

4.3.1.2. Statistical tests for continuous analysis

For the second case, where differential pressure measurements are collected under continuous operation there are a number of statistical control charts that can be utilized. Shewhart developed a control chart in the 1920s in order to monitor and identify changes primarily in the process mean [16], [17]. The Shewhart chart only takes into account sensors measurements at a given time instant [18], [164]. For online analysis, control charts taking into account process memory have shown improved performance, and these include the exponentially weighted moving average (EWMA), and cumulative sum

(CUSUM) chart [165]–[167]. More recently, the generalized likelihood ratio (GLR) and exponential likelihood ratio (ELR) charts, based on statistical hypothesis testing fundamentals, have demonstrated vastly improved fault detection performance [13], [37], [45], [46].

Statistical hypothesis testing methods function by utilizing training data in order to establish what the distribution, and relevant parameters, i.e., process mean and variance are expected to be under normal conditions. In statistical theory, measurements collected under these conditions fall under the null hypothesis and can be used to establish detection thresholds or limits for the different parameters. Observations assumed to be significantly different to the parameters established by the null hypothesis, are assumed to follow an alternate hypothesis. GLR methods function by utilizing the concept of maximum likelihood estimates (MLEs), in order to estimate the parameters of the observations collected under testing conditions, as these parameters are unknown. The GLR method is said to provide the best detection rate, for a fixed false alarm rate, and this has been demonstrated through different works in literature [13], [36], [168], [169].

In this work the GLR technique will be utilized in order to train a model by using differential pressure measurements collected under different operating flow rates to compute thresholds for the different operation regions (flow rates). The model is then utilized in order to classify data collected under test conditions by running multiple GLR charts with the different thresholds in parallel. The GLR chart will only be used to determine if there are changes in the mean. As the variance of a single observation is undefined, the GLR chart designed to detect shifts in the variance performs poorly and

cannot be utilized. Literature demonstrates that a likelihood ratio chart that incorporates process memory (exponentially weighted) is capable of detecting shifts in the variance when only single observations are available at a given time instant, and will therefore be utilized to track differences in the variance [161]. The exponential likelihood ratio (ELR) technique will be utilized in order to train a model to detect changes in the variance of the differential pressure measurements in the same way the GLR technique was used to train a model to detect changes in the mean.

The ELR test statistic designed to detect shifts in the variance is defined as follow [161]:

$$ELR_t = v_t - \ln(v_t), \quad t = 1, 2, \ldots, \tag{61}$$

where, $v_t = \lambda S_t^{*2} + (1-\lambda) v_{t-1}$, $S_t^{*2} = \sum_{j=1}^{n} (x_{tj} - u_0)$, $u_0 = 0$, $v_0 = 1$, and λ is the smoothing parameter that can be assigned a value between 0 and 1. The threshold for the ELR chart can also be computed empirically using training data, or through look up tables available in literature [13].

The illustrative example presented in this section will be analyzed using two data sets using differential pressure measurements collected under single phase flow conditions and multiphase phase flow sections in Sections 4.3.2.1 and 4.3.2.2, respectively. Batch and continuous analysis will be presented for either flow condition.

4.3.2. Illustrative Example

4.3.2.1. Single phase flow conditions

A sample of the differential pressure measurements utilized in order to train the statistical model and charts for both batch and continuous flow cases for single phase flow is illustrated in Figure 36. The flow rates of Flowzan (0.075% wt) in the different regions are 208, 219, and 229 kg/min, respectively. The increases in the flow rate are approximately 5%, and as can be noted from Figure 36 for certain regions it is difficult to visually tell the difference with certainty if there are changes in the mean and variance, as certain observations from two different regions (see Region 1 and 2) sometimes cover the same range.

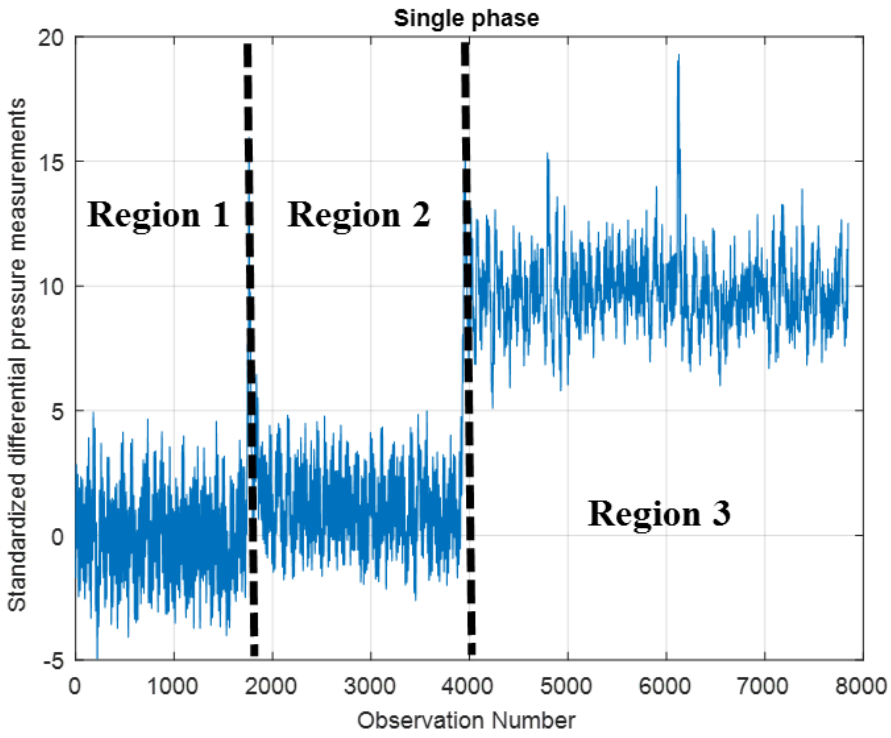

Figure 36. Time series evolution of differential pressure measurements for single phase flow.

4.3.2.1.1. Batch analysis – Single phase flow

Treating measurements collected from three different regions as batch data from different operating flow rates, the two-sample t-test is used in order to determine if the batches have means that have a statistically significant difference, and the F-test for equality of variance is used in order to determine if the batches have variances that that have a statistically significant difference. Utilizing testing data from each region in order to compute mean and variance values for all three regions, they can be compared to the

mean and variance for observations collected under training conditions, i.e., the null hypothesis, in order to determine if they have a statistically significant difference. The results for the two-sample t-test are demonstrated in Table 20, where a value of 0 indicates that the null-hypothesis was not violated, and a value of 1 indicates that the alternate hypothesis is true, i.e., meaning that the means are signficantly different. Similarly, the results for the F-test for quality of variances is demonstrated in Table 21.

Table 20. Decision matrix - Two-sample t-test (single phase flow).

Region		**Training**		
		1	**2**	**3**
Testing	**1**	0	1	1
	2	1	0	1
	3	1	1	0

Table 21. Decision matrix - F-test for equality of variance (single phase flow).

Region		**Training**		
		1	**2**	**3**
Testing	**1**	0	1	1
	2	1	0	1
	3	1	1	0

Utilizng only the differential pressurement measurements, Table 20 shows that the two-sample t-test is able to conclude that there are significant differences in the mean for data collected under different operating flow rates, while Table 21 shows that the F-test for equality of variances is able to conclude that there are significant differences in the mean for data collected under different opereating flow rates. This indicates that both tests are able to efficiently classify differential pressure measurements according to their operating flow rate for single phase flow despite noisy sensor measurements.

4.3.2.1.2. Continuous analysis – single phase flow

Similar to the batch analysis, for continuous operation training data is used from each region to train the GLR and ELR chart to monitor changes in the mean and variance, respectively. The performance of the GLR chart used to monitor changes in the mean is illustrated in Figure 37. Figure 37 (a) shows the GLR threshold obtained when using training data from Region 1, while the GLR thresholds in Figure 37 (b) and (c) are trained using data from Regions 2 and 3 respectively. If a violation in a particular threshold is present, the data does not belong to the class used to train that particular threshold. A zoom of each plot is included to demonstrate if and when the threshold is violated. Although, there is a delay in detection in the transition region between different flow rates, the GLR chart is able to reasonably determine which class of flow rate a particular differential pressure reading belongs to by only monitoring the shift in the mean.

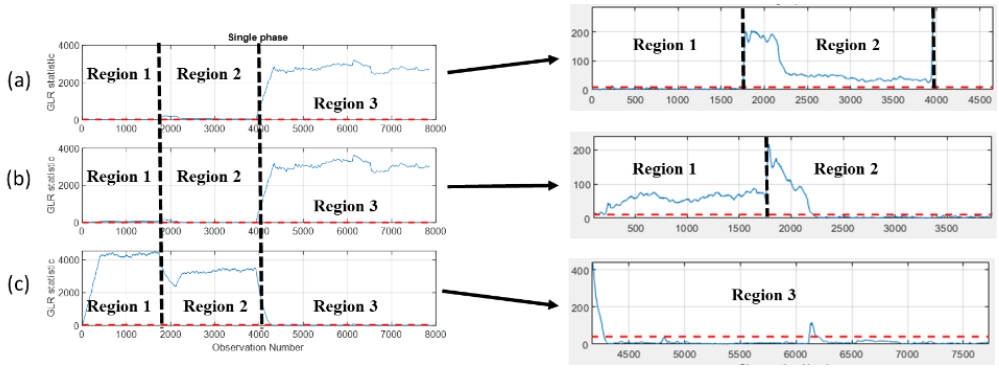

Figure 37. GLR chart to monitor changes in the mean (single phase flow).

Similarly, the performance of the ELR chart used to monitor changes in the variance is illustrated in Figure 38. Figure 38 (a) shows the ELR threshold obtained when using training data from Region 1, while the ELR thresholds in Figure 38 (b) and (c) are trained using data from Regions 2 and 3, respectively. A zoom of each plot is included to demonstrate if and when the threshold is violated. The ELR chart is able to reasonably determine which class of flow rate a particular differential pressure reading belongs to by only monitoring the shift in the variance.

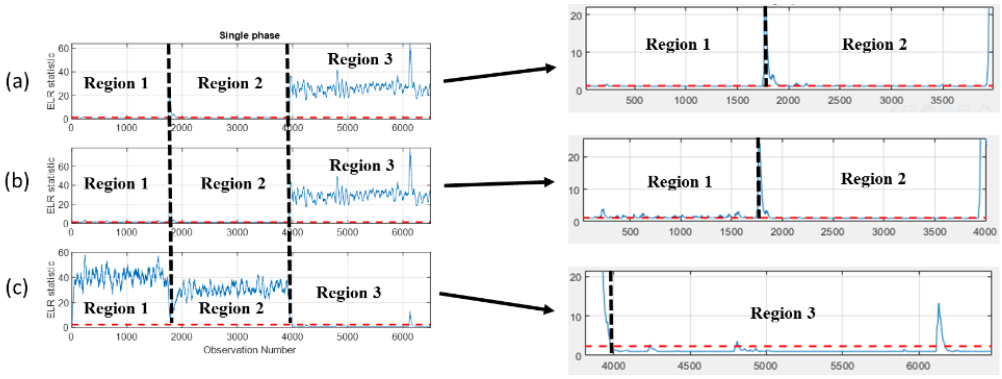

Figure 38. ELR chart to monitor changes in the variance (single phase flow).

These results deomonstrate that both the GLR and ELR tests are able to efficiently classify differential pressure measurements according to their operating flow rate for single phase flow despite noisy sensor measurements.

4.3.2.2. Multiphase flow conditions

A sample of the differential pressure measurements utilized in order to train the statistical model and charts for both batch and continuous flow cases for multiphase flow is illustrated in Figure 39. As in the single-phase flow condition, the flow rates of Flowzan (0.075% wt) in the different regions are 208, 219, and 229 kg/min, respectively, with a fixed flow rate of air introduced to all regions. The increases in the liquid flow rate are approximately 5%, and as can be noted from **Error! Reference source not found.** for c ertain regions it is difficult to visually tell the difference with certainty if there are changes in the mean and variance, as certain observations from two different regions (see Region 2 and 3) cover the same range.

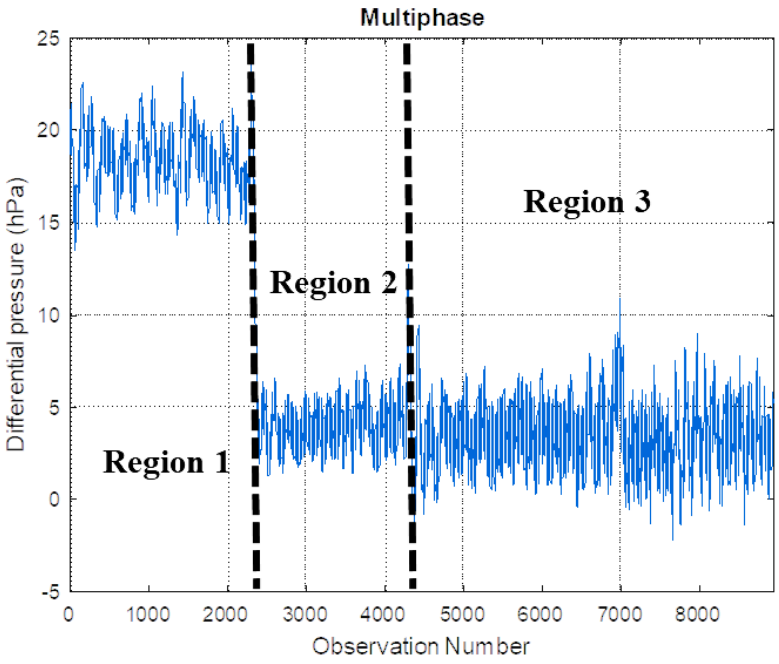

Figure 39. Time series evolution of differential pressure measurements for multiphase flow.

4.3.2.2.1. Batch analysis – Multiphase flow

The results for the two-sample t-test are demonstrated in Table 22, where a value of 0 indicates that the null-hypothesis was not violated, and a value of 1 indicates that the alternate hypothesis is true, i.e., meaning that the means are signficantly different. Similarly, the results for the F-test for quality of variances is demonstrated in Table 23. Utilizng only the differential pressurement measurements, Table 22 shows that the two-sample t-test is able to conclude that there are significant differences in the mean for data collected under different operating flow rates, while Table 23 shows that the F-test for equality of variances is able to conclude that there are significant differences in the mean

for data collected under different opereating flow rates. As with the batch analysis case for single phase flow. This indicates that both tests are able to efficiently classify differential pressure measurements according to their operating flow rate for multiphase flow despite noisy sensor measurements.

Table 22. Decision matrix - Two sample t-test (multiphase flow).

Region		**Training**		
		1	**2**	**3**
Testing	**1**	0	1	1
	2	1	0	1
	3	1	1	0

Table 23. Decision matrix - F-test for equality of variances (mulitphase flow).

Region		**Training**		
		1	**2**	**3**
Testing	**1**	0	1	1
	2	1	0	1
	3	1	1	0

4.3.2.2.2. Continuous analysis – Multiphase flow

The performance of the GLR chart used to monitor changes in the mean is illustrated in Figure 40. Figure 40 (a) shows the GLR threshold obtained when using training data from Region 1, while the GLR thresholds in Figure 40 (b) and (c) are trained using data from Regions 2 and 3 respectively. A zoom of each plot is include to demonstrate if and when the threshold is violated. Although, there is a delay in detection in the transition region between different flow rates, the GLR chart is able to reasonably determine which class of flow rate a particular differential pressure reading belongs to by only monitoring the shift in the mean.

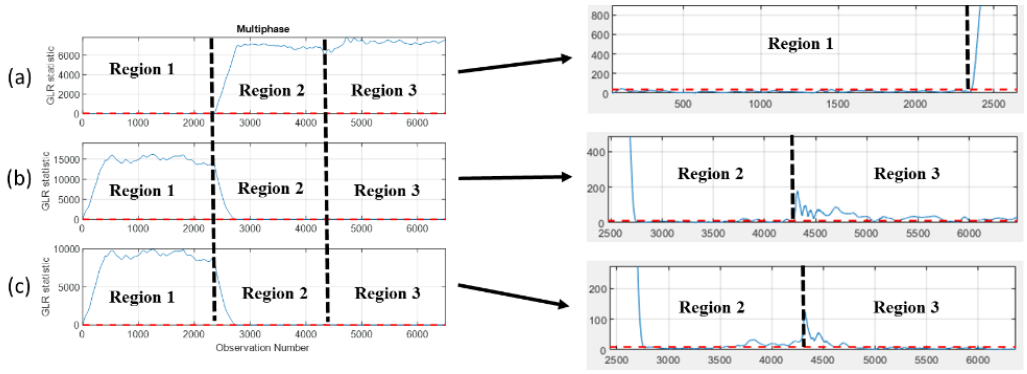

Figure 40. GLR chart to monitor changes in the mean (multiphase flow).

Similarly, the performance of the ELR chart used to monitor changes in the variance is illustrated in Figure 41. Figure 41 (a) shows the ELR threshold obtained when using training data from Region 1, while the ELR thresholds in Figure 41 (b) and (c) are trained using data from Regions 2 and 3, respectively. A zoom of each plot is include to demonstrate if and when the threshold is violated. Once again, although, there is a delay

in detection in the transition region between different flow rates, the ELR chart is able to reasonably determine which class of flow rate a particular differential pressure reading belongs to by only monitoring the shift in the variance.

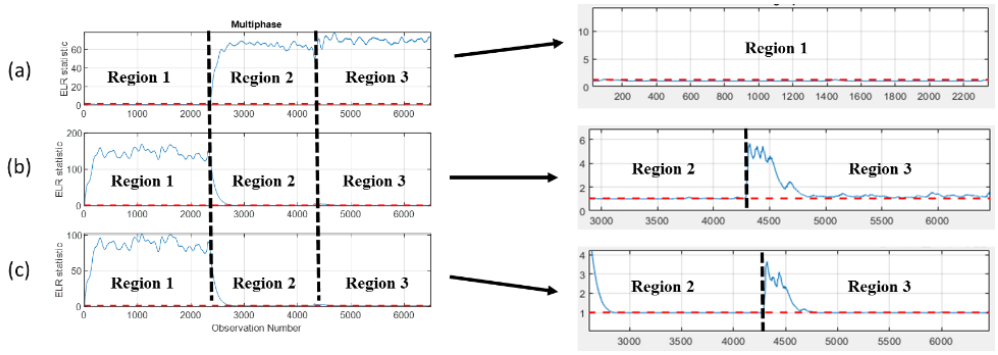

Figure 41. ELR chart to monitor changes in the variance (multiphase flow).

These results deomonstrate that both the GLR and ELR tests are able to efficiently classify differential pressure measurements according to their operating flow rate for single phase flow despite noisy sensor measurements.

4.3.2.3. Discussion on the effect of contamination of noise and/or use of low quality sensors

Although, for the illustrative example utilized in this particular work, classification of flow rates using just the differential pressure measurements provided reliable results, in certain cases it may be possible that the use of low-quality or low-frequency sensors contaminates the data with excessive amounts of noise, making classification problematic. For such cases the authors propose using noise filtering methods such as multiscale

wavelet-based methods, in order to pre-treat the data, before employing the approach presented in this work [35].

4.3.3. Concluding remarks on the classification of sensor measurements from non-Newtonian fluids using batch and online analysis of data

Different statistical methods were utilized in this work in order to assist with the classification of different operating flow rates using only differential pressure measurements. For batch analysis, it was demonstrated that the two-sample t-test and the F-test for equality of variances was sufficient in determining if there was a statistically significant difference in the mean and variance in differential pressure measurements for different operating flow rates, for both single phase and multiphase flow conditions. Similarly, for online analysis of data, it was demonstrated that the GLR and ELR charts could be utilized to classify different operating flow rates of the non-Newtonian fluid using only the current differential pressure measurements to monitor the mean and variance, respectively. These results were obtained despite the presence of noise in the measurement data.

This is advantageous as the redundancy in measurements enables the process engineer to utilize additional sensor measurements, such as differential pressure, in order to determine if there are changes in the flow rate. This redundancy is useful in process monitoring as it enables the process engineer to observe changes in the process when sensors and meters, such as the flow meter are malfunctioning. These results were obtained for an increase in the flow rate of approximately 5%. Although this change is

relatively small, one direction of further work is the exploration of the limitations of the different statistical monitoring charts, such as the GLR technique and other control charts.

It is possible that non-Newtonian fluids can have behavior that is unpredictable under different flow conditions, therefore, a potential direction for future work is to explore the applicability of the proposed techniques for a wider range of operating flow rates, and working fluids.

In this work sensor readings from only a differential pressure sensor were utilized. In reality, for different processes a variety of different sensors can be utilized to measure different quality variables, i.e., temperature etc. The different quality variables are often correlated, and models that utilize the correlation between different variables, e.g., principal component analysis (PCA), can be developed in order to build classification models.

5. CONCLUSIONS

5.1. Summary of contributions

This dissertation sought to design and develop monitoring algorithms for fault detection, diagnosis, and classification, and equipment degradation tracking.

In Section 2, multiple hybrid data-based monitoring algorithms were developed to provide enhanced fault detection, diagnosis, and classification performance. Multiscale principal component analysis (MSPCA) based Generalized Likelihood Ratio (GLR) algorithms were developed to combine the ability of MSPCA to handle data that are noisy, correlated, and non-Gaussian through multiscale wavelet-based representation, with the superior fault detection and classification capabilities of the GLR technique. Fault detection of nonlinear data was accomplished through the utilization of kernel principal component analysis (KPCA) based GLR algorithms that were able to model the nonlinearity through utilization of a high dimensional feature space. Principal component analysis (PCA) based GLR algorithms were developed to highlight the importance of designing and selecting the appropriate GLR technique for your particular monitoring application.

In Section 3, a novel state estimation driven dynamic contour profile-based monitoring algorithm was developed in order to track equipment degradation in multiple operating regimes. The computational simplicity and practical applicability were demonstrated through illustrative examples, both simulated and experimental, to monitor fouling in heat exchangers. This section provided an efficient solution to mitigate

economic losses that cause industries in the United States and the world to lose billions of dollars per annum.

In Section 4, a detailed literature review of chronic leak detection and diagnosis methods for subsea and arctic conditions was used in order to guide the design and development of an experimental setup for leak detection. Dynamic pressure sensor measurements of a non-Newtonian fluid were then utilized in order to classify and distinguish data from multiple operating regimes, i.e., flow rates, using different statistical techniques for batch and continuous analysis of data.

5.2. Future research directions

In Section 2 of this dissertation multiple hybrid data-based monitoring algorithms were developed for fault detection, diagnosis, and classification purposes. Although, each algorithm demonstrated superior performance over existing conventional algorithms, more work is required in order to develop more generalized algorithms, with computational simplicity and decreased complexity, to encourage implementation by broader engineering industries.

In Section 3 of this dissertation an efficient algorithm to monitor equipment degradation was developed. Although, the practical applicability of the algorithm was highlighted through both simulated and real data to track fouling in heat exchangers, this work can lead to a number of interesting contributions with regards to equipment degradation tracking and maintenance for the broader engineering industry. One possible avenue for further work includes the extension of the algorithm to track catalyst

deactivation in multiple operating in a fluidized bed reactor. Another possible avenue for further work includes extension of the algorithm to track equipment degradation in multiple process units, such as heat exchanger networks and carbon capture, utilization, and sequestration (CCUS) networks. Extension of the algorithm to such applications would enable the design and development of optimal maintenance and cleaning schedules considering a number of factors, including economic (operational and capital), safety, and environmental related costs.

In Section 4 of this dissertation the design and development of an experimental setup for chronic leak detection was presented. As this setup was designed to monitor single phase flow it needs to be modified in order to monitor flow for multiphase flow conditions.

Finally, it is important to note that the monitoring algorithms developed in this dissertation have been applied for a wide variety of applications. The development of a software package with a simple graphical user interface (GUI) would increase popularity and interest from the broader academic and industrial communities, thereby encouraging and ensuring implementation in practice.

REFERENCES

[1] W. A. Shewhart, “Economic Quality Control of Manufactured Product,” *Bell Syst. Tech. J.*, vol. 9, no. 2, pp. 364–389, Apr. 1930, doi: 10.1002/j.1538-7305.1930.tb00373.x.

[2] W. A. Shewhart, “Application of statistical methods to manufacturing problems,” *J. Franklin Inst.*, vol. 226, no. 2, pp. 163–186, Aug. 1938, doi: 10.1016/S0016-0032(38)90436-3.

[3] W. A. Shewhart, *Statistical Method from the Viewpoint of Quality Control*, 1st ed. Washington, DC: The Graduate School, The Department of Agriculture, 1939.

[4] V. Venkatasubramanian, R. Rengaswamy, K. Yin, and S. N. Kavuri, “A review of process fault detection and diagnosis: Part I: Quantitative model-based methods,” *Comput. Chem. Eng.*, vol. 27, no. 3, pp. 293–311, Mar. 2003, doi: 10.1016/S0098-1354(02)00160-6.

[5] V. Venkatasubramanian, R. Rengaswamy, and S. N. Kavuri, “A review of process fault detection and diagnosis: Part II: Qualitative models and search strategies,” *Comput. Chem. Eng.*, vol. 27, no. 3, pp. 313–326, Mar. 2003, doi: 10.1016/S0098-1354(02)00161-8.

[6] V. Venkatasubramanian, R. Rengaswamy, S. N. Kavuri, and K. Yin, “A review of process fault detection and diagnosis: Part III: Process history based methods,” *Comput. Chem. Eng.*, vol. 27, no. 3, pp. 327–346, Mar. 2003, doi: 10.1016/S0098-1354(02)00162-X.

[7] H. N. Nounou and M. N. Nounou, “Multiscale fuzzy Kalman filtering,” *Eng. Appl. Artif. Intell.*, vol. 19, no. 5, pp. 439–450, Aug. 2006, doi: 10.1016/j.engappai.2005.11.001.

[8] J. A. Delgado-Aguiñaga and G. Besançon, “EKF-based leak diagnosis schemes for pipeline networks,” *IFAC-PapersOnLine*, vol. 51, no. 24, pp. 723–729, 2018, doi: 10.1016/j.ifacol.2018.09.655.

[9] C. Cao, M. Li, Y. Li, and Y. Sun, “Intelligent fault diagnosis of hot die forging press based on binary decision diagram and fault tree analysis,” *Procedia Manuf.*, vol. 15, pp. 459–466, 2018, doi: 10.1016/j.promfg.2018.07.244.

[10] S. Yin, S. X. Ding, A. Haghani, H. Hao, and P. Zhang, “A comparison study of basic data-driven fault diagnosis and process monitoring methods on the benchmark Tennessee Eastman process,” *J. Process Control*, vol. 22, no. 9, pp. 1567–1581, 2012, doi: 10.1016/j.jprocont.2012.06.009.

[11] F. Harrou, M. N. Nounou, and H. N. Nounou, “Detecting abnormal ozone levels using PCA-based GLR hypothesis testing,” in *2013 IEEE Symposium on Computational Intelligence and Data Mining (CIDM)*, 2013, pp. 95–102, doi: 10.1109/CIDM.2013.6597223.

[12] M. Kano *et al.*, “Comparison of statistical process monitoring methods: application to the Eastman challenge problem,” *Comput. Chem. Eng.*, vol. 24, no. 2–7, pp. 175–181, Jul. 2000, doi: 10.1016/S0098-1354(00)00509-3.

[13] M. R. Reynolds and J. Lou, “An Evaluation of a GLR Control Chart for Monitoring the Process Mean,” *J. Qual. Technol.*, vol. 42, no. 3, pp. 287–310, Jul. 2010, doi:

10.1080/00224065.2010.11917825.

[14] P. Guo and D. Infield, “Wind turbine tower vibration modeling and monitoring by the nonlinear state estimation technique (NSET),” *Energies*, vol. 5, no. 12, pp. 5279–5293, 2012, doi: 10.3390/en5125279.

[15] M. Stafford and N. Williams, “Pipeline leak detection study,” London, UK, 1996.

[16] M. Z. Sheriff and M. N. Nounou, “Improved fault detection and process safety using multiscale Shewhart charts,” *J. Chem. Eng. Process Technol.*, vol. 08, no. 02, pp. 1–16, 2017, doi: 10.4172/2157-7048.1000328.

[17] W. A. Shewhart, “Quality Control Charts,” *Bell Syst. Tech. J.*, vol. 5, no. 4, pp. 593–603, Oct. 1926, doi: 10.1002/j.1538-7305.1926.tb00125.x.

[18] D. C. Montgomery, *Introduction to Statistical Quality Control*, 7th ed. Hoboken, NJ: John Wiley & Sons, Inc., 2013.

[19] S. W. Roberts, “Control Chart Tests Based on Geometric Moving Averages,” *Technometrics*, vol. 1, no. 3, pp. 239–250, Aug. 1959, doi: 10.1080/00401706.1959.10489860.

[20] J. S. Hunter, “The Exponentially Weighted Moving Average,” *J. Qual. Technol.*, vol. 18, no. 4, pp. 203–210, Oct. 1986, doi: 10.1080/00224065.1986.11979014.

[21] E. S. Page, “Continuous Inspection Schemes,” *Biometrika*, vol. 41, no. 1–2, pp. 100–115, Jun. 1954, doi: 10.1093/biomet/41.1-2.100.

[22] E. S. Page, “Control charts with warning lines,” *Biometrika*, vol. 42, no. 1–2, pp. 243–257, 1955, doi: 10.1093/biomet/42.1-2.243.

[23] J. F. MacGregor and T. Kourti, “Statistical process control of multivariate

processes," *Control Eng. Pract.*, vol. 3, no. 3, pp. 403–414, Mar. 1995, doi: 10.1016/0967-0661(95)00014-L.

[24] W. H. Woodall and M. M. Ncube, "Multivariate CUSUM Quality-Control Procedures," *Technometrics*, vol. 27, no. 3, p. 285, Aug. 1985, doi: 10.2307/1269710.

[25] M. C. Testik, G. C. Runger, and C. M. Borror, "Robustness properties of multivariate EWMA control charts," *Qual. Reliab. Eng. Int.*, vol. 19, pp. 31–38, 2003, doi: 10.1002/qre.498.

[26] H. Yamamoto *et al.*, "Dimensionality reduction for metabolome data using PCA, PLS, OPLS, and RFDA with differential penalties to latent variables," *Chemom. Intell. Lab. Syst.*, vol. 98, no. 2, pp. 136–142, 2009, doi: 10.1016/j.chemolab.2009.05.006.

[27] J. Jiao, J. Zhang, and H. R. Karimi, "A partial robust M-regression-based prediction and fault detection method," *Abstr. Appl. Anal.*, vol. 2014, 2014, doi: 10.1155/2014/304754.

[28] I. T. Joliffe, *Principal Component Analysis*, 2nd ed. New York, NY: Springer-Verlag, 2002.

[29] F. Harrou, M. N. Nounou, and H. N. Nounou, "Enhanced monitoring using PCA-based GLR fault detection and multiscale filtering," in *2013 IEEE Symposium on Computational Intelligence in Control and Automation (CICA)*, 2013, pp. 1–8, doi: 10.1109/CICA.2013.6611656.

[30] E. C. M. Nascimento and J. B. L. Martins, "Pharmacophoric Profile: Design of New

Potential Drugs with PCA Analysis," in *Principal Component Analysis - Multidisciplinary Applications*, InTech, 2012, pp. 59–72.

[31] J. Yu, "Fault detection using principal components-based Gaussian mixture model for semiconductor manufacturing processes," *IEEE Trans. Semicond. Manuf.*, vol. 24, no. 3, pp. 432–444, 2011, doi: 10.1109/TSM.2011.2154850.

[32] M. Zhu and A. Ghodsi, "Automatic dimensionality selection from the scree plot via the use of profile likelihood," *Comput. Stat. Data Anal.*, vol. 51, no. 2, pp. 918–930, 2006, doi: 10.1016/j.csda.2005.09.010.

[33] G. Diana and C. Tommasi, "Cross-validation methods in principal component analysis: a comparison," *Stat. Methods Appl.*, vol. 11, no. 1, pp. 71–82, 2002, doi: 10.1007/BF02511446.

[34] H. Hotelling, "Analysis of a complex of statistical variables into principal components.," *J. Educ. Psychol.*, vol. 24, no. 6, pp. 417–441, 1933, doi: 10.1037/h0071325.

[35] B. R. Bakshi, "Multiscale PCA with application to multivariate statistical process monitoring," *AIChE J.*, vol. 44, no. 7, pp. 1596–1610, Jul. 1998, doi: 10.1002/aic.690440712.

[36] M. Z. Sheriff, M. Mansouri, M. N. Karim, H. Nounou, and M. Nounou, "Fault detection using multiscale PCA-based moving window GLRT," *J. Process Control*, vol. 54, pp. 47–64, Jun. 2017, doi: 10.1016/j.jprocont.2017.03.004.

[37] M. Z. Sheriff, M. N. Karim, H. N. Nounou, and M. N. Nounou, "Process monitoring using PCA-based GLR methods: A comparative study," *J. Comput. Sci.*, vol. 27,

pp. 227–246, Jul. 2018, doi: 10.1016/j.jocs.2018.05.013.

[38] B. Schölkopf, A. Smola, and K.-R. Müller, “Kernel principal component analysis,” in *Computer Vision And Mathematical Methods In Medical And Biomedical Image Analysis*, vol. 1327, 1997, pp. 583–588.

[39] J.-M. Lee, C. Yoo, S. W. Choi, P. a. Vanrolleghem, and I.-B. Lee, “Nonlinear process monitoring using kernel principal component analysis,” *Chem. Eng. Sci.*, vol. 59, no. 1, pp. 223–234, 2004, doi: 10.1016/j.ces.2003.09.012.

[40] B. R. Bakshi, “Multiscale analysis and modeling using wavelets,” *J. Chemom.*, vol. 13, no. 3–4, pp. 415–434, May 1999, doi: 10.1002/(SICI)1099-128X(199905/08)13:3/4<415::AID-CEM544>3.0.CO;2-8.

[41] H. Aradhye, B. Bakshi, R. Strauss, and J. Davis, “Multiscale SPC using wavelets: theoretical analysis and properties,” *AIChE J.*, vol. 49, no. 4, pp. 939–958, Apr. 2003, doi: 10.1002/aic.690490412.

[42] M. N. Nounou and B. R. Bakshi, “Multiscale methods for denoising and compression,” in *Wavelets in Chemistry*, B.Walczak, Ed. Elsevier Science B.V., 2000, pp. 119–150.

[43] J. Davis, M. Piovoso, K. A. Hoo, and B. R. Bakshi, “Process Data Analysis and Interpretation,” in *Advances in chemical engineering*, vol. 25, 1999, pp. 1–103.

[44] D. C. Montgomery and G. C. Runger, *Applied Statistics and Probability for Engineers*, 5th ed. Hoboken, NJ: John Wiley & Sons, Inc., 2011.

[45] M. R. Reynolds Jr. and J. Lou, “A GLR control chart for monitoring the process variance,” in *Frontiers in Statistical Quality Control 10*, W. P. Lenz HJ., Schmid

W., Ed. 2012, pp. 3–17.

[46] M. R. Reynolds, J. Lou, J. Lee, and S. A. I. Wang, “The Design of GLR Control Charts for Monitoring the Process Mean and Variance,” *J. Qual. Technol.*, vol. 45, no. 1, pp. 34–60, 2013.

[47] R. Isermann, “Model-based fault-detection and diagnosis - Status and applications,” *Annu. Rev. Control*, vol. 29, pp. 71–85, 2005, doi: 10.1016/j.arcontrol.2004.12.002.

[48] M. M. Mansouri, H. N. Nounou, and M. N. Nounou, “Nonlinear control and estimation in induction machine using state estimation techniques,” *Syst. Sci. Control Eng.*, vol. 2, pp. 642–654, 2014, doi: http://dx.doi.org/10.1080/21642583.2014.956842.

[49] A. Noor, E. Serpedin, M. Nounou, and H. N. Nounou, “Inferring gene regulatory networks via nonlinear state-space models and exploiting sparsity,” *IEEE/ACM Trans. Comput. Biol. Bioinforma.*, vol. 9, no. 4, pp. 1203–1211, Jul. 2012, doi: 10.1109/TCBB.2012.32.

[50] M. Liu, S. Zang, D. Zhou, and and D. Z. Liu, Ming, Shu Zang, “Fast leak detection and location of gas pipelines based on an adaptive particle filter,” *Int. J. Appl. Math. Comput. Sci.*, vol. 15, no. 4, pp. 541–550, 2005, doi: 10.1038/39865.

[51] D. Simon, *Optimal State Estimation: Kalman, H Infinity, and Nonlinear Approaches*, 1st ed. New Jersey: Wiley-Interscience, 2006.

[52] Y. Kim, S. Sul, and M. Park, “Speed sensorless vector control of an induction motor using an extended Kalman filter,” in *IEEE Industry Applications Society Annual*

Meeting Industry Applications Society Annual Meeting, 1992, pp. 594–599, doi: 10.1109/IAS.1992.244341.

[53] S. J. Julier and J. K. Uhlmann, "A new extension of the Kalman filter to nonlinear systems," in *Signal Processing, Sensor Fusion, and Target Recognition VI*, 1865, doi: https://doi.org/10.1117/12.280797.

[54] E. A. Wan and R. Van Der Merwe, "The unscented Kalman filter for nonlinear estimation," in *IEEE 2000 Adaptive Systems for Signal Processing, Communications, and Control Symposium*, 2000.

[55] J. J. Downs and E. F. Vogel, "A plant-wide industrial process control problem," *Comput. Chem. Eng.*, vol. 17, no. 3, pp. 245–255, 1993, doi: 10.1016/0098-1354(93)80018-I.

[56] D. X. Tien, K.-W. Lim, and L. Jun, "Comparative Study of PCA Approaches in Process Monitoring and Fault Detection," *30th Annu. Conf. IEEE Ind. Electron. Soc.*, vol. 3, pp. 2594–2599, 2004, doi: 10.1109/IECON.2004.1432212.

[57] A. Bathelt, N. L. Ricker, and M. Jelali, "Revision of the Tennessee Eastman Process Model," *IFAC-PapersOnLine*, vol. 48, no. 8, pp. 309–314, 2015, doi: 10.1016/j.ifacol.2015.08.199.

[58] E. L. Russell, L. H. Chiang, and R. D. Braatz, *Fault detection and diagnosis in industrial systems*. New York, NY: Springer-Verlag, 2001.

[59] M. Z. Sheriff, C. Botre, M. Mansouri, H. Nounou, M. Nounou, and M. N. Karim, "Process Monitoring Using Data-Based Fault Detection Techniques: Comparative Studies," in *Fault Diagnosis and Detection*, InTech, 2017.

[60] M. Mansouri, M. Nounou, H. Nounou, and N. Karim, “Kernel PCA-based GLRT for nonlinear fault detection of chemical processes,” *J. Loss Prev. Process Ind.*, vol. 40, pp. 334–347, 2016, doi: 10.1016/j.jlp.2016.01.011.

[61] M. Z. Sheriff, F. Harrou, and M. Nounou, “Univariate process monitoring using multiscale Shewhart charts,” in *2014 International Conference on Control, Decision and Information Technologies (CoDIT)*, 2014, pp. 435–440.

[62] M. Z. Sheriff, “Improved Shewhart chart using multiscale representation,” Texas A&M University, 2015.

[63] M. Mansouri *et al.*, “Statistical Fault Detection of Chemical Process - Comparative Studies,” *J. Chem. Eng. Process Technol.*, vol. 07, no. 01, pp. 1–10, 2016, doi: http://dx.doi.org/10.4172/2157-7048.1000282.

[64] M. Z. Sheriff, M. N. Karim, M. N. Nounou, H. Nounou, and M. Mansouri, “Fault detection of nonlinear systems using an improved KPCA method,” in *2017 4th International Conference on Control, Decision and Information Technologies (CoDIT)*, 2017, pp. 0036–0041, doi: 10.1109/CoDIT.2017.8102563.

[65] M. Z. Sheriff, M. N. Karim, M. N. Nounou, H. Nounou, and M. Mansouri, “Monitoring of chemical processes using improved multiscale KPCA,” in *2017 4th International Conference on Control, Decision and Information Technologies (CoDIT)*, 2017, pp. 0049–0054, doi: 10.1109/CoDIT.2017.8102565.

[66] M. Z. Sheriff and M. N. Nounou, “Enhanced performance of shewhart charts using multiscale representation,” in *2016 American Control Conference (ACC)*, 2016, pp. 6923–6928, doi: 10.1109/ACC.2016.7526763.

[67] R. Isermann, “On the applicability of model-based fault detection for technical processes,” *Control Eng. Pract.*, vol. 2, no. 3, pp. 439–450, 1994, doi: 10.1016/0967-0661(94)90781-1.

[68] E. G. J. Huang, “An improved fault detection methodology for semiconductor applications based on multi-regime identification,” University of Cincinnati, 2013.

[69] T. A. Johansen and R. Murray-Smith, “Multiple model approaches to nonlinear modelling and control,” in *Multiple model approaches to nonlinear modelling and control*, 1st ed., T. A. Johansen and R. Murray-Smith, Eds. Bristol, PA: Taylor & Francis, 1997, pp. 1–360.

[70] J. Penman, “Feasibility of using unsupervised learning, artificial neural networks for the condition monitoring of electrical machines,” *IEE Proc. - Electr. Power Appl.*, vol. 141, no. 6, p. 317, 1994, doi: 10.1049/ip-epa:19941263.

[71] G. Craessaerts, J. De Baerdemaeker, and W. Saeys, “Fault diagnostic systems for agricultural machinery,” *Biosyst. Eng.*, vol. 106, no. 1, pp. 26–36, 2010, doi: 10.1016/j.biosystemseng.2009.12.004.

[72] L. Selak, P. Butala, and A. Sluga, “Condition monitoring and fault diagnostics for hydropower plants,” *Comput. Ind.*, vol. 65, no. 6, pp. 924–936, 2014, doi: 10.1016/j.compind.2014.02.006.

[73] D. M. Ghiocel and M. J. Roemer, “New probabilistic risk-based fault diagnosis procedure for gas turbine engine performance,” *Collect. Tech. Pap. - AIAA/ASME/ASCE/AHS/ASC Struct. Struct. Dyn. Mater. Conf.*, vol. 4, no. c, pp. 2807–2813, 1999, doi: 10.2514/6.1999-1572.

[74] W. J. Rebello, S. L. Richlen, and F. Childs, “The cost of heat exchanger fouling in the US industries,” 1988.

[75] U. B. Deshannavar, M. S. Rafeen, M. Ramasamy, and D. Subbarao, “Crude oil fouling: A review,” *J. Appl. Sci.*, vol. 10, no. 24, pp. 3167–3174, 2010, doi: 10.3923/jas.2010.3167.3174.

[76] T. K. Hou, S. N. Kazi, A. B. Mahat, C. B. Teng, A. Al-Shamma’a, and A. Shaw, “Industrial Heat Exchanger: Operation and Maintenance to Minimize Fouling and Corrosion,” in *Heat Exchangers - Advanced Features and Applications*, no. May, 2017, pp. 193–207.

[77] J. C. Wong, K. A. McDonald, and A. Palazoglu, “Classification of abnormal plant operation using multiple process variable trends,” *J. Process Control*, vol. 11, no. 4, pp. 409–418, 2001, doi: 10.1016/S0959-1524(00)00011-1.

[78] F. Y. Wang, P. Bahri, P. L. Lee, and I. T. Cameron, “A multiple model, state feedback strategy for robust control of non-linear processes,” *Comput. Chem. Eng.*, vol. 31, no. 5–6, pp. 410–418, 2007, doi: 10.1016/j.compchemeng.2006.05.008.

[79] U. J. F. Aarsnes, F. Di Meglio, R. Graham, and O. M. Aamo, “A methodology for classifying operating regimes in underbalanced-drilling operations,” *SPE J.*, vol. 21, no. 2, pp. 423–433, 2016, doi: 10.2118/178920-PA.

[80] D. N. Togobitskaya, P. I. Otorvin, A. I. Bel’kova, and A. Y. Grin’ko, “Automated system for monitoring and controlling the slag regime in blast-furnace smelting,” *Metallurgist*, vol. 48, no. 3–4, pp. 147–152, 2004, doi: 10.1023/B:MELL.0000037175.94442.d1.

[81] E. Lapira, D. Brisset, H. Davari Ardakani, D. Siegel, and J. Lee, "Wind turbine performance assessment using multi-regime modeling approach," *Renew. Energy*, vol. 45, pp. 86–95, 2012, doi: 10.1016/j.renene.2012.02.018.

[82] Z. Zhu, Z. Song, and A. Palazoglu, "Process pattern construction and multi-mode monitoring," *J. Process Control*, vol. 22, no. 1, pp. 247–262, 2012, doi: 10.1016/j.jprocont.2011.08.002.

[83] R. Zimroz and A. Bartkowiak, "Two simple multivariate procedures for monitoring planetary gearboxes in non-stationary operating conditions," *Mech. Syst. Signal Process.*, vol. 38, no. 1, pp. 237–247, 2013, doi: 10.1016/j.ymssp.2012.03.022.

[84] S. Natarajan and R. Srinivasan, "Multi-model based process condition monitoring of offshore oil and gas production process," *Chem. Eng. Res. Des.*, vol. 88, no. 5–6, pp. 572–591, 2010, doi: 10.1016/j.cherd.2009.10.013.

[85] N. Basha, M. Z. Sheriff, C. Kravaris, H. Nounou, and M. Nounou, "Multiclass data classification using fault detection-based techniques," *Comput. Chem. Eng.*, vol. 136, pp. 1–11, 2020, doi: 10.1016/j.compchemeng.2020.106786.

[86] M. Rodrigues, D. Theilliol, M. Adam-Medina, and D. Sauter, "A fault detection and isolation scheme for industrial systems based on multiple operating models," *Control Eng. Pract.*, vol. 16, no. 2, pp. 225–239, 2008, doi: 10.1016/j.conengprac.2006.02.020.

[87] A. Bhagwat, R. Srinivasan, and P. R. Krishnaswamy, "Multi-linear model-based fault detection during process transitions," *Chem. Eng. Sci.*, vol. 58, no. 9, pp. 1649–1670, 2003, doi: 10.1016/S0009-2509(03)00008-3.

[88] A. S. Naik, S. Yin, S. X. Ding, and P. Zhang, “Recursive identification algorithms to design fault detection systems,” *J. Process Control*, vol. 20, no. 8, pp. 957–965, 2010, doi: 10.1016/j.jprocont.2010.06.018.

[89] Y. S. Ng and R. Srinivasan, “An adjoined multi-model approach for monitoring batch and transient operations,” *Comput. Chem. Eng.*, vol. 33, no. 4, pp. 887–902, 2009, doi: 10.1016/j.compchemeng.2008.11.014.

[90] A. Bhagwat, R. Srinivasan, and P. R. Krishnaswamy, “Fault detection during process transitions: A model-based approach,” *Chem. Eng. Sci.*, vol. 58, no. 2, pp. 309–325, 2003, doi: 10.1016/S0009-2509(02)00520-1.

[91] Y. S. Ng and R. Srinivasan, “Multivariate Temporal Data Analysis Using Self-Organizing Maps. 2. Monitoring and Diagnosis of Multistate Operations,” *Ind. Eng. Chem. Res.*, vol. 47, no. 20, pp. 7758–7771, Oct. 2008, doi: 10.1021/ie071022y.

[92] S. J. Zhao, J. Zhang, and Y. M. Xu, “Monitoring of processes with multiple operating modes through multiple principle component analysis models,” *Ind. Eng. Chem. Res.*, vol. 43, no. 22, pp. 7025–7035, 2004, doi: 10.1021/ie0497893.

[93] Y. H. Ali, R. Abd Rahman, and R. I. R. Hamzah, “Artificial neural network model for monitoring oil film regime in spur gear based on acoustic emission data,” *Shock Vib.*, vol. 2015, pp. 1–12, 2015, doi: 10.1155/2015/106945.

[94] A. K. Das and C. K. Y. Leung, “Power spectral entropy of acoustic emission signal as a new damage indicator to identify the operating regime of strain hardening cementitious composites,” *Cem. Concr. Compos.*, vol. 104, no. April, p. 103409, 2019, doi: 10.1016/j.cemconcomp.2019.103409.

[95] L. Travé-Massuyès and R. Milne, “Gas-turbine condition monitoring using qualitative model-based diagnosis,” *IEEE Expert. Syst. their Appl.*, vol. 12, no. 3, pp. 22–31, 1997, doi: 10.1109/64.590070.

[96] D. Edelin, N. Bariteau, Y. Etourneau, L. Traonvouez, and J. Soto, “Experimental investigation of the air side fouling of finned tube heat exchangers,” *Heat Mass Transf. und Stoffuebertragung*, vol. 55, no. 10, pp. 2713–2722, 2019, doi: 10.1007/s00231-019-02612-2.

[97] A. Fguiri, R. Jradi, C. Marvillet, and M. R. Jeday, “Heat exchangers fouling in phosphoric acid concentration,” *Heat Mass Transf. und Stoffuebertragung*, vol. 56, no. 7, pp. 2313–2324, 2020, doi: 10.1007/s00231-020-02858-1.

[98] R. Jradi, C. Marvillet, and M. R. Jeday, “Modeling and comparative study of heat exchangers fouling in phosphoric acid concentration plant using experimental data,” *Heat Mass Transf. und Stoffuebertragung*, 2020, doi: 10.1007/s00231-020-02888-9.

[99] E. Diaz-Bejarano, F. Coletti, and S. Macchietto, “Modeling and Prediction of Shell-Side Fouling in Shell-and-Tube Heat Exchangers,” *Heat Transf. Eng.*, vol. 40, no. 11, pp. 845–861, 2019, doi: 10.1080/01457632.2018.1446814.

[100] Z. Han, Z. Xu, and X. Yu, “CFD modeling for prediction of particulate fouling of heat transfer surface in turbulent flow,” *Int. J. Heat Mass Transf.*, vol. 144, p. 118428, 2019, doi: 10.1016/j.ijheatmasstransfer.2019.07.078.

[101] U. Ojaniemi, T. P. Pättikangas, A. Jäsberg, E. Puhakka, and A. Koponen, “CFD simulation of fouling of plate heat exchanger by Phosphate Calcium,” in

Proceedings of International Conference on Heat Exchanger Fouling and Cleaning – 2019, 2019, no. Table 1, pp. 45–52.

[102] S. García and A. Trueba, "Fouling in Heat Exchangers," in *Inverse Heat Conduction and Heat Exchangers*, IntechOpen, 2019, pp. 1–26.

[103] E. Guelpa and V. Verda, "Automatic fouling detection in district heating substations: Methodology and tests," *Appl. Energy*, vol. 258, no. February 2019, p. 114059, 2020, doi: 10.1016/j.apenergy.2019.114059.

[104] A. M. Demin, A. P. Naumenko, O. A. Reutova, and A. I. Odinets, "Economic evaluation of use of heat exchange equipment diagnostic software at diesel hydrotreating unit," *J. Phys. Conf. Ser.*, vol. 1260, no. 3, 2019, doi: 10.1088/1742-6596/1260/3/032009.

[105] E. Diaz-Bejarano, F. Coletti, and S. MacChietto, "A Model-Based Method for Visualization, Monitoring, and Diagnosis of Fouling in Heat Exchangers," *Ind. Eng. Chem. Res.*, vol. 59, no. 10, pp. 4602–4619, 2020, doi: 10.1021/acs.iecr.9b05490.

[106] Incropera Frank P. and D. P. DeWitt, *Fundametals of heat and mass transfer*, 5th ed. Wiley, 2001.

[107] M. S. Peters and K. D. Timmerhaus, *Plant design and economics for chemical engineers*, 4th ed. McGraw-Hill, 1991.

[108] M. A. Mehrabian and M. Hemmat, "The overall heat transfer characteristics of a double pipe heat exchanger: Comparison of experimental data with predictions of standard correlations," *Comput. Eng.*, vol. 30, pp. 607–618, 2001.

[109] “National Inventory Report 1990-2012: Greenhouse Gas Sources and Sinks in Canada,” 2014.

[110] N. Behari, M. Z. Sheriff, M. A. Rahman, M. Nounou, I. Hassan, and H. Nounou, “Chronic leak detection for single and multiphase flow: A critical review on onshore and offshore subsea and arctic conditions,” *J. Nat. Gas Sci. Eng.*, vol. 81, p. 103460, Sep. 2020, doi: 10.1016/j.jngse.2020.103460.

[111] J. Wan, Y. Yu, Y. Wu, R. Feng, and N. Yu, “Hierarchical leak detection and localization method in natural gas pipeline monitoring sensor networks,” *Sensors*, vol. 12, no. 1, pp. 189–214, 2012, doi: 10.3390/s120100189.

[112] J. C. Martins and P. Seleghim, “Assessment of the performance of acoustic and mass Balance methods for leak detection in pipelines for transporting liquids,” *J. Fluids Eng.*, vol. 132, no. 1, p. 011401, 2010, doi: 10.1115/1.4000736.

[113] T. M. El-Shiekh, “Leak detection methods in transmission pipelines,” *Energy Sources, Part A Recover. Util. Environ. Eff.*, vol. 32, no. 8, pp. 715–726, 2010, doi: 10.1080/15567030903058618.

[114] S. Ali *et al.*, “SimpliMote: A Wireless Sensor Network Monitoring Platform for Oil and Gas Pipelines,” *IEEE Syst. J.*, vol. 12, no. 1, pp. 778–789, 2018, doi: 10.1109/JSYST.2016.2597171.

[115] S. Rashid, U. Akram, and S. A. Khan, “WML: Wireless sensor network based machine learning for leakage detection and size estimation,” *Procedia Comput. Sci.*, vol. 63, no. Euspn, pp. 171–176, 2015, doi: 10.1016/j.procs.2015.08.329.

[116] S. Rashid, U. Akram, S. Qaisar, S. A. Khan, and E. Felemban, “Wireless sensor

network for distributed event detection based on machine learning," *Proc. - 2014 IEEE Int. Conf. Internet Things, iThings 2014, 2014 IEEE Int. Conf. Green Comput. Commun. GreenCom 2014 2014 IEEE Int. Conf. Cyber-Physical-Social Comput. CPS 20*, no. iThings, pp. 540–545, 2014, doi: 10.1109/iThings.2014.93.

[117] M. E. Zurko, S. Chiasson, and M. Smith, "Numerical analysis of heavy oil-water flow and leak detection in vertical pipelines," *Adv. Chem. Eng. Sci.*, vol. 3, pp. 9–15, 2013, doi: http://dx.doi.org/10.4236/aces.2013.31002.

[118] C. Ma, S. Yu, and J. Huo, "Negative pressure wave-flow testing gas pipeline leak based on wavelet transform," in *2010 International Conference on Computer, Mechatronics, Control and Electronic Engineering*, 2010, vol. 5, pp. 306–308, doi: 10.1109/CMCE.2010.5609975.

[119] C. Ge, G. Wang, and H. Ye, "Analysis of the smallest detectable leakage flow rate of negative pressure wave-based leak detection systems for liquid pipelines," *Comput. Chem. Eng.*, vol. 32, no. 8, pp. 1669–1680, 2008, doi: 10.1016/j.compchemeng.2007.08.011.

[120] P. Stouffs and M. Giot, "Pipeline balance: leak detection based on mass importance of the packing term," *J. Loss Prev. Process Ind.*, vol. 6, no. 5, pp. 307–312, 1993.

[121] M. Dinis, A. Wojtanowicz, and S. Scott, "Leak detection in liquid subsea flowlines with no recorded feed rate," vol. 121, no. September, pp. 161–166, 1999, doi: 10.1115/1.2795976.

[122] R. Toriumi *et al.*, "Differential absorption lidar at 1.67 μm for remote sensing of methane leakage emissions from process units differential absorption lidar at 1 . 67

μ m for remote sensing of methane leakage," *Jpn. J. Appl. Phys.*, vol. 38, no. 1, pp. 110–114, 1999.

[123] T. Iseki, T. Hideo, and K. Kimura, "A portable remote methane sensor using a tunable diode laser," *Meas. Sci. Technol.*, vol. 11, no. 6, pp. 594–602, 2000, doi: 10.1088/0957-0233/11/6/302.

[124] N. S. Gopalsame and A. P. C. Raptis, "Millimeter-wave radar sensing of airbone chemicals," *IEEE Trans. Microw. Theory Tech.*, vol. 49, no. 4, pp. 646–653, 2001.

[125] N. Kasai, C. Tsuchiya, T. Fukuda, K. Sekine, T. Sano, and T. Takehana, "Propane gas leak detection by infrared absorption using carbon infrared emitter and infrared camera," *NDT &E Int.*, vol. 44, no. 1, pp. 57–60, 2011, doi: 10.1016/j.ndteint.2010.09.006.

[126] C. L. Bennett, M. R. Carter, and D. J. Fields, "Hyperspectral Imaging in the Infrared using LIFTIRS," in *International symposium on optical science, engineering and instrumentation*, 1995.

[127] P. M. Bach and J. K. Kodikara, "Reliability of Infrared Thermography in Detecting Leaks in Buried Water Reticulation Pipes," *IEEE J. Sel. Top. Appl. Earth Obs. Remote Sens.*, vol. 10, no. 9, pp. 4210–4224, 2017, doi: 10.1109/JSTARS.2017.2708817.

[128] A. Banica, D. Miller, and B. T. Tolton, "Results of field trials of Realsens, an airborne natural gas leak detection technology," in *7th International Pipeline Conference*, 2008, pp. 1–6.

[129] P. S. Murvay and I. Silea, "A survey on gas leak detection and localization

techniques," *J. Loss Prev. Process Ind.*, vol. 25, no. 6, pp. 966–973, 2012, doi: 10.1016/j.jlp.2012.05.010.

[130] A. B. M. Akib, N. Bin Saad, and V. Asirvadam, "Pressure point analysis for early detection system," in *Proceedings - 2011 IEEE 7th International Colloquium on Signal Processing and Its Applications, CSPA 2011*, 2011, no. 2, pp. 103–107, doi: 10.1109/CSPA.2011.5759852.

[131] J. Mashford, D. De Silva, D. Marney, and S. Burn, "An approach to leak detection in pipe networks using analysis of monitored pressure values by support vector machine," in *NSS 2009 - Network and System Security*, 2009, pp. 534–539, doi: 10.1109/NSS.2009.38.

[132] Marques, C., Ferreira, M. J., and J. G. Rocha, "Leak detection in water-distribution plastic pipes by spectral analysis of acoustic leak noise," in *IECON 2009 - 35th Annual Conference of IEEE Industrial Electronics (IECON)*, 2009, pp. 2092–2097, doi: 10.1109/IECON.2009.5415109.

[133] M. Kim and S. Lee, "Detection of leak acoustic signal in buried gas pipe based on the time – frequency analysis," *J. Loss Prev. Process Ind.*, vol. 22, no. 6, pp. 990–994, 2009, doi: 10.1016/j.jlp.2008.08.009.

[134] S. B. Beck, M. D. Curren, N. D. Sims, and R. Stanway, "Pipeline network features and leak detection by cross-correlation analysis of reflected waves," *J. Hydraul. Eng.*, vol. 131, no. 8, pp. 715–723, 2005, doi: 10.1061/(ASCE)0733-9429(2005)131:8(715).

[135] W. Mpesha, S. L. Gassman, and M. H. Chaudhry, "Leak detection in pipes by

frequency response method," *J. Hydraul. Eng.*, vol. 127, no. 2, pp. 134–147, 2001, doi: ISSN 0733-9429/01/0002-0134–0147.

[136] A. Lay-Ekuakille, A. Trotta, and G. Vendramin, "FFT-based spectral response for smaller pipeline leak detection," in *2009 IEEE Intrumentation and Measurement Technology Conference, I2MTC 2009*, 2009, no. May, pp. 328–331, doi: 10.1109/IMTC.2009.5168469.

[137] A. Lay-Ekuakille, C. Pariset, and A. Trotta, "Leak detection of complex pipelines based on the filter diagonalization method: Robust technique for eigenvalue assessment," *Meas. Sci. Technol.*, vol. 21, no. 11, 2010, doi: 10.1088/0957-0233/21/11/115403.

[138] A. Lay-Ekuakille, G. Vendramin, and A. Trotta, "Robust Spectral Leak Detection of Complex Pipelines Using Filter Diagonalization Method," *IEEE Sens. J.*, vol. 9, no. 11, pp. 1605–1614, 2009, doi: 10.1109/JSEN.2009.2027410.

[139] A. Lay-Ekuakille, G. Vendramin, and A. Trotta, "Spectral analysis of leak detection in a zigzag pipeline: A filter diagonalization method-based algorithm application," *Meas. J. Int. Meas. Confed.*, vol. 42, no. 3, pp. 358–367, 2009, doi: 10.1016/j.measurement.2008.07.007.

[140] M. A. Adegboye, W. K. Fung, and A. Karnik, "Recent advances in pipeline monitoring and oil leakage detection technologies: Principles and approaches," *Sensors (Switzerland)*, vol. 19, no. 11, 2019, doi: 10.3390/s19112548.

[141] E. Hauge, O. M. Aamo, and J. M. Godhavn, *Model based pipeline monitoring with leak detection*, vol. 7, no. PART 1. IFAC, 2007.

[142] D. Kurtis L, “Leak Detection in Pipelines using the Extended Kalman Filter and the Extended Boundary Approach,” University of Saskatchewan, 2007.

[143] A. Lay-Ekuakille, P. Vergallo, and A. Trotta, “Impedance method for leak detection in zigzag pipelines,” *Meas. Sci. Rev.*, vol. 10, no. 6, pp. 209–213, 2010, doi: 10.2478/v10048-010-0036-0.

[144] D. Covas, H. Ramos, and A. B. de Almeida, “Standing wave difference method for leak detection in pipeline systems,” *J. Hydraul. Eng.*, vol. 131, no. 12, pp. 1106–1116, 2005, doi: 10.1061/(ASCE)0733-9429(2005)131:12(1106).

[145] D. Isa and R. Rajkumar, “Pipeline defect prediction using support vector machines,” *Appl. Artif. Intell.*, vol. 23, no. 8, pp. 758–771, 2009, doi: 10.1080/08839510903210589.

[146] M. Di Blasi, R. M. Baptista, and C. Muravchik, “Pipeline leak localization using pattern recognition and a bayes detector,” *6th Int. Pipeline Conf.*, no. June 2015, pp. 1–8, 2006, doi: 10.1115/IPC2006-10211.

[147] X. Li and G. J. Li, “Leak detection of municipal water supply network based on the cluster-analysis and fuzzy pattern recognition,” *2010 Int. Conf. E-Product E-Service E-Entertainment, ICEEE2010*, no. 50878140, pp. 1–5, 2010, doi: 10.1109/ICEEE.2010.5660550.

[148] Z. J. Zhou, C. H. Hu, D. L. Xu, J. B. Yang, and D. H. Zhou, “Bayesian reasoning approach based recursive algorithm for online updating belief rule based expert system of pipeline leak detection,” *Expert Syst. Appl.*, vol. 38, no. 4, pp. 3937–3943, 2011, doi: 10.1016/j.eswa.2010.09.055.

[149] D. L. Xu *et al.*, “Inference and learning methodology of belief-rule-based expert system for pipeline leak detection,” *Expert Syst. Appl.*, vol. 32, no. 1, pp. 103–113, 2007, doi: 10.1016/j.eswa.2005.11.015.

[150] G. Geiger, T. Werner, and D. Matko, “Knowledge-based leak monitoring for pipelines,” *IFAC Proc. Vol.*, vol. 34, no. 27, pp. 249–254, 2001, doi: 10.1016/S1474-6670(17)33600-5.

[151] S. L. Scott and M. A. Barrufet, “Worldwide assessment of industry leak detection capabilities for single & multiphase pipelines; Project Report Prepared for the Minerals Management Service Under the MMS/OTRC Cooperative Research Agreement 1435-01-99-CA-31003 Task Order 18133,” College Station, 2003.

[152] C. J. Thiberville, Y. Wang, P. Waltrich, W. C. Williams, and S. I. Kam, “Evaluation of software-based early leak-warning system in Gulf of Mexico subsea flowlines,” *SPE Prod. Oper.*, no. November, pp. 802–828, 2018, doi: https://doi.org/10.2118/187417-MS.

[153] S. I. Kam, “Mechanistic modeling of pipeline leak detection at fixed inlet rate,” *J. Pet. Sci. Eng.*, vol. 70, no. 3–4, pp. 145–156, 2010, doi: 10.1016/j.petrol.2009.09.008.

[154] O. Akinsete and A. Oshingbesan, “Leak Detection in Natural Gas Pipelines Using Intelligent Models,” in *SPE Nigeria Annual International Conference and Exhibition*, 2019, no. August, pp. 5–7, doi: 10.2118/198738-MS.

[155] O. Fidaner, “Downhole Multiphase Flow Monitoring Using Fiber Optics,” in *SPE Annual Technical Conference and Exhibition*, 2017, no. October, pp. 9–11, doi:

10.2118/187415-MS.

[156] J. Worsley, C. Minto, D. Hill, A. Godfrey, and J. Ashdown, “Fibre Optic Four Mode Leak Detection for Gas, Liquids and Multiphase Products,” in *Abu Dhabi International Petroleum Exhibition and Conference*, 2014, vol. 2, pp. 1567–1578, doi: 10.2118/171824-MS.

[157] P. Thodi, M. Paulin, L. Forster, J. Burke, and G. Lanan, “Arctic Pipeline Leak Detection using Fiber Optic Cable Distributed Sensing Systems,” in *OTC Arctic Technology Conference*, 2014, doi: 10.4043/24589-MS.

[158] B. Eisler, “Leak Detection Systems and Challenges for Arctic Subsea Pipelines,” in *OTC Arctic Technology Conference*, 2011, doi: 10.4043/22134-MS.

[159] J. Zhang, A. Hoffman, A. Kane, and J. Lewis, “Development of Pipeline Leak Detection Technologies,” in *2014 10th International Pipeline Conference*, 2014, doi: https://doi.org/10.1115/IPC2014-33619.

[160] L. Billmann and R. Isermann, “Leak detection methods for pipelines,” *Automatica*, vol. 23, no. 3, pp. 381–385, 1987, doi: 10.1016/0005-1098(87)90011-2.

[161] J. Zhang, C. Zou, and Z. Wang, “A control chart based on likelihood ratio test for monitoring process mean and variability,” *Qual. Reliab. Eng. Int.*, vol. 26, no. 1, pp. 63–73, 2010, doi: 10.1002/qre.1036.

[162] R. A. Sultan, M. A. Rahman, S. Rushd, S. Zendehboudi, and V. C. Kelessidis, “Validation of CFD model of multiphase flow through pipeline and annular geometries,” *Part. Sci. Technol.*, vol. 37, no. 6, pp. 681–693, 2019, doi: 10.1080/02726351.2018.1435594.

[163] “Liquid Flowzan ® Biopolymer XPT - Safety Data Sheet,” Conroe, TX, 2019.

[164] A. Cinar, A. Palazoglu, and F. Kayihan, *Chemical Process Performance Evaluation*, 1st ed. Boca Raton, FL: CRC Press, 2007.

[165] P. Čisar and S. Čisar, “Optimization methods of EWMA statistics,” *Acta Polytech. Hungarica*, vol. 8, no. 5, pp. 73–87, 2011.

[166] P. Musonda, M. Hocine, N. Andrews, P. Tubert-Bitter, and C. P. Farrington, “Monitoring vaccine safety using case series cumulative sum charts,” *Vaccine*, vol. 26, no. 42, pp. 1–22, 2008.

[167] A. Chen and Y. K. Chen, “Design of EWMA and CUSUM control charts subject to random shift sizes and quality impacts,” *IIE Trans.*, vol. 39, no. 12, pp. 1127–1141, 2007.

[168] F. Harrou, M. Nounou, and H. Nounou, “Statistical Detection of Abnormal Ozone Levels Using Principal Component Analysis,” *Int. J. Eng. ...*, no. 06, pp. 54–59, 2012.

[169] C. Botre, M. Mansouri, M. Nounou, H. Nounou, and M. N. Karim, “Kernel PLS-based GLRT method for fault detection of chemical processes,” *J. Loss Prev. Process Ind.*, vol. 43, pp. 212–224, 2016, doi: 10.1016/j.jlp.2016.05.023.